FINAL REPORT

FOR

RADIATION DAMAGE

IN

LITHIUM-CONTAINING SOLAR CELLS

(21 JUNE 1966 THROUGH 20 MARCH 1968)

CONTRACT NO. NAS 5-10239

Prepared by

G. BRUCKER, T. FAITH, A.G. HOLMES-SIEDLE,
AND R. NEADLE
ASTRO-ELECTRONICS DIVISION
DEFENSE ELECTRONIC PRODUCTS
RADIO CORPORATION OF AMERICA
PRINCETON, NEW JERSEY 08540

FOR

NATIONAL AERONAUTICS AND SPACE ADMINISTRATION
GODDARD SPACE FLIGHT CENTER
GREENBELT, MARYLAND

FINAL REPORT

RADIATION DAMAGE IN LITHIUM-CONTAINING SOLAR CELLS

21 June 1966 through 20 March 1968

Contract No. NAS 5–10239

Goddard Space Flight Center

Contracting Officer: Mr. A. L. Essex
Technical Monitor: Dr. P. H. Fang

Prepared by

G. Brucker, T. Faith, A. G. Holmes-Siedle, and R. Neadle

Astro-Electronics Division
Defense Electronic Products
Radio Corporation of America
Princeton, New Jersey 08540

Project Supervisor: Dr. A. G. Holmes-Siedle
Project Scientist: Dr. G. J. Brucker

for

National Aeronautics and Space Administration
Goddard Space Flight Center
Greenbelt, Maryland

PREFACE

This is the final report on the work performed under Contract No. NAS5-10239, "Radiation Damage in Lithium-Containing Solar Cells", by the Physical Research Laboratory of the Astro-Electronics Division (AED) of the Radio Corporation of America, Mr. Martin Wolf, Manager. The Project Supervisor was Dr. A.G. Holmes-Siedle and the Project Scientist was Dr. G.J. Brucker.

The Technical Monitor of the program was Dr. P.H. Fang of the Goddard Space Flight Center, National Aeronautics and Space Administration. Dr. Fang also selected and supplied the GFE device samples used in this program.

Mr. F. Kolondra, Member of the Technical Staff of the RCA Laboratories, contributed to the experimental work by operating the 1-MeV Van de Graaff generator and assisting with measurements and calculations.

The work described in this report was performed over a period of twenty-one months. The results obtained during the first twelve months were reported in detail in the "Annual Progress Report" on this contract, issued June 1967. The work described in the Annual Progress Report is referenced where the subject matters involve a level of detail inappropriate for inclusion in a final report. However, where necessary, material has been repeated in order to present here an adequate history of the overall project.

This report was submitted by the authors April 1968.

ABSTRACT

The interactions of lithium with defects induced in silicon solar cells by 1-Mev electron bombardment have been investigated. Solar cells used as test vehicles were supplied by NASA and test diodes similar to solar cells were made. The principal techniques used in the study to investigate the interaction of lithium with a radiation induced damage center were (1) the capacitance method of measuring donor (lithium) concentration, (2) the electron-voltaic method of measuring diffusion length, and (3) the measurement of diffusion length vs. excess carrier density. Recovery of solar cells appeared to follow a diffusion-limited kinetic model. Recovery theory was shown to correlate with measurements of lithium density profiles and direct measurements of the effective lithium-diffusion constant. The electric field arising from the ratio of donor-concentration gradient to donor concentration is, in some cases, sufficiently large to affect the collection of minority carriers. The effect of the electric field is particularly important when the diffusion length is reduced to a low value by electron bombardment; at that point the concept of a diffusion length begins to lose its physical meaning.

A large group of government-furnished cells, originally bombarded during the initial contract period, were periodically re-evaluated. There appeared to be an optimum concentration of lithium for good stability and recovery, ranging from ≈ 2 to 5×10^{15} cm^{-3} for the damage level used in this study ($\Phi = 10^{16}$ e/cm^2, $d\Phi/dt \approx 3 \times 10^{15}$ $e/cm^2/hr$). Cells with smaller concentrations of lithium than $2 \times 10^{15} cm^{-3}$ exhibited less recovery and complete depletion of lithium. Cells with greater concentration of lithium than $5 \times 10^{15} cm^{-3}$ exhibited redegradation in power (6% to 44%, relative to maximum annealed value) and/or short-circuit current. The oxygen-rich cells (initial lithium concentration $\approx 2 \times 10^{15} cm^{-3}$) and cells with an additional phosphorus layer near the junction are still annealing after a post-irradiation time of approximately one year. These latter two types of cells appear very promising and their development should be vigorously pursued. All test diodes showed good stability under all conditions. Lightly damaged diodes ($\Phi = 10^{12}$ to 10^{13} e/cm^2) exhibited complete diffusion-length recovery and heavily damaged diodes ($\Phi \approx 10^{15}$ e/cm^2) exhibited partial recovery.

During this contract, several guidelines to good lithium solar-cell design have emerged. These have included data giving guidance on (1) choice of silicon starting material, (2) choice of lithium concentration and distribution, (3) the effects of differing illumination levels on performance, (4) prediction of recovery rates, (5) non-destructive hardness evaluation tests, and (6) prediction of the effects of protons and neutrons.

TABLE OF CONTENTS

TABLE OF CONTENTS (Continued)

LIST OF ILLUSTRATIONS

LIST OF ILLUSTRATIONS (Continued)

LIST OF ILLUSTRATIONS (Continued)

LIST OF TABLES

SECTION I
INTRODUCTION

A. GENERAL

This study was concerned with the physical mechanisms underlying the electrical neutralization, by lithium, of radiation-induced defects in bulk silicon and in silicon junction devices of the solar-cell type. A more detailed knowledge of the mechanism-of-action of lithium is needed to establish the best processes for the fabrication of solar cells and to determine the ultimate stability obtainable in cells of this type. The objective of the present work was to determine the parameters which affect the resistance of experimental solar cells to charged-particle radiation. Within this framework, the primary objective was to interrelate the observed recovery phenomena in lithium-doped devices to the known mechanisms of migration and binding of lithium in silicon, and to the known defect structures in silicon.

This report describes extensive measurements of lithium concentration profiles in solar-cell structures, the performance of the structures before and after particle irradiation, and the correlation of such concentration measurements with the recovery properties of radiation-damaged cells, as indicated by the recovery rate of diffusion lengths and photovoltaic characteristics of the devices. The feasibility of the use of lithium doping as a means of hardening a practical operational solar cell to radiation depends on the degree of long-term stability of these cells both before and after irradiation. A study of long-term stability of a large group of irradiated government-furnished cells (GFE) was initiated during the period 1966-1967. This study was continued in the present work and additional cells, some being furnished by NASA and others fabricated in-house, were added to this study during this contract period.

B. BACKGROUND

In previous work by RCA (Ref. 1), it was discovered that the presence of lithium as a dopant in silicon solar cells significantly affected the radiation properties of the cells, causing an unusual, if not unique, recovery of damage effects so rapid that it became noticeable minutes after irradiation. This discovery led to the prospect that an operational solar-cell power source of greatly enhanced lift-time in space could be designed, using lithium-doped cells. This concept, the first true "hardening" of cells by special doping, had, in addition, a potential application to other solid-state devices that are sensitive to minority-carrier lifetime degradation.

Subsequent work showed that, when cells made from high-resistivity n-type silicon with low oxygen content were doped with lighium, they spontaneously recovered from

damage introduced by 1-MeV electrons, 16.8 MeV protons, and fission or 14 MeV neutrons (Refs. 1, 2, and 3). It was further shown that other impurities played a role in the behavior of lithium-diffused diodes (Ref. 4). For example, in lithium cells made from silicon containing a high oxygen concentration, the self-healing process after irradiation was much slower, recovery taking months rather than hours.

The study of impurity effects was carried out in a systematic way on test diodes (test vehicles modeled on solar cells but better adapted to the experiment)[1], fabricated by the experimenters from bulk silicon of well-characterized properties. A continuing, parallel evaluation program carried out on government furnished, lithium-doped solar cells supplied supplementary information on typical production-type solar cells with a variety of material parameters.

An important phenomenon observed in studies on lithium in silicon by other workers (Ref. 4) was the gradual redegradation of some lithium cells after recovery from radiation damage. This effect most commonly occurred over a period of a few hundred hours after irradiation. The 1-MeV electron fluences investigated by these workers were in the range 10^{14} to 10^{15} e/cm^2. In the present program, the study of long-term stability involved cells irradiated to a much higher electron fluence, namely, 10^{16} e/cm^2. Such cells were stored and re-measured regularly in a cumulative "stability test", which continues to give information.

The measurement of diffusion length as a function of excess-carrier density in both lithium-doped and lithium-free cells by the electron-voltaic method clearly demonstrated that there were several stages in the interaction of lithium with radiation-induced damage centers. In addition, the temporal dependence of diffusion length vs. excess carrier density indicated that the interaction of lithium with other damage centers (for example, A- and E- centers) altered the dependence of diffusion length on excess carrier density.

C. TECHNICAL APPROACH

Several dozen special test diodes were made and, along with several dozen lithium solar cells made by other contractors (selected and supplied by NASA), were evaluated for diffusion length, lithium profiles, stability, and radiation sensitivity. An important new development was the application of junction capacitance techniques to accurately evaluate the strongly varying concentrations of lithium vs. distance within a few microns of the junction. This led to two important new types of information. The first derives

---

[1] *"Test diodes" in this report refer to special samples of lithium cells, similar to solar cells in junction depth, thickness, etc., but specially adapted for diffusion-length measurement and controlled fabrication from special ingots of silicon. They are usually 0.2 x 0.2 x 0.020 in. and have opaque front contacts. "GFE" cells refer to cells selected from other NASA development contracts and supplied as "government-furnished equipment" to RCA.*

from a new application of a previously known technique. Using this technique, several values of the rates of lithium removal vs electron flux (carrier removal rates) could be obtained from the same cell and analyzed as a function of lithium concentration. This approach served to elucidate the lithium-defect interactions occurring in the cell. The second new type of information is novel in that, for the first time, it has been observed that the migration of lithium at room temperature is measurable electrically in solar cells under reverse bias; this raised the possibility of calculating an effective lithium mobility in the cell. Such a parameter is very important as a basic material property indicating impurity/defect concentrations.

Questions concerning the nonuniformity of lithium doping on the behavior of damaged solar cells as well as the details of the production of defects (both those responsible for carrier and lifetime loss) in irradiated cells remained to be answered at the commencement of this project. In order to obtain more basic information on the production rates of defects which affected bulk conductivity (carrier removal) in lithium-doped silicon without the complication of a non-uniform distribution of lithium, the program included Hall-effect and transient-lifetime measurements on bars of silicon uniformly doped with lithium. The Hall measurements were carried out with equipment built and reported on in previous work (Ref. 5). The apparatus was designed for low-temperature measurements. It permits the viewing of the beam distribution over the area occupied by the sample, measurements of the electron beam current in a Faraday Cup, rapid insertion and extraction of the sample from the beam and interruption of the beam during measurements of the Hall constant in situ. In addition to the Hall-effect measurements, transient lifetime measurements were made on the Hall samples in the same apparatus. Modification of the apparatus was required to make the transient-lifetime measurements. This involved a new feedthrough to shorten the pulse-lead connections since the capacitance of long leads would destroy the pulse shape of the signal.

The Van de Graaff generator was converted to pulsed-beam operation by the addition of a mercury-switch pulser in the high-voltage terminal of the generator. This method of operation, first described by Wertheim (Ref. 6), involves biasing the cathode assembly to cut off the electron beam. The pulse generator provides a fast pulse which restores the cathode-to-ground potential for the duration of the pulse. This turns the electron-beam "on" for the same period of time. In the present arrangement, the pulser is capable of producing a repetition rate of ≈ 8 pulses per second with a pulse rise time of 2 to 4 nsec, a fall time of 10 to 20 nsec, and a width of 20 to 200 nsec. The various pulse characteristics were obtained by using lumped-delay lines with the required pulse characteristics. The experimental technique used here was to make a d-c Hall and conductivity measurement at a given temperature, then switch the Van de Graaff generator to pulse operation and determine lifetimes from the rate of decay of the conductivity of the Hall bar, induced by electron pulses. Minority carrier lifetime was measured in this way at several injection levels.

SECTION II

STABILITY OF TEST DIODES AND GFE CELLS BEFORE IRRADIATION

A. FABRICATION OF TEST DIODES

The test diodes fabricated for this contract effort were prepared, as in previous work (Ref. 7) by diffusing boron from a boron-nitride source into n-type silicon wafers (the concentrations selected were 1, 10, and 30 ohm-cm Lopex; 1, 10, and 30 ohm-cm float-zone; and 10 ohm-cm quartz crucible) at 950°C for 30 minutes. Lithium was then diffused into the diodes by immersing them in a 1% lithium, 99% tin bath at 400°C for over 120 hours.

Toward the end of the initial contract period (Ref. 7), attempts were made to improve test-diode diffusion length by including a gettering process between the boron-diffusion and lithium-diffusion stages. The purpose of the gettering process was to leach out fast-diffusing impurities, such as copper and gold which serve to increase carrier recombination. A slurry of P_2O_5 in ethoxy ethanol, painted on the back surface of boron-diffused Lopex and quartz-crucible samples and heated at 800°C for 16 hours gave significant increases in diffusion length (Ref. 7, Table XIII).

In the course of the present contract, a variant of this process using glass doped with a 15%-phosphorus concentration was chosen as the gettering agent. The latter process has the advantage of providing a stable encapsulation for the wafer during heating to 800°C. After depositing $\approx$5000 Å of the phosphorus-doped glass on the base side of the wafers at high temperature, the wafers were heated to 800°C for 16 hours in an inert atmosphere. They were then allowed to cool slowly to room temperature (several hours) and were subsequently diced into 0.2-in. squares. Several of the cells were then diffused with lithium, while a few control cells were not diffused. Throughout the gettering and lithium diffusion stages, the wafers had a coating of deposited undoped glass over the junction side to protect the boron-containing skin from attack by lithium. The lithium diffusion was accomplished through the back face.

Lithium concentrations near the junction in these cells were regularly measured. In previous reports, a two-voltage capacitance bridge measurement of lithium concentration was made, averaged, and termed: "Li_{jo}." In the present work, once the importance of the lithium gradient was recognized, a more advanced method of specifying lithium concentration, based on measurements at several voltages, was developed. However, for comparison with past work (Ref 7), values of lithium concentration adjacent to the junction (the same as Li_{jo},) but now termed N_{LO}, for consistency (see Section IV), are given here.

Test diodes fabricated under this contract are listed in Tables I and II. Lithium-diffused diodes are listed in Table I, diodes with no lithium, i.e., control diodes, in Table II. Starting resistivities of the phosphorus-doped n-type crystals, growth methods, and diffusion lengths (for three different dates) before irradiation are also given[2,3]. Diffusion length was obtained by the electron-voltaic method using a 1 MeV electron beam (Ref. 8). The diodes (or "cells," as they will be referred to hereafter) are identified by letter (e.g., crystal A is 10-ohm-cm Lopex) and number (cell A-3-2 is cell No. 2 from wafer No. 3 of crystal A). Either "C" or "CA" is added to identify a control cell.

TABLE I. DIFFUSION LENGTH STABILITY OF LITHIUM-DOPED TEST DIODES BEFORE IRRADIATION

LOPEX					FLOAT ZONE					QUARTZ CRUCIBLE		
Cell	Initial Resistivity ρ_o (Ω - cm)	Diffusion Length, L (microns) 11/67	1/68	3/68	Cell	Initial Resistivity ρ_o (Ω - cm)	Diffusion Length, L (microns) 11/67	1/68	3/68	Cell	Initial Resistivity ρ_o (Ω - cm)	Diffusion Length, L (microns) 3/68
A-3-1	10	118		105	D-1-1	1	94	85	73	G-1-1	12 to 16	40
A-3-2	↓			109	D-1-2	↓	71		49	G-1-2	↓	41
A-3-3				109	D-1-3				72	G-1-5		50
A-4-1		132		120	D-1-4				60	G-2-1		33
A-4-2				109	D-2-1		87	83	79	G-2-2		37
A-4-3				112	D-2-2		86		87	G-2-3		34
A-4-4				93	D-2-3				86	G-2-4		27
A-5-1		94		69	D-2-4	↓			99	G-2-5	↓	41
A-5-2				72	E-1-1	10	100	101	98			
A-5-3	↓			116	E-1-2	↓	94		86			
B-1-2	1			105	E-1-3				67			
B-2-1	↓			141	E-1-4				55			
B-2-2				125	E-2-1		129	135	122			
B-3-1				100	E-2-2		96		91			
B-3-2	↓			97	E-2-3	↓			83			
C-2-1	30		100	82	E-2-4				102			
C-2-2	↓		94	90	F-1-1	30	104	119	106			
C-2-3			95	91	F-1-2	↓	97	104	98			
C-2-4			97	91	F-1-3				75			
C-2-5			84	74	F-1-4				97			
C-3-2			76	81	F-2-1		79	87				
C-3-3			72	70	F-2-2		69	84	77			
C-3-4			83	73	F-2-3				32			
C-4-1			57	53	F-2-4	↓			68			
C-4-2			58	54								
C-4-3			64	57								
C-4-4			61	52								
C-4-5	↓		57	53								

[2] *Lithium-diffused diodes fabricated and irradiated in the early stages of the contract are listed in Table I. These, namely A-1-2, A-1-4, A-2-1, A-2-2, A-2-3, C-1-5, and C-1-7 will be discussed in the sections that follow.*

[3] *All test diodes and GFE cells are listed together with their original parameters in Appendix B.*

TABLE II. DIFFUSION LENGTH STABILITY OF CONTROL TEST DIODES BEFORE IRRADIATION

LOPEX				FLOAT ZONE				QUARTZ CRUCIBLE			
Cell	Initial Resistivity ρ_o (Ω - cm)	Diffusion Length, L (microns)		Cell	Initial Resistivity ρ_o (Ω - cm)	Diffusion Length, L (microns)		Cell	Initial Resistivity ρ_o (Ω - cm)	Diffusion Length, L (microns)	
		11/67	3/68			11/67	3/68			11/67	3/68
A-2-4C	10	47	44	D-1-6C	1	66	65*	G-1-6C	12 to 16		33
A-3-7CA	↓	45	44	D-1-7CA	↓	53		G-1-7C	↓		33
A-4-7CA		55		D-1-8CA		65	67*	G-2-6C		67	63
A-5-7CA	↓	29	35	D-2-6C		50	46*	G-2-7C	↓	53	50
B-1-7CA	1		23	D-2-7CA		53	72*				
B-2-7CA	↓		30	D-2-8CA	↓	46	56*				
C-2-6C	30	55	45*	E-1-6C	10	62	65*				
C-2-7C	↓	52	39*	E-1-7CA	↓	42	53*				
C-2-8C		39	29*	E-1-8CA		58	57				
C-3-6C			57	E-2-6C		29	32				
C-3-7C			53	E-2-7CA		33	31				
C-4-6C		32	30*	E-2-8CA	↓	33					
C-4-7C	↓	37	34*	F-1-6C	30	39					
				F-1-7CA		42					
				F-1-8CA		47					
				F-2-6C		32	37				
				F-2-7CA		32	36				
				F-2-8CA	↓	31	32				

*Indicates that the beam from the 1-MeV Van de Graaff generator was unstable when measurements were made.

Averaging the initial diffusion lengths in Tables I and II for all cells except those from G-crystal (quartz-crucible) it was found that the average diffusion length for 52 lithium-doped cells was 89 microns and the average for 31 control cells was 44 microns. It is evident from these values that the process used to incorporate lithium in the cell is somehow effective in increasing the minority-carrier lifetime in the cell.

Other than the presence of lithium, the only difference between the lithium and control cells is that the lithium cells have undergone a 400°C anneal during the lithium diffusion. It was considered possible that the 400°C temperature during lithium diffusion resulted in a lower equilibrium concentration of recombination defects. To check this possibility the control cells were made in two groups. One group incorporated a 400°C anneal for a duration of three days in an inert atmosphere, thereby duplicating the thermal conditions of the lithium diffusion. Control cells of this group are identified by the suffix "CA".

The other control group did not receive the 400°C anneal; cells in this group are identified by the suffix "C". Measurements showed that the average initial diffusion length for the 17 "CA" control cells fabricated in this work was 42 microns whereas the 18 "C" control cells averaged 46 microns. Clearly, the 400°C anneal did not cause an increase in diffusion length. It is therefore evident that the presence of lithium

in the lithium-diffused cells is responsible for the higher diffusion lengths of these cells. It is reasonable to expect that the lithium should form a complex with the defects present, which cause low diffusion length, the result being a defect of lower cross-section for recombination than the initial defects.

The efficacy of the phosphorous glass gettering process was tested by omitting this process in the fabrication of cells from wafer No. 4 of C crystal, i. e., C-4- cells. The average initial diffusion length for the five C-4- lithium cells was 59 microns; that of all other lithium cells from C crystal (eight in number) was 88 microns. For control cells from C crystal, the average initial diffusion length for two ungettered cells was 35 microns; for five gettered cells, 51 microns. This data, although the number of samples is relatively small, tends to confirm the efficacy of the gettering process previously observed.

B. STABILITY OF UNIRRADIATED TEST DIODES

Diffusion-length stability of the lithium-diffused cells before irradiation was tested by measurements at approximately two-month intervals, as shown in Table I. Control-cell measurements taken on two separate dates provide an index of the reproducibility of the diffusion-length measurement. In Table II all (23) repeated measurements are in agreement within ±10% except for four cases (C-2-7C, C-2-8C, D-2-7CA, and E-1-7CA) in which the second measurements were taken while the beam from the Van de Graaff generator was unstable. The reproducibility of diffusion length measurement to within ±10%, which has been verified in many other measurements, is assumed to be the error in the measurement. Referring back to Table I, 3 out of 15 lithium-doped cells measured, decreased in diffusion length over a four-month period, by an amount greater than 20%: these were A-5-1, 27% decrease; D-1-1, 22% decrease; and D-1-2, 31% decrease. The only other significant decrease was in A-3-1, 11%, which is still within the limits of error of the measurement. Of the 20 cells completed later and measured over a two-month period, none of the cells decreased beyond the limits of experimental error (20%) although five cells showed a decrease of greater than 10%. It is too early at this point to draw any conclusions from these tests which will be continued.

C. GFE CELLS

Solar cells fabricated by Heliotek (He) and Texas Instruments (TI) are being tested in this work. Table III contains a listing of most of these cells[4] also giving the starting resistivities of the n-type, phosphorus-doped base silicon and the crystal growth methods. Electron-voltaic-diffusion lengths and short-circuit-current densities, open-circuit voltages, and maximum power densities taken from photo-response characteristics are listed for two sets of measurements four months apart. A filtered tungsten light, adjusted to an incident power of 100 mW/cm^2 at the front surface of the cells, was used in the I-V (photo-response) measurements.

---

[4] *Eight TI cells irradiated in November, but not listed here, will be discussed in Section III, Paragraph B.3.*

TABLE III. PERFORMANCE STABILITY OF GFE CELLS BEFORE IRRADIATION

Cell	Initial Resistivity ρ_o (Ω - cm)	Growth Method	November 1967				March 1968			
			L (microns)	J_{sc} (mA/cm^2)	V_{oc} (volts)	P_{max} (mW/cm^2)	L (microns)	J_{sc} (mA/cm^2)	V_{oc} (volts)	P_{max} (mW/cm^2)
He651	20	Lopex	33	26.3	.535	9.8	34	27.2	.550	10.3
670			41	27.7	.545	10.8	42	28.6	.560	10.6
673			25	24.3	.522	8.8	26	25.0	.537	9.4
676			31	25.9	.519	9.1	33	26.6	.541	9.7
694			29	25.8	.525	9.4	29	26.8	.546	9.7
796		FZ	29	26.0	.525	9.5	29	26.9	.543	10.3
798			40	27.6	.518	10.4	42	28.6	.553	11.1
808			30	26.4	.532	9.6	31	27.2	.553	10.0
810			39	27.9	.532	9.6	37	28.9	.539	10.0
815			42	28.3	.535	11.0	38	29.1	.557	8.5
866			42	29.0	.532	10.8	40	30.2	.550	11.5
867			39	28.6	.523	10.7	40	29.9	.542	11.8
868			31	26.5	.527	9.9	30	28.0	.542	10.7
870			41	28.0	.525	10.5	40	29.6	.542	11.2
871			51	29.6	.540	11.2	54	31.6	.560	12.4
872							31	28.0	.535	10.6
873				29.0	.544	11.6	44	30.0	.552	11.4
875				28.1	.531	10.7	37	29.1	.540	10.9
876				27.6	.523	9.2	34	28.6	.535	11.0
878				28.3	.532	11.1	36	26.1	.547	11.2
879				30.1	.542	11.9	44	30.9	.551	12.3
881				29.6	.539	11.2	48	30.4	.552	10.1
882				29.6	.532	11.4	51	30.5	.547	11.9
884				30.2	.530	10.8	53	31.2	.547	11.3
885				28.9	.530	10.9	46	29.8	.539	11.3
886				29.1	.528	10.7	45	30.4	.550	11.5
887				30.6	.527	10.8	58	31.8	.537	11.4
890				26.4	.521	9.9	34	27.5	.542	10.7
He891				29.5	.535	11.3	51	30.8	.550	11.5
He892				28.9	.532	11.0	44	29.8	.550	11.4
TI976	200	Lopex	100	32.0	.568	12.1	108	33.8	.585	12.9
TI979	200	Lopex	122	32.4	.569	11.8	135	34.3	.571	11.0

The diffusion lengths remained remarkably constant over the four months from November 1967 to March 1968 as did nearly all of the I-V characteristics. The consistent $\approx$ 5% increase in the photo-response parameters from November to March is believed to be due to instrument settings and not to a significant physical change. Significant changes seen in only four cells: He 815 showed a decrease in power from 11.0 to 8.5 mW/cm^2; He 876 showed an increase from 9.2 to 11.0 mW/cm^2; He 881 showed a decrease from 11.2 to 10.1 mW/cm2; and He 878 showed a short-circuit current-density decrease from 28.3 to 26.1 mA/cm^2. All of these cells were stored at room temperature, in room light, and in an open circuit condition. Several of the cells were subsequently irradiated. A representative group will be retained for further pre-bombardment testing.

SECTION III
CELL STABILITY AFTER RECOVERY FROM IRRADIATION

A. TEST DIODES

The plan for irradiation of test diodes had the dual objective of studying annealing kinetics at varying impurity levels and fluences and also of allowing the detection of redegradation after irradiation by the lower electron fluences. Such redegradation has been seen to occur especially in Lopex-silicon lithium cells at fairly light damage levels, sometimes only a few days following irradiation. Thus, seven of the cells were irradiated by fairly small 1-Mev electron fluence levels and their diffusion lengths observed thereafter as a function of time.

Diffusion-length measurements were made during periods ranging up to 179 days on several test diodes fabricated in-house for this contract. All of these had high initial diffusion lengths (>90 microns) and thus exhibited enhanced sensitivity to damage under bombardment by low fluence levels. Cells were initially irradiated to low fluences (10^{12} to 10^{13} e/cm^2). Three cells of the group (A-1-2, A-2-2, and C-1-5) were subsequently irradiated to a fluence of 1.4×10^{15} e/cm^2. The diffusion lengths and radiation histories of four of these cells during a period of 179 days ($\sim$4300 hours) are shown in Figure 1. Cell A-1-4, which had been irradiated to cumulative fluences of 10^{13}, 2×10^{13}, 2.1×10^{13}, and 3.1×10^{13} e/cm^2 (administered on the 15th, 29th, 48th, and 50th days respectively) maintained a diffusion length within 22% of its initial value of 128 microns throughout this period, except for short annealing periods after irradiation (<1 day after 10^{13} e/cm^2 and $\approx$2 hrs after an increment of 10^{12} e/cm^2). Cell C-1-7, which was bombarded by an increment of 10^{12} e/cm^2 on the 48th day and of 10^{13} e/cm^2 on the 50th day, maintained a constant length ($\approx$90 microns) since the eighth day, although a decrease from 120 to 90 microns occurred during the eight days between the first two measurements. Over a period of 129 days following the last irradiation the diffusion length of each cell remained constant to within 10% of its value.

Cell A-1-2 and C-1-5 also showed good stability with high diffusion length prior to irradiation (48 days) and also for 12 days after irradiation to a fluence of 1.1×10^{13} e/cm^2. These two cells were then irradiated to a fluence of 1.6×10^{15} e/cm^2. The diffusion lengths subsequently recovered from five to about 30 microns ($\sim$98% of damage sites annealed in terms of Eq. (1) given in Section IV.A.) over a period of $\sim$10 days. For a period of 109 days following recovery, each cell maintained the 30-micron diffusion length to within 10%.

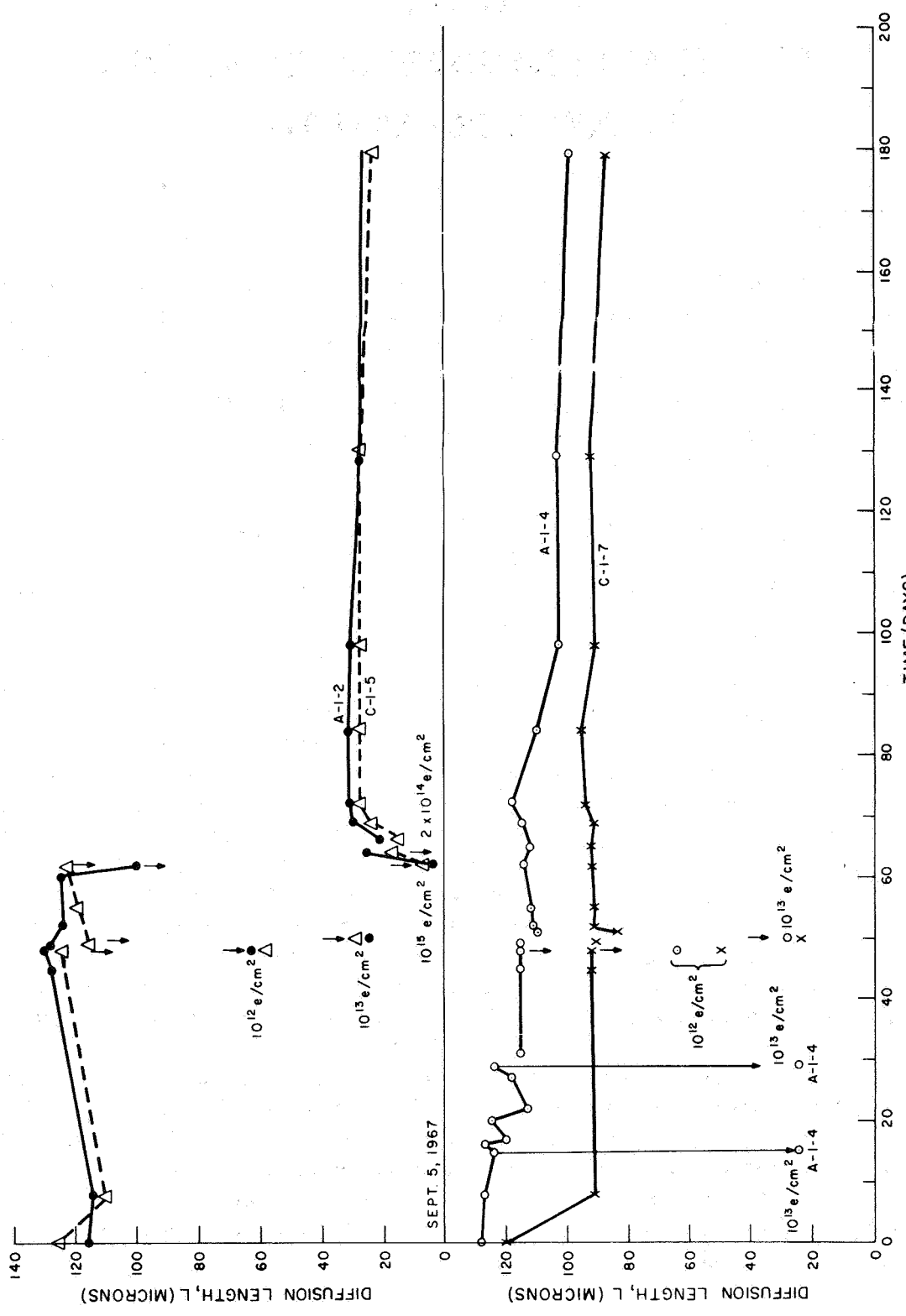

Figure 1. Diffusion Lengths and Radiation Histories of Four Cells

Diffusion-length plots vs. time for cells A-2-1, A-2-2, and A-2-3 (which were lithium diffused at a later date than those shown in Figure 2 are given in Figure 2. These cells are characterized by very low lithium concentrations ($\sim 10^{14}$ cm^{-3} near the junction). Each of these cells was irradiated to a fluence of 10^{12} e/cm^2 on the third day of the test. Annealing was slow; approximately four days of annealing at room temperature were required to achieve the pre-irradiation diffusion lengths. Subsequently, each of the cells continued to show an increase in diffusion length above the initial value. On the 17th day, cell A-2-2 was irradiated to 1.2×10^{15} e/cm^2. After this irradiation, very little annealing took place. The diffusion length remained constant at approximately four microns over a period of 117 days. It will be shown in Section IV that this behavior is due to the fact that after bombardment no free lithium remained near the junction. This absence of free lithium is also confirmed by the injection-level measurements on the cell, which are discussed in Section VI. Cells A-2-1 and A-2-3 which received no further irradiation since the third day of the test have remained constant within 10% for 100 days, both having diffusion lengths greater than 100 microns through this period.

In summary, seven test diodes were tested for diffusion-length stability for periods greater than 100 days, after irradiation to fluences of $\sim 10^{13}$ e/cm^2 or $\sim 10^{15}$ e/cm^2. All of these diodes were fabricated from Lopex silicon. All seven diodes showed both complete diffusion-length recovery and stability of recovered diffusion length after fluences of 10^{12} and 10^{13} e/cm^2 for the duration of the tests; i.e., A-1-2, A-2-2, and C-1-5: 12 to 14 days; A-1-4, A-2-1, A-2-3, and C-1-7: over 100 days ($\sim$2500 hrs.) to date. One of the diodes (A-2-2) was found to be completely depleted of lithium in the junction region after $\sim 10^{15}$ e/cm^2. As expected, this diode showed no subsequent diffusion-length recovery. The two diodes not completely depleted of lithium by $\sim 10^{15}$ e/cm^2 fluence (A-1-2 and C-1-5), showed substantial diffusion-length recovery (from 5 to 30 microns) and stability of recovered diffusion length for over 100 days. Any decreases in recovered diffusion length during this time were within the $\pm 10\%$ experimental error.

B. GFE CELLS

1. Cells Irradiated in December 1966 to 10^{14} e/cm^2

Four cells furnished during the initial contract period and irradiated on Dec. 16, 1966 to a fluence of 10^{14} e/cm^2 were given photo-response and diffusion-length tests periodically after recovery. Cell He 55-1 was fabricated by Heliotek (Ref. 9). The other three cells were fabricated by Hoffman (Ref. 10). The results of the tests are shown in Table IV. It may be seen that He 55-1 had significantly higher initial values than the other cells and that all cells showed practically complete recovery in photo-response. Only in the case of diffusion length were the values soon after recovery consistently lower than the initial values. The photo-response parameters after recovery remained constant within 10% from December 1966 through June 1967.

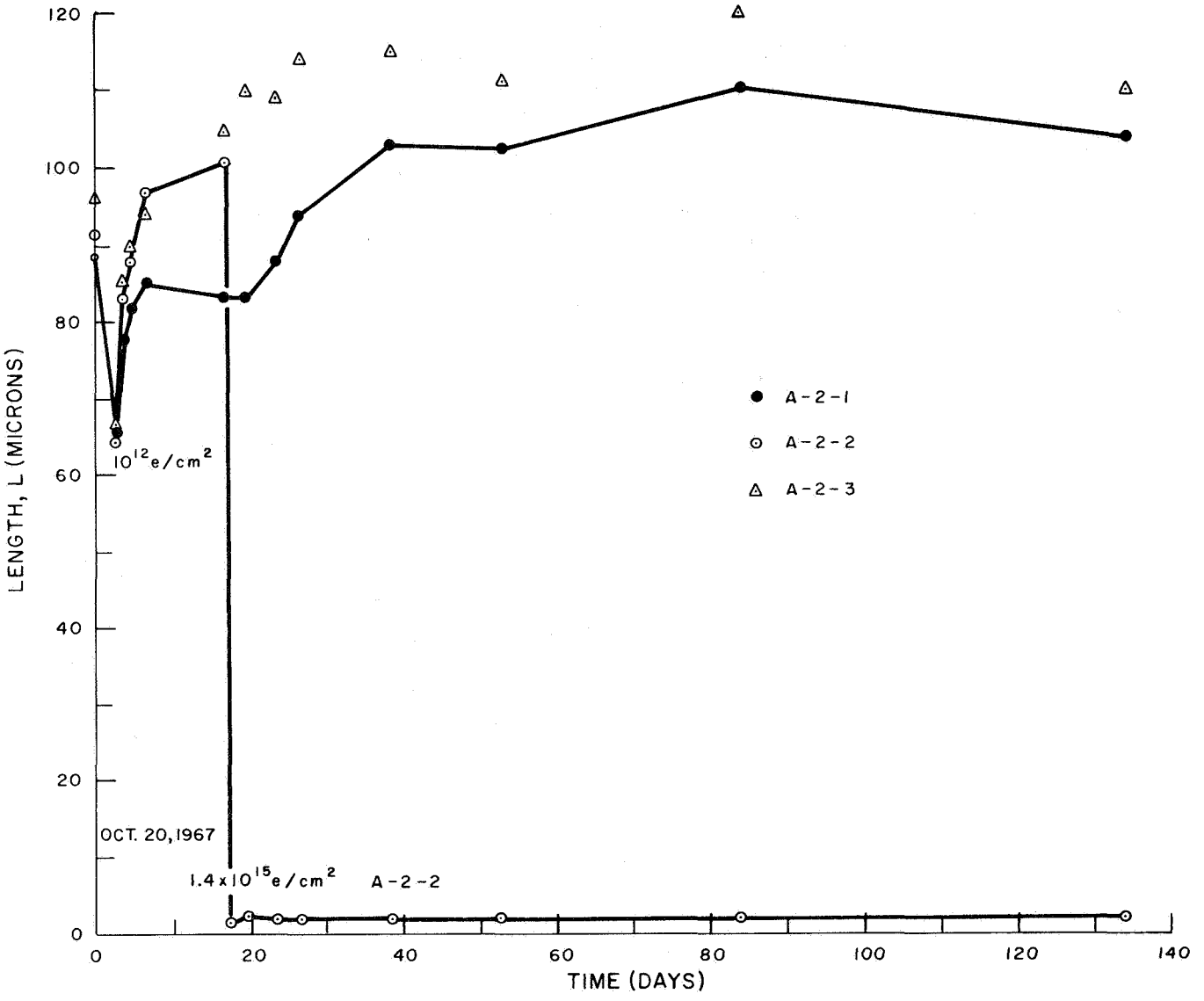

Figure 2. Diffusion Length as Function of Time for Three Cells

The error in the photo-response readings is estimated at ±5% based on reproducibility of readings on many stable cells. Severe redegradation (~50%) in power in cell He 55-1 was observed in the November, 1967 readings. This redegradation, which occurred between 6 and 11 months after recovery, was accompanied by only slight decreases in short-circuit current and open-circuit voltage, and no decrease in diffusion length. A decrease in filling factor, $P_{max}/J_{sc}V_{oc}$, was responsible for the power drop, indicating that a contact problem was responsible. The Hoffman cells have remained stable at the post-recovery values for over 14 months, with a slight upward trend evident in Ho 5-1 and Ho 6-1. It is noted that capacitance measurements (Ref. 11 and Appendix C of this report) made before irradiation showed that the lithium

TABLE IV. POST-IRRADIATION STABILITY OF PERFORMANCE PARAMETERS FOR GFE CELLS IRRADIATED DECEMBER 1966

Cell	ρ_o and Growth Method	Initial Performance: 12/66				Fluence 12/16/66	After Recovery						
							December 1966			January-February 1968			
		L (microns)	J_{sc} (mA/cm^2)	V_{oc} (volts)	P_{max} (mW/cm^2)	ϕ	J_{sc}	V_{oc}	P_{max}	L	J_{sc}	V_{oc}	P_{max}
HE55-1	20 FZ	51	29.2	.553	9.2	10^{14}	26.4	.540	9.0	34	26.5	.540	8.3
HO33-2	10 FZ	26	24.4	.500	6.6	10^{14}	23.1	.488	6.2	23	24.6	.490	6.3
HO5-1	100 FZ	33	24.7	.500	7.7	10^{14}	25.0	.492	8.0	29	24.7	.490	7.6
HO6-1	1000 FZ	39	23.3	.514	6.4	10^{14}	23.3	.506	8.0	35	23.1	.510	7.5

Cell	After Recovery (Cont'd)									
	June 1967			November 1967				March 1968		
	J_{sc}	V_{oc}	P_{max}	L	J_{sc}	V_{oc}	P_{max}	J_{sc}	V_{oc}	P_{max}
HE55-1	25.0	.540	8.3	33	24.9	.513	4.4	26.2	.535	4.9
HO33-2	22.8	.500	6.6	25	23.4	.480	6.2	25.0	.500	6.9
HO5-1	25.0	.495	7.7	34	24.0	.485	8.0	26.6	.497	8.5
HO6-1	24.5	.520	8.4	26	24.9	.500	8.6	26.2	.518	9.1

density, N_{LO}, at a distance $\sim 1\ \mu$ from the junction was: He 55-1, 1.7×10^{15} cm^{-3}; Ho 33-2, 1.5×10^{14} cm^{-3}; Ho 5-1, 2.4×10^{14} cm^{-3}; Ho 6-1, 4.3×10^{14} cm^{-3}. Thus, the cells with good long-term stability were very lightly doped with lithium.

2. Cells Irradiated in February/March 1967 to 10^{16} e/cm^2

This study of long-term stability was initiated during the initial contract period. During February and March, 1967, a large group of government-furnished cells were irradiated to 10^{16} e/cm^2 at a flux rate of approximately 3×10^{15} e/cm^2/hr. Periodic measurements of diffusion lengths and photo-response characteristics have been made. Table V lists values of J_{sc} and P_{max} obtained from these measurements. Readings made before bombardment, then approximately one hour, four days, three months, eight months, and one year after bombardment are included. Pre-irradiation values of lithium concentration, N_{LO}, (lithium ions/cm^3) near the junction, taken from capacitance-bridge measurements (Ref. 11 and Appendix C of this report) are also included. The cells, which were manufactured by Heliotek (He) and Texas Instruments (TI), are listed in order of increasing N_{LO}. Cells whose identifying number is followed by L are made from Lopex silicon, and those followed by Q are quartz-crucible grown; all others are float-zone refined silicon. Figure 3 shows curves of P_{max} vs N_{LO} before irradiation (initial), 4 days after bombardment, ~3 months after bombardment (June, 1967), and ~1 year after bombardment (Feb., 1968). He 248P and He 249P represent a special group of cells with a diffused, highly doped phosphorous

TABLE V. RESULTS OF LONG-TERM STABILITY STUDY OF GFE CELLS
(ϕ = 10^{16} e/cm^2 in February/March 1967)

Cell		Initial Performance				Post-Irradiation Performance									
		December 1966				1/Hour		4 Days		June 1967		November 1967		February 1968	
		ρ_o (Ω-cm)	N_{Lo} (10^{-15} cm^3)	J_{sc} (mA/cm^2)	P_{max} (mW/cm^2)	J_{sc} (mA/cm^2)	P_{max} (mW/cm^2)	J_{sc} (mA/cm^2)	P_{max} (mW/cm^2)	J_{sc} (mA/cm^2)	P_{max} (mW/cm^2)	J_{sc} (mA/cm^2)	P_{max} (mW/cm^2)	J_{sc} (mA/cm^2)	P_{max} (mW/cm^2)
Group 1	TI167*	20	.75	30.8	10.8	10.8	2.3	10.9	2.2	12.9	3.0	14.5	2.9	15.4	3.2
	HE342	100	1.2	29.6	--	--	--	--	--	18.3	--	19.6	3.3	21.5	4.1
	TI63	20	1.5	29.6	10.4	9.5	2.0	11.2	2.1	15.7	3.4	17.6	3.9	19.3	4.5
	TI171	20	1.7	28.5	6.3	9.4	1.6	11.6	1.8	16.2	2.8	18.7	3.7	20.6	4.3
	HE341*	100	1.7	28.5	--	--	--	--	--	21.0	--	20.4	2.6	22.0	3.3
Group 2	TI112Q	20	2.0	28.0	10.5	9.5	2.5	10.2	2.7	17.4	4.0	19.7	4.9	20.6	5.6
	TI113Q	20	2.0	27.5	9.9	9.2	2.5	9.8	2.7	16.8	--	19.0	5.2	20.2	5.8
	TI168	20	2.0	28.8	11.1	9.9	2.5	13.5	3.3	16.7	4.0	17.6	4.4	18.6	4.8
	HE340	100	2.2	28.6	--	--	--	--	--	21.2	--	21.2	2.9	22.9	3.8
	TI42	20	2.2	28.6	9.2	8.3	2.0	12.2	3.0	15.1	3.9	16.3	4.2	17.2	4.6
	TI161	20	5.0	27.2	10.8	8.9	2.6	17.1	5.1	17.4	5.3	17.4	5.5	18.2	5.8
Group 3	TI128L	20	7.0	28.5	10.8	9.1	2.5	16.7	5.0	16.0	4.9	15.7	3.4	16.2	3.6
	TI127L	20	8.2	30.2	10.2	9.4	2.6	17.8	5.2	16.9	4.9	15.3	3.0	13.8	2.7
	TI132L*	20	9.2	29.8	--	10.7	1.5	16.2	4.8	15.2	4.1	15.8	4.0	16.2	4.1
	TI166	20	.10	25.2	8.7	9.6	2.5	15.8	4.5	14.8	4.2	15.1	4.1	15.5	4.1
	HE248P	1000	--	24.8	8.4	16.6	3.8	22.3	6.1	22.5	5.0	22.2	6.3	23.5	7.0
	HE249P	1000	--	24.2	8.4	14.2	3.5	20.6	5.7	23.7	6.3	22.2	6.9	22.8	7.4

*Irradiated to incremental flux of 10^{15} e cm^2 after November 1967 readings.

region near the junction. These last two cells will be discussed separately. The rest of the cells will be discussed in three Groups: Group 1, low ($N_{LO} < 2 \times 10^{15}$ cm^{-3}); Group 2, intermediate ($2 \times 10^{15} \leq N_{LO} \leq 5 \times 10^{15}$ cm^{-3}); and Group 3, high ($N_{LO} \geq 7 \times 10^{15}$ cm^{-3}) lithium concentrations in the junction region.

Cells belonging to Group 1 recovered in J_{sc} and P_{max}, slowly, but steadily since bombardment. The low lithium density is probably responsible for the slow recovery. At the end of the contract period all of the cells in this group had values of P_{max} greater than 4 mW/cm^2 and presumably will continue to increase towards the $\sim$5.2 mW/cm^2 reported for a 10 Ω-cm n/p cell (Ref. 12) after 10^{16} e/cm^2 bombardment. Cell TI 167, however, has shown no significant recovery since June ($\sim$3 mW/cm^2) and it must be assumed that this cell, which had the lowest initial lithium concentration of all the cells in this test, has exhausted its free lithium supply near the junction and consequently will recover no further. Cells He 341 and He 342 (and also He 340 of Group 2) display interesting features. These three cells, which were made from high resistivity (100 Ω-cm) starting material, showed good recovery of minority-carrier lifetime as seen from diffusion-length measurements and J_{sc} measurements. In November He 341 had the highest diffusion length (21 microns) of the cells in Group 1, and He 340 the highest in Group 2 (18 microns). From Table V it is seen that these three cells also have the highest values of J_{sc} of all the cells in Groups 1 and 2. In spite of this, they have three of the lowest values of P_{max} of the cells in Groups 1 and 2; the only P_{max} reading below these being that for TI 167, a cell with presumably no free lithium remaining. The reason for this low power is the very low filling factor, $P_{max}/J_{sc}V_{oc} \sim 0.4$, found in the photo-response curves of these cells. This low filling factor is attributed to the high resistivity starting material, which, together with the high bombardment fluence, results in a low post-irradiation impurity concentration. This could lead to series resistance problems either at the base contact or in parts of the body of the cell where lithium was heavily depleted. The other cells of Groups 1 and 2 (with 20 Ω-cm starting material) had significantly higher filling factors, suggesting that series resistance problems can be adequately dealt with by judicious choice of initial silicon resistivity. This observation goes far in answering some objections to the lithium cell (Ref. 13).

Group 2 cells with "intermediate" 2 to 5 x 10^{15} cm^{-3}) lithium concentrations near the junction differ from Group 1 cells in their post-irradiation behavior only in degree. They show consistent and continuing recovery just as do Group 1 cells, however, due to the higher lithium density, the recovery has been more rapid and these cells (excepting He 340 discussed above) now display values of P_{max} comparable to that obtained for 10 Ω-cm n/p cells (Ref. 12) irradiated to 10^{16} e/cm^2, as shown in Figure 3. In fact the cell of this group (TI 166) with highest initial lithium concentration (5 x 10^{15} cm^{-3} near the junction) had recovered to a power of greater than 5 mW/cm^2 as early as June 1967. This is significant in that the radiation dose of 10^{16} e/cm^2 of 1 Mev electrons is the equivalent of several year's dose in a particularly high-radiation earth orbit. It is particularly interesting to compare the time behavior of the two quartz-crucible cells of this group (TI 112Q and TI 113Q) with that of the

float-zone cells (TI 42, TI 161 and TI 168). This comparison is made in Figure 4 which is a graphic representation of the P_{max} values in Table V. The solid and dotted lines represent the average values for quartz-crucible and float-zone cells respectively. The slow but steady increase in quartz-crucible cell performance stands out in contrast to the rapid initial increase followed by a very slow long-term increase in float-zone cells. As of the last measurements the quartz-crucible cells are significantly (> 5%) ahead of the float-zone cells in power output. The contrasting initial behavior has been reported (Refs. 4 and 14) and explained (Ref. 14) previously in terms of formation of LiO^+ complexes which lower the effective lithium diffusion constant in oxygen-rich quartz-crucible cells. The observed long-term behavior of the quartz-crucible cells also agrees with this observation. The even slower long-term recovery in float-zone cells could be explained in two different ways. First the rapid initial flow of lithium to defects could cause local depletion of lithium near the junction, leaving some recombination centers after the initial fast recovery unsatisfied in their demand for lithium. Lithium would have to diffuse across large distances to satisfy these centers. A second, and more likely, explanation is that over the long-term, recovery has to compete with redegradation, i.e., recovery and redegradation mechanisms may be occurring simultaneously. Post-recovery redegradation of preformance in lithium-doped cells has been observed here (Group 3 cells) and elsewhere (Ref. 4), and its cause although not well understood has been suggested to be the precipitation of lithium from the supersaturated solution that exists in the lithium doped p/n silicon cell. (The solubility of lithium at room temperature in n-type silicon is $\sim 10^{13}$ cm^{-3}.) In any case, if redegradation mechanisms are active in the float-zone cells represented in Figure 4, they have been more than compensated by recovery mechanisms. No significant drop in filling factor has occurred in these cells.

All four of the Group 3 cells showed significant redegradation between the 4th day after bombardment (March 10, 1967) and the 240th day (November 1967). In cell TI 127L this redegradation continued between the 240th and the 360th day to the extent that the value of P_{max} on the 260th day approximated that obtained one hour after bombardment. The other Group 3 cells have remained constant within experimental error since the 240th day. It should be noted that three of the four cells in Group 3 were Lopex cells and that the cell suffering the least severe degradation was TI 166, the float-zone cell. The sampling, however, is too small, and the variables too numerous to state whether the degradation is due to the crystal growth method, especially since the three Lopex cells are those with the highest-lithium concentrations of the Group.

Cells He 248P and 249P, with a highly doped-phosphorous region near the junction have displayed particularly good behavior after irradiation. Though preirradiation power values (8.4 mW/cm^2 in each cell) were low, the resistance of the cells to irradiation was high, as seen from the values 1 hour after bombardment. Recovery then continued steadily with time. As of the latest reading, approximately one year after bombardment, the cells had values of 7.0 and 7.4 mW/cm^2 for P_{max} i.e., $\sim 40\%$ above the value for a 10 Ω-cm n/p cell after 10^{16} e/cm^2 and the highest value exhibited in this series.

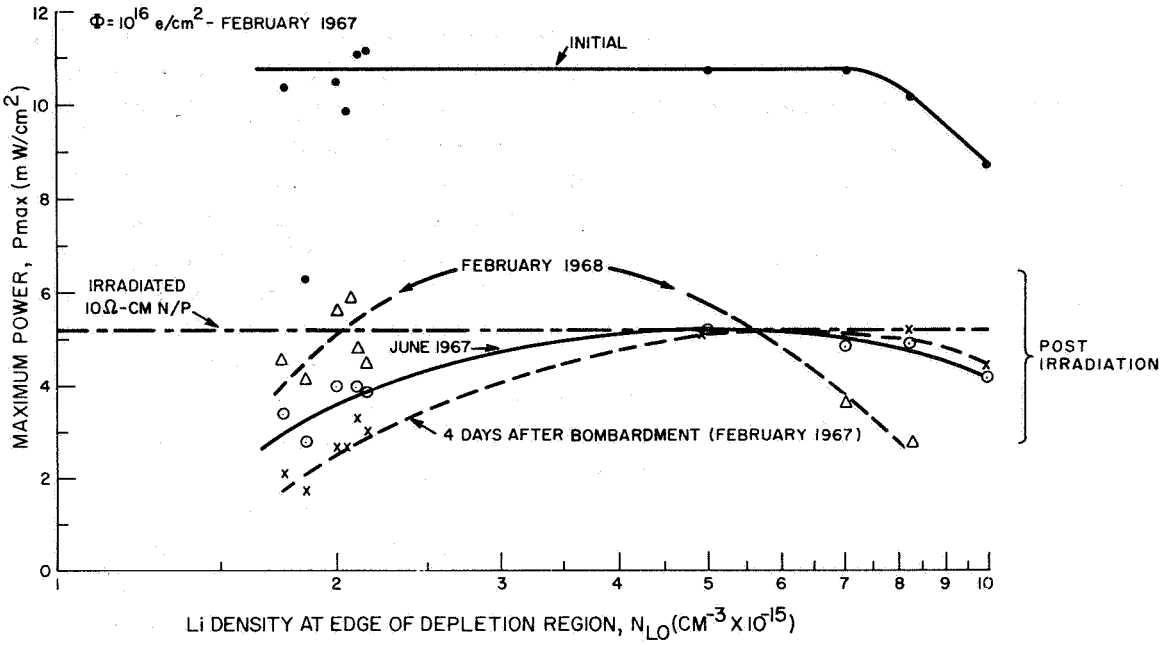

Figure 3. Maximum Power as a Function of Lithium Concentration, Before and After Irradiation

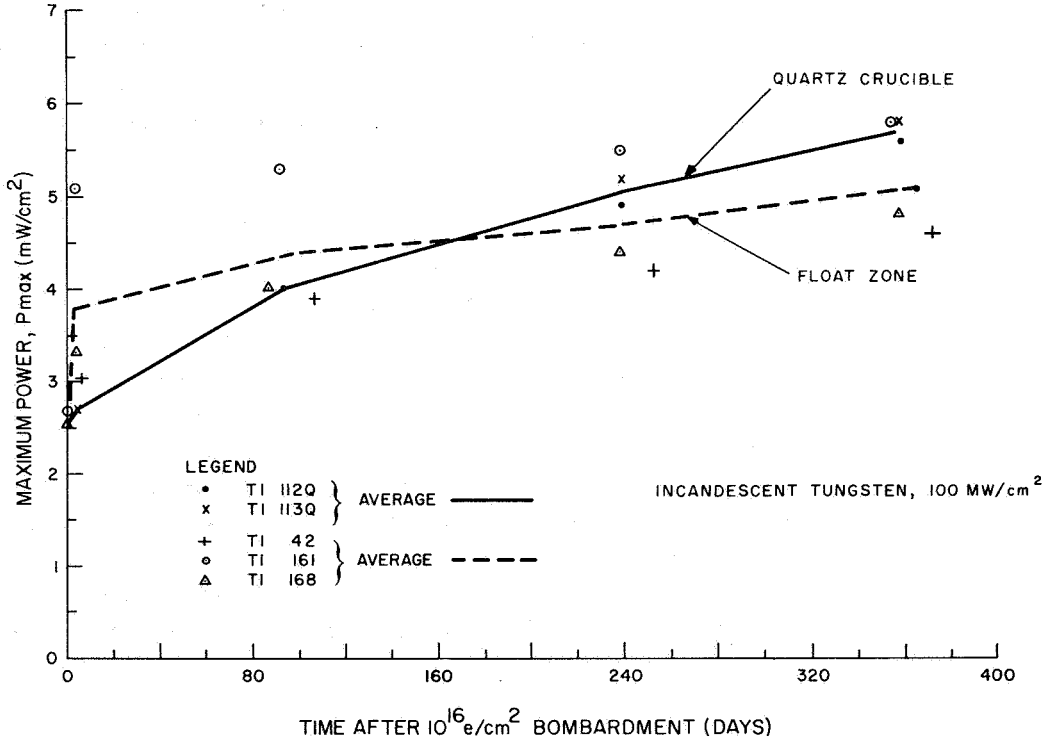

Figure 4. Comparison of the Time Behavior of Two Quartz Crucible and Three Float-Zone Cells

3. GFE Cells Irradiated in November 1967 to 10^{14} or 10^{15} e/cm^2

Eight GFE (TI) cells received during the final contract period were irradiated in November 1967. These cells were all characterized by high initial diffusion length ($\gtrsim$ 96 microns) and good photo-response characteristics ($P_{max} \gtrsim 12$ mW/cm^2). Four of the cells (TI 948, 949, 950, and 951) were irradiated to $\sim 1.6 \times 10^{15}$ e/cm^2) fluence during an injection-level experiment, as described later in Section VI. The other four cells (TI 952, 977, 978, and 981) were irradiated to 10^{13} e/cm^2, monitored during recovery as described in Section IV, irradiated in 10^{14} e/cm^2, and monitored again during recovery. Subsequent diffusion length and photo-response characteristics were taken at $\sim$ 1 month intervals. Stability results from the cells irradiated to $\sim 10^{15}$ e/cm^2 are given in Figure 5. The values which are given are the averaged values of the four cells. All cells were made from 20 Ω-cm float-zone silicon and all displayed similar behavior. The "error bars" in Figure 5 indicate the range of values obtained for the four cells rather than the experimental error of the measurement. Where no bar is shown, all values were essentially equal. The results show that the post recovery values of all cell parameters remained substantially constant for a period of 120 days; no redegradation occurred. Table VI lists results of stability measurements on the four TI cells irradiated to 10^{14} e/cm^2 and monitored for recovery characteristics. The 20 Ω-cm float-zone cell, TI 952 has remained stable since recovery. Measurements on cell TI 981, which is 200 Ω-cm Lopex, showed a minor decrease in diffusion length, the decrease still being within worst-case experimental errors, but with good photo-response stability. The other two cells, TI 977 and 978, both 200 Ω-cm Lopex, showed similar minor decreases in diffusion length. In addition, a larger redegradation in power was evident, which, in the case of TI 978 (19%) was outside the error of the measurement. This power degradation occurred between the 65th and 113th day after bombardment.

4. Summary of Post-Recovery Tests on GFE Cells

A total of 29 cells have undergone long-term (>100 days to > 14 months) post bombardment stability tests. Six of these cells showed significant redegradation; the remainder remained stable, with the possible exception of two cells (TI 977 and 981) which showed some trend toward degradation after $\sim$100 days. Of the 19 float-zone cells tested only two showed significant power degradation. Conversely, four of six Lopex cells have degraded significantly, one back to its post-bombardment value. However, it is not certain that the silicon growth technique is the important factor, since in three cases the cells were also of very high lithium content and very heavily irradiated. The four other cells tested (two of quartz crucible silicon and, two containing a phosphorous barrier layer) are still increasing (recovering) in power output $\sim$ 1 year after bombardment.

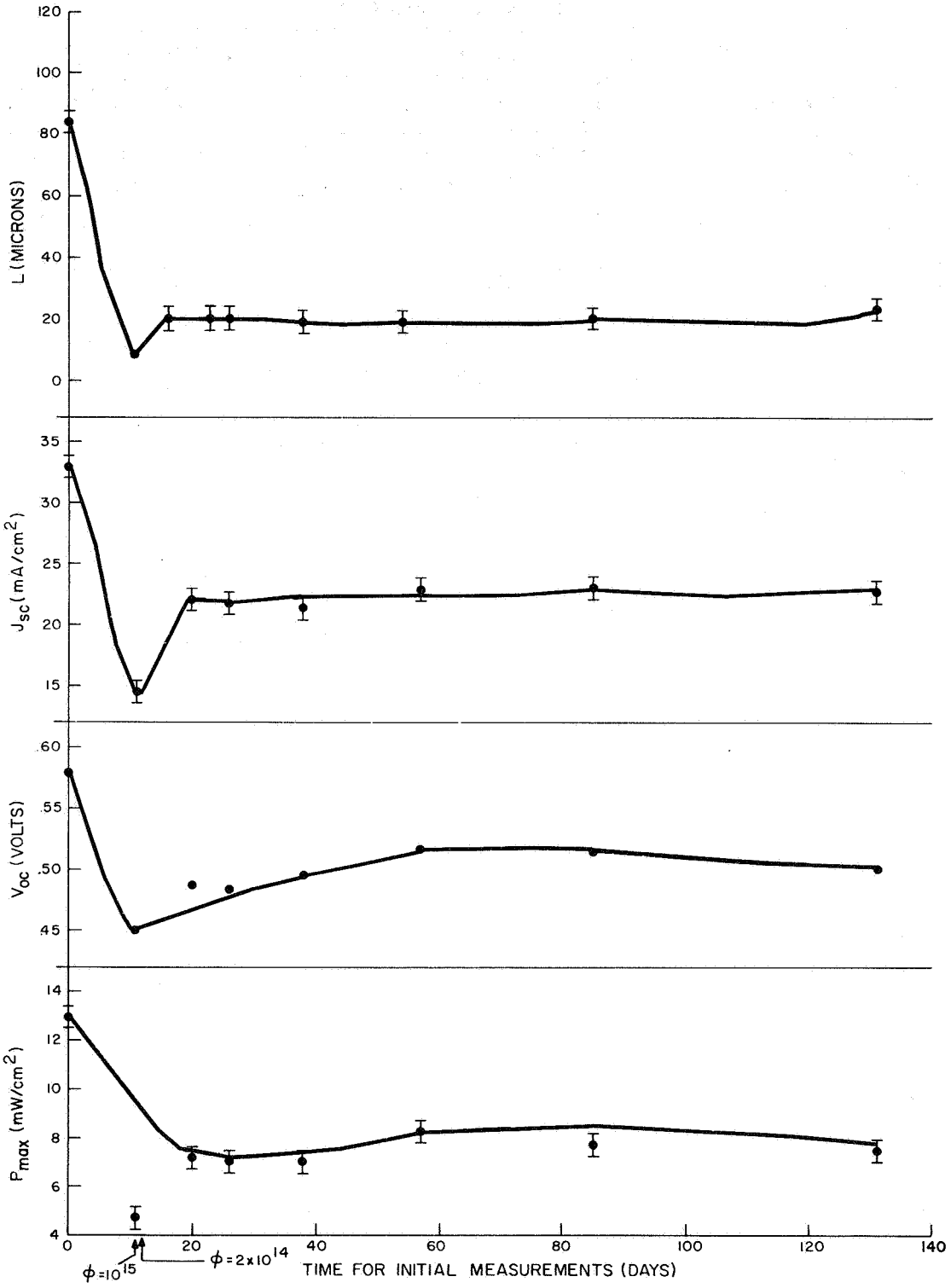

Figure 5. Stability Results from Cells Irradiated to 10^{15} e-cm^2

TABLE VI. POST-IRRADIATION STABILITY OF PERFORMANCE PARAMETERS FOR GFE CELLS IRRADIATED NOVEMBER 1967

Cell	ρ_o (Ω-cm) and Growth Method	Initial Performance: 10/67				Fluence 11/8/67	L_1	After Recovery							
								November 11, 1967				November 16, 1967			
		L (microns)	J_{SC} (mA/cm^2)	V_{OC} (volts)	P_{max} (mW/cm^2)	ø	(microns)	L_2	J_{sc}	V_{oc}	P_{max}	L_2	J_{sc}	V_{oc}	P_{max}
TI952	20 FZ	91	33.0	.564	12.6	10^{14}	14	62	28.5	.550	10.4	62	28.2	.548	10.3
TI977	200 Lopex	100	34.3	.554	12.0	10^{14}	16	66	29.1	.540	9.9	65	28.4	.539	9.5
TI978	200 Lopex	100	34.5	.574	13.4	10^{14}	16	67	29.3	.545	10.4	67	28.8	.549	10.0
TI981	200 Lopex	121	35.5	.562	12.4	10^{14}	15	76	30.2	.540	10.2	73	29.5	.541	10.0

After Recovery (Cont'd.)

Cell	December 1967				January 1968				March 1, 1968			
	L_2	J_{sc}	V_{oc}	P_{max}	L_2	J_{sc}	V_{oc}	P_{max}	L_2	J_{sc}	V_{oc}	P_{max}
TI952	56	30.0	.578	11.1	59	29.3	.570	10.9	59	28.9	.554	10.2
TI977	57	30.2	.570	10.4	56	29.3	.558	10.9	56	28.6	.539	8.9
TI978	60	30.6	.568	10.3	58	27.2	.558	10.0	58	29.2	.533	8.5
TI981	63	31.5	.568	10.5	65	30.8	.564	10.9	66	30.2	.551	10.3

*Immediately after bombardment.

SECTION IV
RECOVERY CHARACTERISTICS

A. ANALYSIS OF DATA

A theoretical treatment of diffusion-length recovery as a function of time after irradiation was given previously. (Ref. 7) The analysis was based on a diffusion-limited-kinetic model (Ref. 15) where unequal concentrations of the annealing species are present. The annealing species were assumed to consist of essentially immobile lithium-vacancy (Li-V) damage sites carrying a single negative charge, and mobile lithium ions Li^+. The $(Li\text{-}V)^-$, being negatively charged, would have a large capture cross section for minority carriers (i.e., holes) in the n-type base region. As Li^+ diffused to and combined with $(Li\text{-}V)^-$, a complex Li_2V with zero charge and therefore low-capture cross-section, would be formed. The proposed recovery process thus involves the formation of a Li_2V complex.

Although present data, given in Paragraph D of this section, indicates that the phosphorus-vacancy E-center, $(P\text{-}V)^-$, might be more prevalent than $(Li\text{-}V)^-$, the recovery kinetics would be the same in either case, a P-V-Li complex being formed by combination of lithium with the-E-center. The appropriate equations are developed in Appendix D. For the circumstances of the present recovery experiments, namely, for low fluences, where the defect density immediately after irradiation is much lower than the lithium density, the appropriate recovery equation after ~ 2 minute transient is

$$f_r^{-1} = \exp 4\pi N_L D_L r_o t \qquad (1)$$

where

f_r is the fraction of damage remaining

N_L is lithium concentration

D_L is diffusion constant of lithium

r_o is defect capture radius

t is time

Equation (1) is related to the basic diffusion-length data through

$$f_r^{-1} = \frac{\left(\frac{1}{L_1^2}\right) - \left(\frac{1}{L_o^2}\right)}{\left(\frac{1}{L_2^2}\right) - \left(\frac{1}{L_o^2}\right)} \qquad (2)$$

where

L_1 is diffusion length immediately after bombardment

L_2 is diffusion length, at a time t, after bombardment has ceased

It can be seen from Eq. (1) and (2) that the pertinent physical parameters in the recovery process are D_L, r_o, and N_L. Eq. (2) contains the product $4\pi r_o D_L N_L$. Therefore, a thorough test of the proposed model requires independent measurements of the individual parameters. Much of the work in the present reporting period has been directed toward the measurement of N_L and D_L through use of capacitance techniques.

B. MEASUREMENT OF LITHIUM DENSITY, N_L

The capacitance method of obtaining lithium donor concentration as a function of distance from the junction is outlined in Appendix C. The technique of measurement is as follows: doping densities are obtained by applying a reverse bias to the p-n junction and measuring the capacitance of the junction as a function of voltage. As the reverse bias is increased the width of the depletion region (i. e. , field region) increases, sweeping through a small portion of the base region near the junction. By measuring increments of voltage and capacitance, the overall doping concentration, N_D, vs. distance from the junction, w, can be obtained. Lithium concentration, N_L, is then obtained by subtraction of the phosphorus doping from N_D.

Figure 6 illustrates the results obtained from capacitance measurements with donor concentration profiles of cell A-2-2 taken on three different days together with the profile of a control cell, A-2-4C, from the same crystal and wafer. Since A-2-4C has no lithium and therefore no mobile donors, its donor density must remain constant provided the cell is not heavily irradiated, which was the situation for this control cell. The donor density of A-2-4C was measured on six different occasions during the present contract to check the reproducibility of the capacitance data. Each of these independent measurements yielded the same concentration profile shown in Figure 6 with a ±10% spread in the data. The lithium density, N_L, at any point, w, in A-2-2 is obtained from Figure 6 by subtracting the phosphorus doping density obtained from measurement of A-2-4C, namely 4×10^{14} cm^{-3}, from the total doping density N_D. Cell A-2-2 is one of the very lightly lithium-doped cells discussed in Section IIIA. The doping densities measured Oct. 19 and Nov. 2, before the $\sim 10^{15}$ e/cm^2 bombardment, show substantially

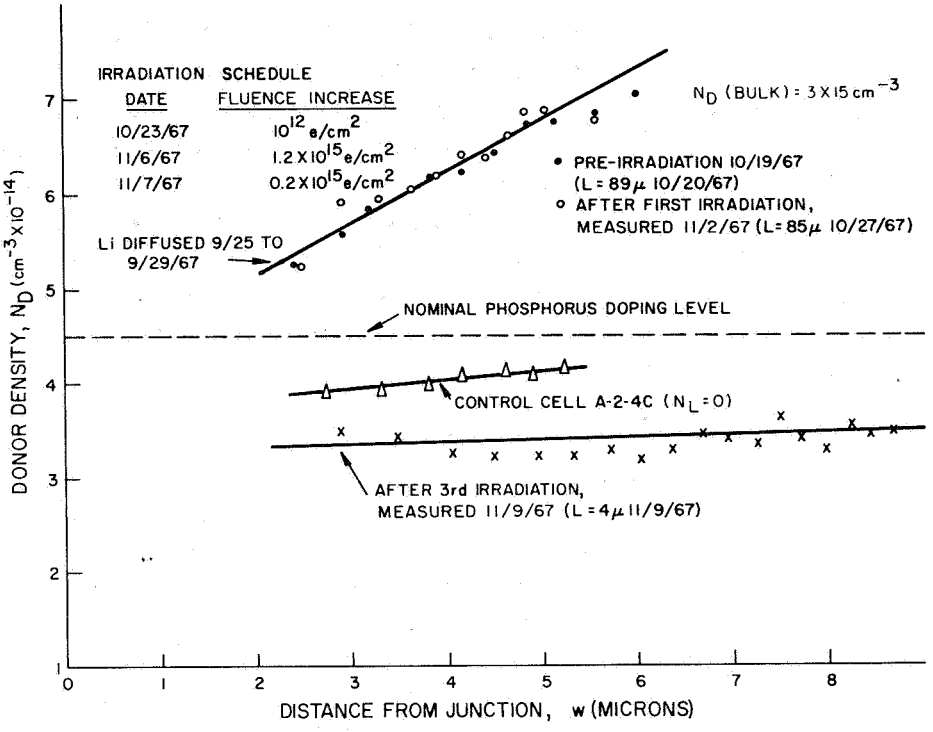

Figure 6. Donor Concentration Profiles of Cell A-2-2 Compared with Profile of Control Cell A-2-4C

equal concentration profiles. The low doping level in this cell allowed the depletion region to sweep out further for a given voltage than for more heavily doped cells. In this cell it was possible to probe over a range of $\sim$6 microns. In many heavily doped cells this range was reduced to $\leq$ 2 microns. The Nov. 9 profile, taken after bombardment at $\sim 10^{15}$ e/cm^2, shows a concentration profile considerably below the phosphorus doping level of the control cell out to beyond 8 microns from the p/n junction. The diffusion length at the time this measurement was made was 4 microns. The apparent absence (as seen from the concentration profile) of lithium donors from the region of current collection and the subsequent absence of recovery as seen from the constancy of diffusion length over 114 days subtantiates the hypotheses (a) that lithium complexes are involved in the damage centers, and (b) that lithium participates actively in the recovery process.

The bulk donor density, $N_{D(BULK)}$, obtained from 4-point probe resistivity measurements (Ref. 16) (before bombardment) is listed in Figure 6 at 3.5×10^{15} cm^{-3}. This value, when compared to the values obtained from the profiles near the junction, is indicative of a fact first recognized in the previous year's work (Ref. 7) and seen consistently in the present work; namely, that the lithium donor density near the junction

is at least an order of magnitude lower than the bulk lithium donor density. This, together with the large gradient of lithium concentration near the junction, makes it evident that the value of N_L to be inserted in Eq (2) should be weighted average over the collection volume of the cell rather than the value adjacent to the junction [N_{Lo} in this report, Li_{fo} in previous reports (Refs. 7 and 17)] inserted previously.
Layer resistivity measurements (Refs. 7 and 18) have given information on lithium donor concentrations in solar cells from the back face of the cell base to within ~. 002 inch (w = 50 microns) from the junction. Capacitance measurements yield the density from the edge of the depletion region up to several microns from the junction depending on the donor level and range of reverse bias applied to the cell. Thus, there is still the very important region, extending from 5 or 10 microns to ~50 microns from the junction, for which there is no information on lithium density.

In the early phases of this work a Boonton Electronics model 74D capacitance bridge was employed for these measurements. More recent work has employed a Boonton model 71A Inductance-Capacitance meter.[5] The advantage of the latter is that a DVM output from the meter provides instantaneous capacitance readings whereas the bridge required manual balancing. Thus, while bridge readings required ~20 seconds with the cell under bias the inductance-capacitance meter reading required only ~1 second. This proved important since significant lithium motion occurred with the cell under bias and the new method enabled significant extension of the bias range, and thus the range of w covered. Readings have been made routinely up to 20V reverse bias, some cells have readings up to 100V. Somewhere in this region of voltage, lithium motion becomes prohibitive. Unfortunately the upper limit of w covered is still small - approximately 4 microns for heavily doped cells to 12 microns for lightly doped cells. Thus, a large fraction of the collection region (i. e. , out to two diffusion lengths or ~100 microns) remains uncharted and an extrapolation must be made for the specification of N_L.

Another effect of the presence of the lithium gradient, (dN_D/dw) is a built-in electric field, $\mathcal{E}$, given by

$$\mathcal{E} = -\frac{dF}{dw} = -\frac{kT}{q}\frac{1}{N_D}\left(\frac{dN_D}{dw}\right),$$

where

F is Fermi level (in volts)

k is Boltzmann's constant

[5] *Measurements were also made on a (then, developmental) meter Model 71C, which Boonton Electronics made available for this effort on a cost-free loan. Because of this assistance, valuable data under new measurement conditions was obtained.*

q is electron charge

T is temperature

Thus, in cell A-2-2 before heavy bombardment the field at the edge of the depletion region, i.e., at w = 2.5 microns was 28 V/cm and at w = 6 microns was 20 V/cm. Even higher fields were found to exist in cells with higher lithium concentrations (up to 600 V/cm at the edge of the depletion width). These gradient-induced fields were found in both test diodes and GFE cells. The effect of this field is to accelerate minority-carriers (holes) from the base region toward the junction thereby creating a field-aided diffusion (Ref. 19) situation. If the field is significant over a large fraction of the collection volume the concept of diffusion length loses its validity and the minority-carrier life-time, τ, is obtained from the short-circuit current measurement only after solution of the continuity equation (which gives minority-carrier density, p, vs. w) together with the current equation given by

$$J_{sc} = q\left(p\mu_p \mathcal{E} - D_p \frac{dp}{dw}\right) \tag{4}$$

where

J_{sc} is current density

μ_p is minority-carrier mobility

D_p is minority-carrier diffusion constant

As will be seen in Paragraph C of this section, where several density profiles are presented, the region of significant field ($\gtrsim 10$ V/cm) is probably confined to w < 10 microns. In recovery from light irradiation ($\sim 10^{13}$ e/cm^2), as studied in this work, the linear portion of the annealing curves occurs for L > 30 microns so that the field effect should not cause large deviations from theory, however, after higher fluences ($\gtrsim 10^{15}$ e/cm^2) where $L_i \lesssim 10$ microns, the field effect is expected to contribute heavily to current collection.

The capacitance measurements have also yielded information on carrier removal and precipitation after irradiation. Concentration profiles are shown in Figure 7 for cell A-1-2. A detailed history of lithium donor concentration was obtained by measurements made on eight different days as listed in the figure. The corresponding minority-carrier diffusion lengths and bombardment fluences are also listed. Four-point probe resistivity measurements (Ref. 16), which were made before the back contact was put on the cell,

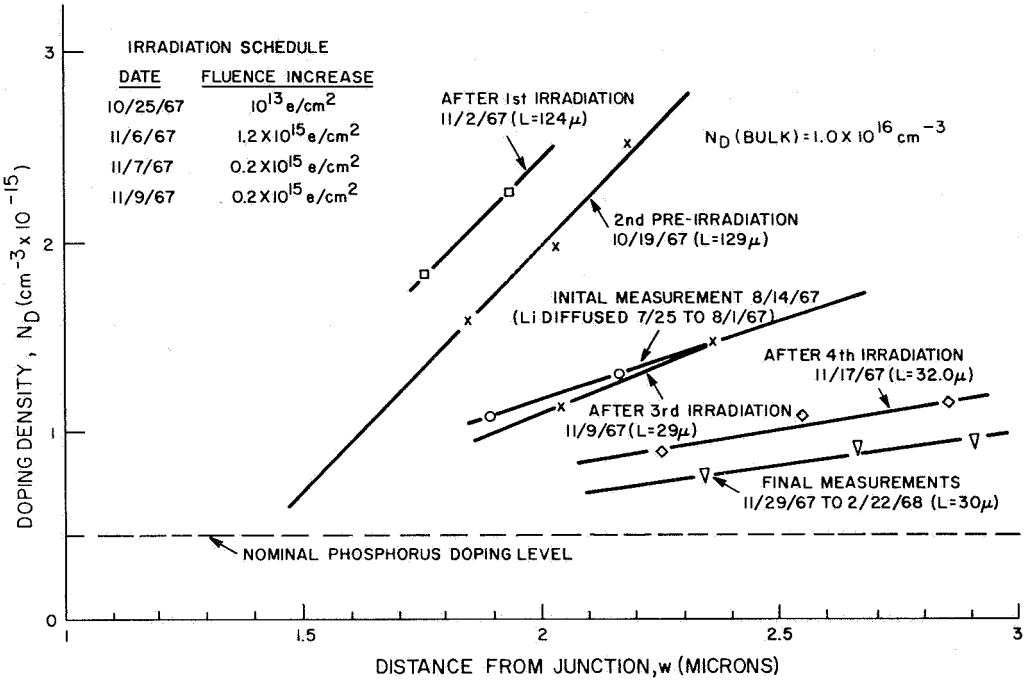

Figure 7. Concentration Profiles for Cell A-1-2

showed that the doping level averaged over the bulk of the base region was 10^{16} cm^{-3}. Four sets of concentration profiles made on August 14, September 7, September 14, and October 19, before the cell was irradiated, show a definite spontaneous increase in lithium doping level. This increase was also noted in cells A-1-4, C-1-5, and C-1-7. It occurs presumably due to diffusion of lithium from the more highly doped bulk (N_D $\sim 10^{16}$ cm^{-3}) toward the junction region. The diffusion length remained constant (within ±10%) throughout this period of time. A fifth reading, made on November 2, eight days after bombardment by 10^{13} e/cm^2, showed a further increase in lithium density. The diffusion length was still within ±10% of its original value after recovery. The cell was then heavily bombarded (November 6 and 7) to a total fluence of 1.4×10^{15} e/cm^2 and after this irradiation, both the lithium donor concentration and the spatial gradient of the lithium concentration dropped sharply (November 9 profile). The drop in lithium donor concentration gradient shows the strong dependence on lithium concentration of the introduction rate for carrier removal. Another irradiation ($\Delta\phi \approx 0.2 \times 10^{15}$ e/cm^2) was made on November 9. After recovery from this irradiation had taken place, a profile made on November 17 showed a further sharp decrease in lithium concentration and concentration gradient. The decrease of lithium concentration after bombardment by a fluence of 1.2×10^{15} e/cm^2 (the decrease in phosphorus donor concentration was neglected) was approximately 1.3×10^{15} cm^{-3} at w = 2 microns. The additional loss at

w= 2 microns after bombardment by an incremental fluence of 0.2×10^{15} e/cm^2 was $\approx 0.3 \times 10^{15}$ cm^{-3}.

A profile taken on November 29 showing a small addition carrier removal since November 16 (with no further diffusion length annealing) led to the suspicion that precipitation was occurring. Subsequent measurements, however, (December 11, January 17, and February 22) have shown the density profile to remain constant at the November 29 values. Thus, it is likely that no precipitation has occurred since November 29. It is possible that two processes were occurring, namely depletion due to precipitation and enrichment due to movement of lithium from the bulk region. This, however, would be expected to be accompanied by a change in diffusion length, which was not observed.

Lithium donor profiles were investigated in the same way on four TI cells (TI 948, 949, 950, 951) after heavy bombardment. The cells were all made from 20 ohm-cm float-zone silicon and all showed similar behavior before and after irradiation. Dated profiles for cell TI 951 are given in Figure 8 with the corresponding diffusion lengths and irradiation history. As with the test diodes, the profiles show a decrease in donor concentration gradient as well as a decrease in the level of concentration. The carrier

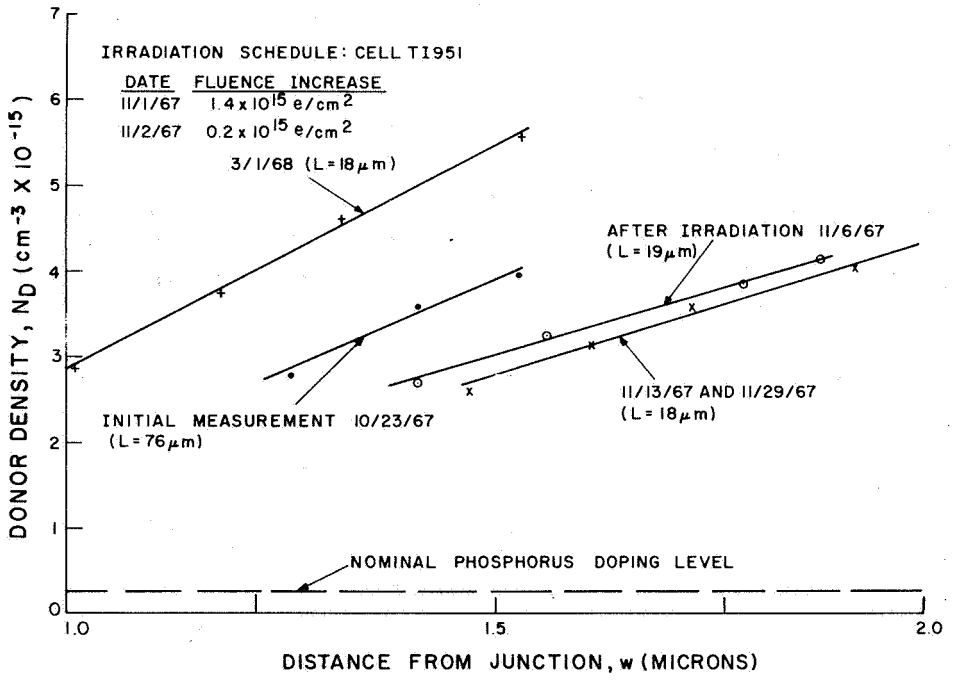

Figure 8. Dated Profiles for Cell TI-951 With Corresponding Diffusion Lengths and Irradiation History

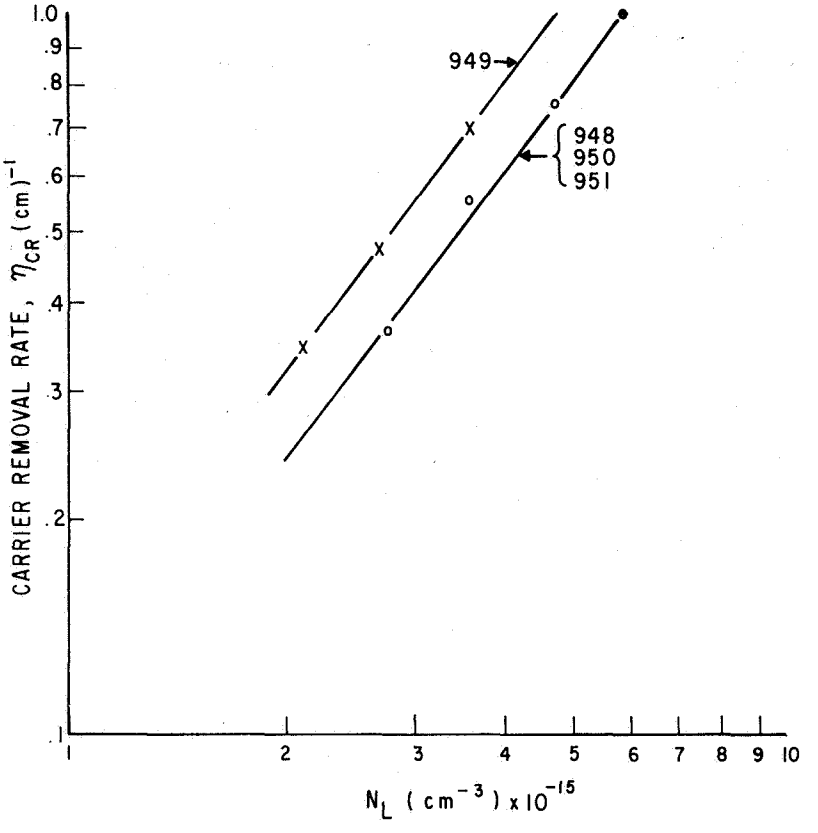

Figure 9. Carrier Removal Rate as a Function of Initial Li Concentration

removal rate, η_{CR}, which is the decrease in carrier density divided by the electron fluence, is given in Figure 9 as a function of the measured initial lithium concentration at various depths in the cell. Cells TI 948, 950, and 951 follow the same curve; the curve for TI 949 gives a removal rate about 30% higher than the other cells. This 30% difference is within the combined error of the capacitance (±10%) and fluence measurements (±20%)[6] in these experiments. The slope of both curves is approximately 1.3.

[6] *Fluence was estimated and not measured by a Faraday cup in the regular way. This estimate was required since it was the value of ϕ administered during the injection level measurement.*

Donor concentration profiles remained constant throughout the month of November. A recent reading (March 1) however, shows a significant increase in lithium density near the junction indicating that lithium has diffused in from the bulk region of the base.

C. MEASUREMENT OF EFFECTIVE LITHIUM DIFFUSION CONSTANT, D_L

Mass transport of lithium has been observed previously in lithium drift-compensated devices and has been utilized to measure the mobility of lithium in these devices (Ref. 20). The diffusion constant of free lithium in silicon of high purity was found to be 2×10^{-14} cm^2/sec at room temperature (Ref. 21). However, impurities in the silicon (e.g., oxygen, boron) can form chemical complexes with lithium, thereby reducing the effective lithium diffusion constant. When studying recovery kinetics it is therefore important to obtain direct measurements of the lithium diffusion constant for each individual silicon sample used. In the present work, lithium drift at room temperature in a junction field has been utilized, for the first time to the authors' knowledge, to obtain a direct measurement of an effective lithium diffusion constant in solar cells. A brief outline of the method follows. An initial measurement of cell capacitance at zero bias is obtained. Then small d-c reverse bias is applied to the cell. (The bias level was 3 V in the present experiments.) This bias is maintained steadily over a period of time (~10 minutes) except at periodic (~30 seconds) intervals when the bias is switched off and the capacitance at zero volts bias remeasured. The bias is then immediately re-applied after the (≈1 second) time required for the zero bias reading. A plot of change in zero-volts capacitance vs. time under reverse bias together with a knowledge of the donor density profile in the region of the applied electric field (due to the reverse bias) enables the calculation of the local lithium mobility, i.e., the mobility near the junction. The lithium diffusion constant may then be obtained by use of the Einstein relation.

Donor density profiles have shown lithium to be present in significant amounts at the edge of the depletion region in spite of the large internal electric fields (up to 600 V/cm) caused by the lithium gradient. In the depletion region itself the lithium density is much lower since the fields are an order of magnitude higher and, consequently, any lithium ions entering this region are carried toward the p-side rather rapidly. When a reverse bias of sufficient magnitude is applied, the field resulting at the edge of the depletion region causes rapid mass transport of lithium into the junction. This lithium donor motion is equivalent to the movement of one plate of a parallel-plate capacitor toward the other plate, e.g., if the voltage between the plates remains constant the capacitance increases. In the case of the solar cell at zero bias, this voltage is the p/n junction potential drop. This is a function of the lithium doping density at the junction edge. If lithium is transported due to an applied reverse bias the donor density and, consequently the junction voltage must change. The change in junction capacitance, dC, is then given by

$$dC = \frac{1}{V_o} dQ - \frac{Q}{V_o^2} dV_o, \tag{5}$$

where Q is the total charge in the depletion region and V_o is the p/n junction potential drop at zero bias.

Several cells have been tested for the purpose of comparing the magnitudes of the two terms in Eq. (5). It has been found that for a capacitance change of ~50 pf a change in donor density of ~2% occurs. Using the Fermi function, the change in junction voltage is found to be

$$dV_o = \frac{kT}{q} \ln \left(\frac{N_{D2}}{N_{D1}} \right) \tag{6}$$

where N_{D1} and N_{D2} are, respectively, the densities at the junction edge before and after the application of bias. For a 2% change in density $dV_o = 5 \times 10^{-4}$ V; for an average of 5×10^{15} cm^{-3} (1.4 and 5 times the densities measured in nominal 10 and 30 Ω-cm control cells, respectively) in a depletion region 2 microns thick, $Q = 4.8 \times 10^{-9}$ coulombs and the second term of Eq. (5) is equal to 4.5 pf, or less than 10% of the total change in capacitance. Thus, the approximation

$$dC \approx \frac{dQ}{V_o} \tag{7}$$

is justified.

The flux of lithium ions, (dQ/q) crossing the boundary into the depletion region is given by

$$\frac{dQ}{q} = N_{Lo} \mu_{Lo} \mathcal{E}_A A \, dt, \tag{8}$$

where

$\mathcal{E}_A$ is value of electric field at the depletion region edge due to applied bias

μ_{LO} is effective Li mobility near the junction

A is cell area

The electric field, $\mathcal{E}_A$, can be found by integration of Poisson's Equation:

$$\mathcal{E}_A = \frac{q}{\epsilon} \int_{w_o}^{w_3} N_D(w)\, dw \tag{9}$$

where

ϵ is permitivity of silicon

w_o is width of the depletion region for zero volts reverse bias

w_3 is width of the depletion region for three volts reverse bias

$N_D(w)$ is obtained from donor density profiles

(Values of $\mathcal{E}_A$ with cells under 3V bias are $\sim 10^4$V/cm.) Having computed $\mathcal{E}_A$, the effective lithium mobility is obtained by combining Eq. (7) and (8)

$$\mu_{Lo} = \frac{V_o}{N_{Lo} q \mathcal{E}_A A} \frac{dC}{dt}, \tag{10}$$

and the effective lithium diffusion constant near the junction, D_{Lo}, is found from the Einstein relation

$$D_{Lo} = \frac{kT}{q} \mu_{Lo}. \tag{11}$$

The sources of error in this measurement are

1. The approximation in Eq. (7) $\left[\lesssim 10\%\right]$;
2. The error in the measurement of lithium density, N_{Lo}, which contains two parts:
   a. Error in measurement of total donor density, N_{Do} ($\pm 10\%$)
   b. Error in measurement of phosphorus density N_p taken from the control cell ($\pm 10\%$)

   The total error in N_{Lo} becomes very large when $(N_{Do} - N_p) \lesssim N_p$;

3. The error due to the lithium density gradient and the gradient of the applied field, E_A, it having been implicitly assumed in Eq. (8) that these values are constant (fortunately, the gradients are in opposite directions and so tend to cancel);

4. The error in the slope of the capacitance-time measurement ~(±10%).

The overall error is estimated at ±30% when $(N_{Do} - N_p) \gtrsim 2N_p$.

Curves of $(C - C_o)$ vs time, the slopes of which give (dC/dt), are shown for six different test diodes in Figures 10, 11, and 12. All of the curves are approximately linear throughout most of the duration of measurements as was anticipated in the analysis. After ~300 seconds of bias some of the curves decreased in slope. It is believed that this was due to traversal of the junction by the small amounts of lithium initially in the depletion region. (The distance traversed by "free" lithium i.e., lithium having diffusion constant of 2×10^{-14} cm^2/sec during 300 seconds in a 10^4 V/cm field is ~0.1 micron, about 5% of the junction width.) Figures 13, 14, and 15 give donor density profiles of the cells represented in Figures 10 through 12. Of the cells shown in Figures 13 through 15 only A-3-3 satisfies the condition $(N_{Do} - N_p) \gtrsim 2N_p$. This cell was from a group of seven A-cells all showing similar doping profiles and diffusion constants. The diffusion constant obtained for cell A-3-3 was 5.5×10^{-16} cm^2/sec. This is a factor of ≈40 less than the free lithium diffusion constant. The role of oxygen in reducing the effective lithium diffusion constant has been established by Pell (Ref. 11) who gives the ratio of the effective lithium diffusion constant D_L in oxygen-containing lithium to that for free lithium in silicon, D_F, as

$$\frac{D_L}{D_F} = \frac{1}{1 + \frac{[O]}{C}} , \tag{12}$$

where C is a rate constant equal to 10^{15} cm^{-3} at room temperature and $[O]$ is the oxygen concentration. If, then, it is assumed that oxygen is responsible for the low diffusion constant in the A-cells, $[O]$ would be ~4×10^{16} cm^{-3}. This is in agreement with measurements made elsewhere (Ref. 12) which found $[O] \lesssim 5 \times 10^{16}$ cm^{-3} for Lopex silicon.

Unlike the A-cells the E-cells (10 Ω-cm F-Z) show large differences from cell to cell. The diffusion constant evaluations in these cells contained large errors due to the small values of N_{Lo}. The values obtained for E-1-1, E-1-3, and E-2-3 were 1.2×10^{-15}, ≈2×10^{-14} and 3.9×10^{-15} cm^2/sec, respectively, reflecting oxygen densities of 1.6×10^{16}, $\lesssim 10^{15}$, and 4.1×10^{15}cm^{-3}, if oxygen were assumed to be the lithium-immobilizing impurity.

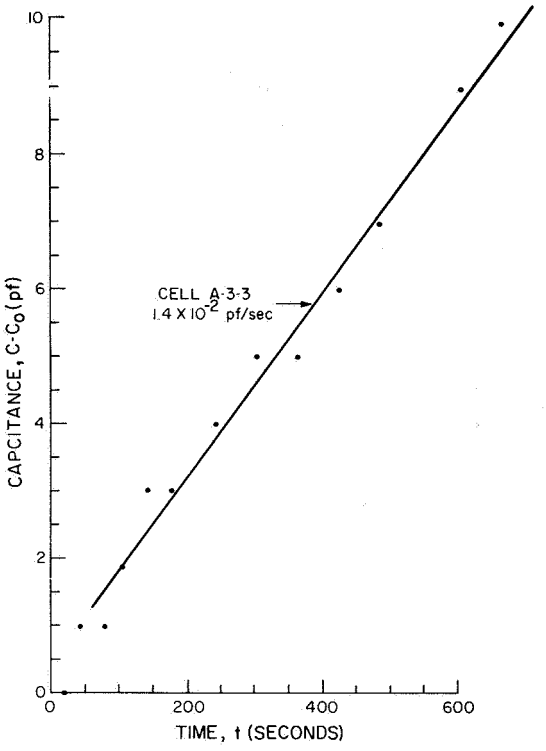

Figure 10. $C-C_o$ as a Function of Time for Cell A-3-3

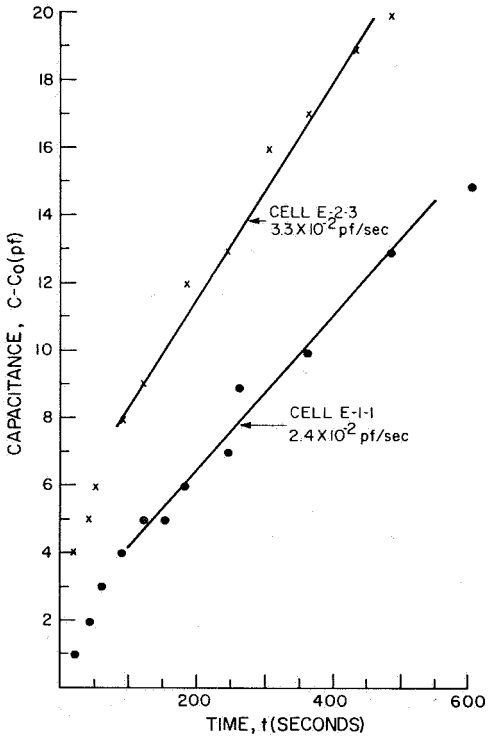

Figure 11. $C-C_o$ as a Function of Time for Cells E-1-1 and E-2-3

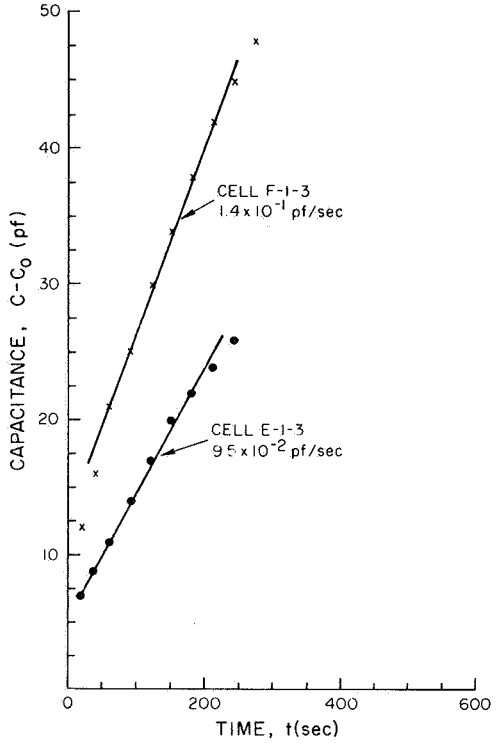

Figure 12. C-C_o as a Function of Time for Cells E-1-3 and F-1-3

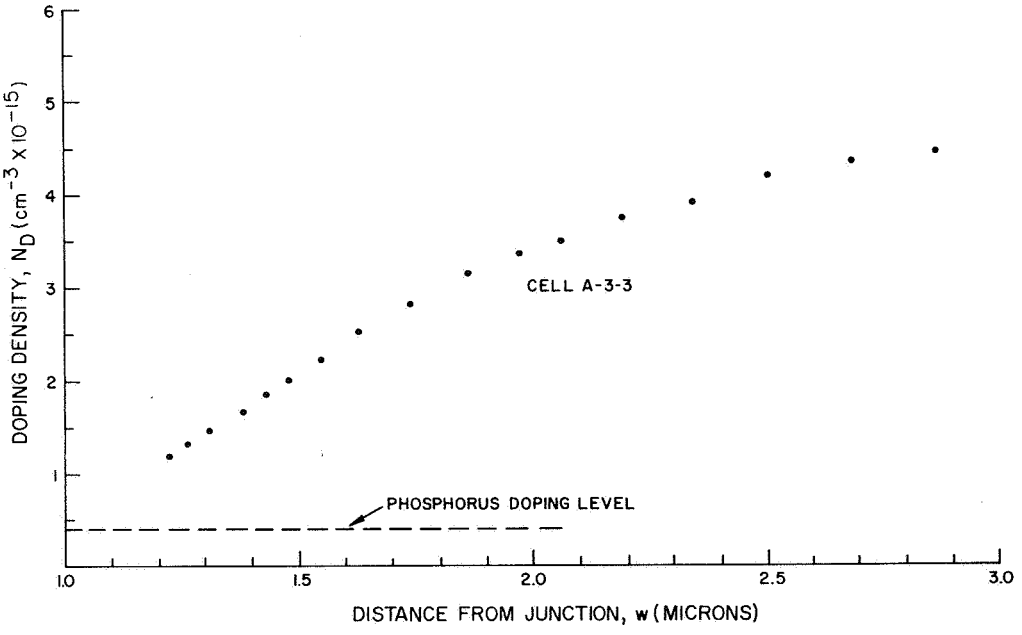

Figure 13. Donor Density Profile for Cell A-3-3

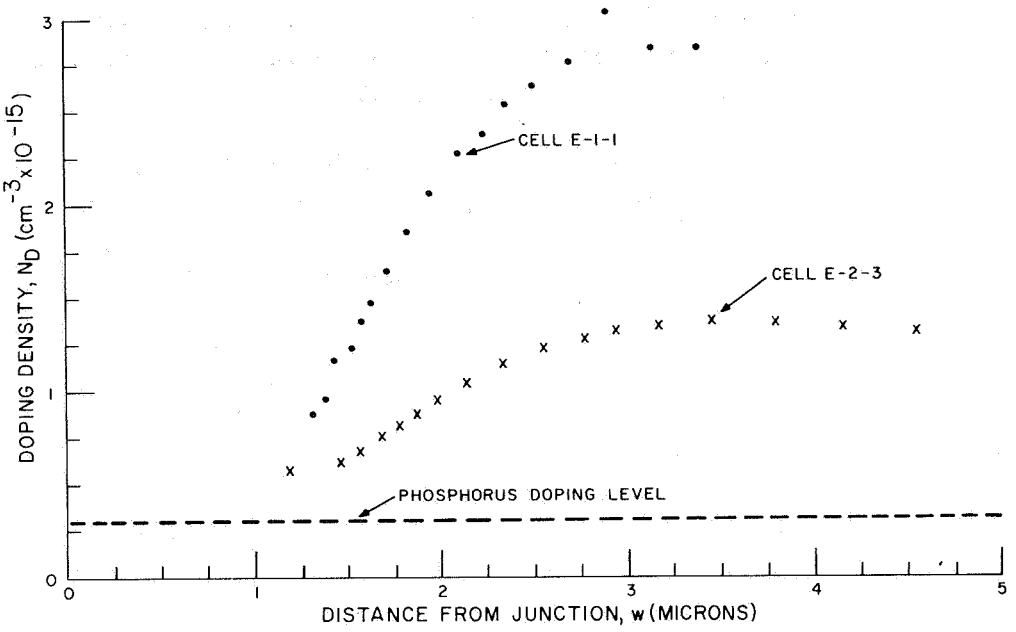

Figure 14. Donor Density Profile for Cells E-1-1 and E-2-3

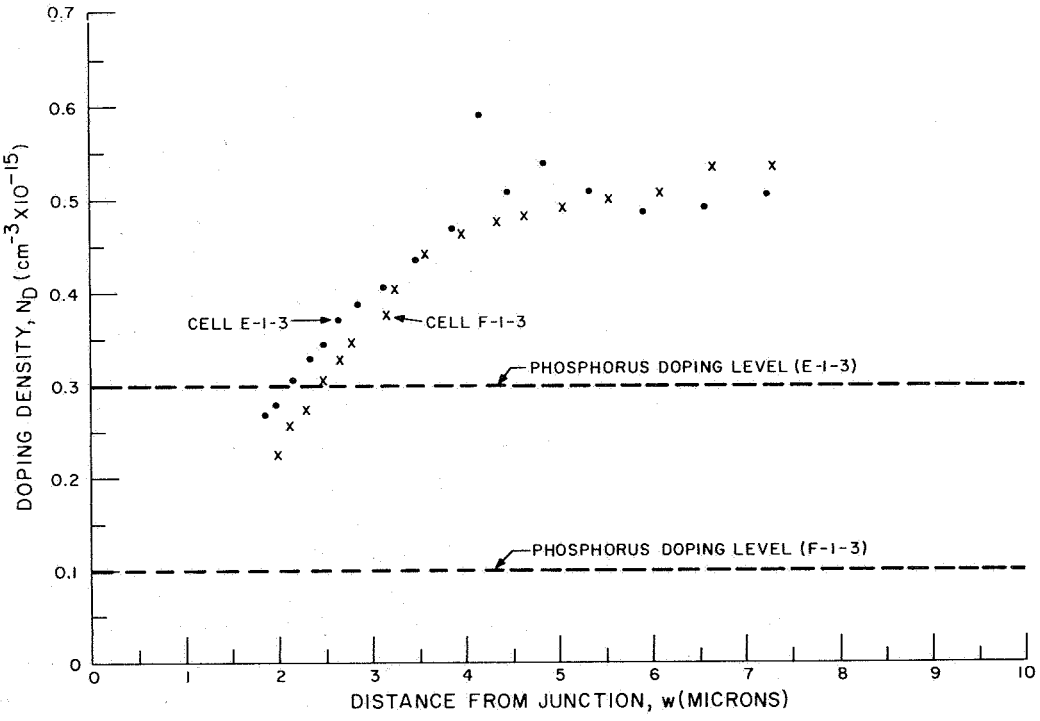

Figure 15. Donor Density Profile for Cells E-1-3 and F-1-3

Cells of 30 Ω-cm starting material also displayed large variations from cell to cell. Diffusion constants ranged from 4.3×10^{-16} to 2.8×10^{-15} cm^2/sec for three C-cells (Lopex) and from 2×10^{-15} to 1.5×10^{-14} for four F-cells (F-Z). It should be noted that cells made from Lopex silicon consistently showed a higher apparent oxygen content than float-zone cells. This is in general agreement with results obtained elsewhere (Ref. 22).

Of course, other lithium binding species may be involved as well as oxygen. Dislocations or point defects, for instance, could have an equivalent effect.

The large variation in apparent oxygen concentration in the C-, E-, and F-cells indicates that the measured diffusion constants may reflect local effects due perhaps to such crystal imperfections (Ref. 22) or to impurities introduced either during boron diffusion or the 800°C anneal rather than to oxygen whose concentration should be relatively more uniform throughout the cell and crystal. This is feasible due to the proximity of the region probed to the boron-containing region and the surface. The present method thus may not represent the average value of the diffusion constant throughout the collection region required for the term D_L in Equations 1 and 2. Results of recovery curves to be presented in Paragraph D of this Section indeed show poor correlation with these measured values.

A pattern generally adhered to by the cells is worthy of note here. The internal electric field, E, due to the gradient dN_D/dw can be found from the donor density profiles by Equation (3). It can be expected that cells with low diffusion constants should be able to support larger internal fields at the depletion region edge than those with high diffusion constants. Figure 16, a plot of the internal field vs. measured lithium diffusion constant for the cells undergoing the complete set of capacitance measurements, shows that this was generally the case. Each point on the curve represents a cell. The solid curve represents $ED_L = 7 \times 10^{13}$ V cm/sec or, equivalently, $E\mu_L = 2.8 \times 10^{-11}$ cm/sec. The product $E\mu_L$ gives an indication of the lithium drift velocity near the edge of the depletion region with the cell short-circuited under zero illumination. Cells above the $E\mu_L$ curve would tend to lose lithium to the junction more rapidly than those below the curve. This criterion might be a useful index of the shelf-life of a practical solar cell. Assuming that the lithium ion donors over the first 3 microns from the junction experience the same field strengths (which is true within a factor of ≈ 3) and that $E\mu_L \approx 3 \times 10^{-11}$ cm/sec, the lithium content in these 3 microns would have to be completely replaced by ions at greater distances from the junction over a period $\approx 10^7$ sec (≈ 100 days). It may not be a coincidence that this time constant is of the same order as that for redegradation phenomena and the slow recoveries discussed in Section III. The $\approx 10^{12}$ cm^{-2} lithium ions reaching the p-side in this time are insignificant compared to the $\approx 10^{16}$ cm^{-2} boron ions in the p-skin ($\approx 10^{20}$ ions $\approx cm^3$ over ≈ 0.5 microns), and thus no significant compensation of the p-region need be considered.

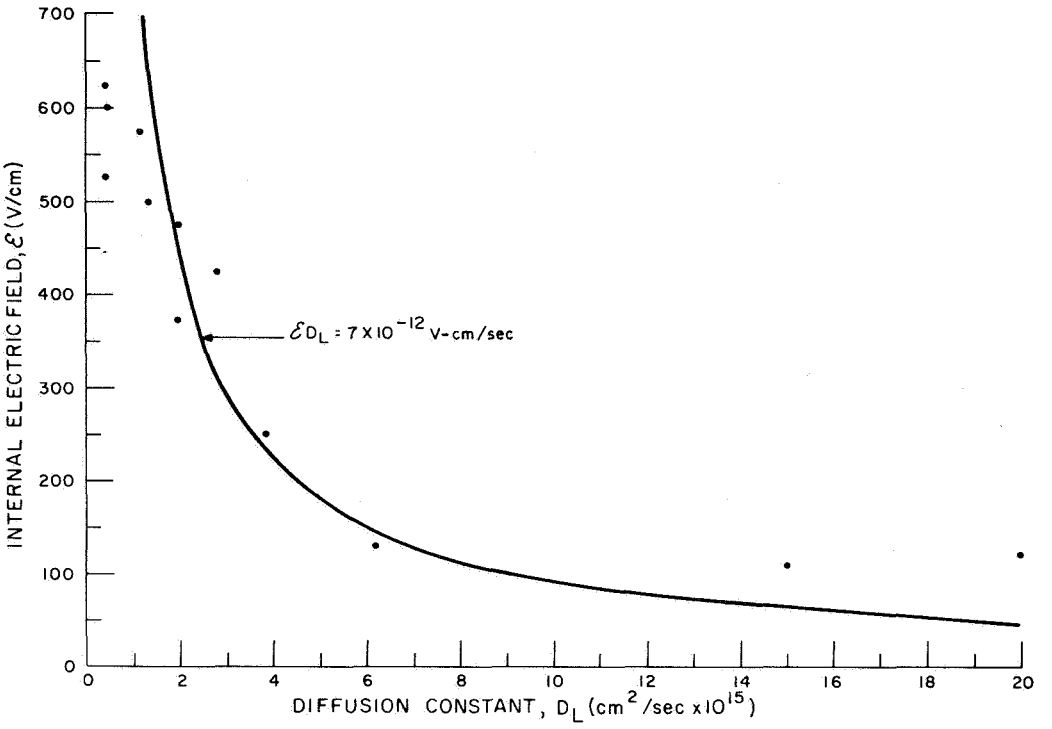

Figure 16. Internal Field as a Function of Measured Li Diffusion Constant

Applied biases have been used (Ref. 21) to affect the mass motion of lithium across a p/n junction. In the course of exploring the effects of applied reverse bias on the lithium-doped cells in the present work, some cells were subjected to larger biases over longer times than was the case in the diffusion-constant measurements. Donor density plots of one such cell, C-2-1, are shown in Figure 17. The first plot was taken before application of a reverse bias; the second, after 16 hours at 10 V reverse bias. The initial depletion region width at zero bias, w_o, and the initial and final depletion widths at 10 V reverse bias, w_{10i} and w_{10f}, respectively, are indicated in the Figure. The plots show that significant loss of lithium occurred in the region of the applied field and that some lithium from the region beyond the applied field moved into the field region to partially compensate for this loss. Within ~ 1 micron beyond the field region the densities before and after bias closely approximate each other. This mass motion of lithium offers the intriguing possibility of redistributing the lithium distribution by applied voltages after the cell has been made. This could be useful, or at least of scientific interest in cells which have locally been depleted of lithium by intense radiation. Unfortunately, however, this technique would be limited to the very small regions near the junction (a few microns) where the voltage drop occurs.

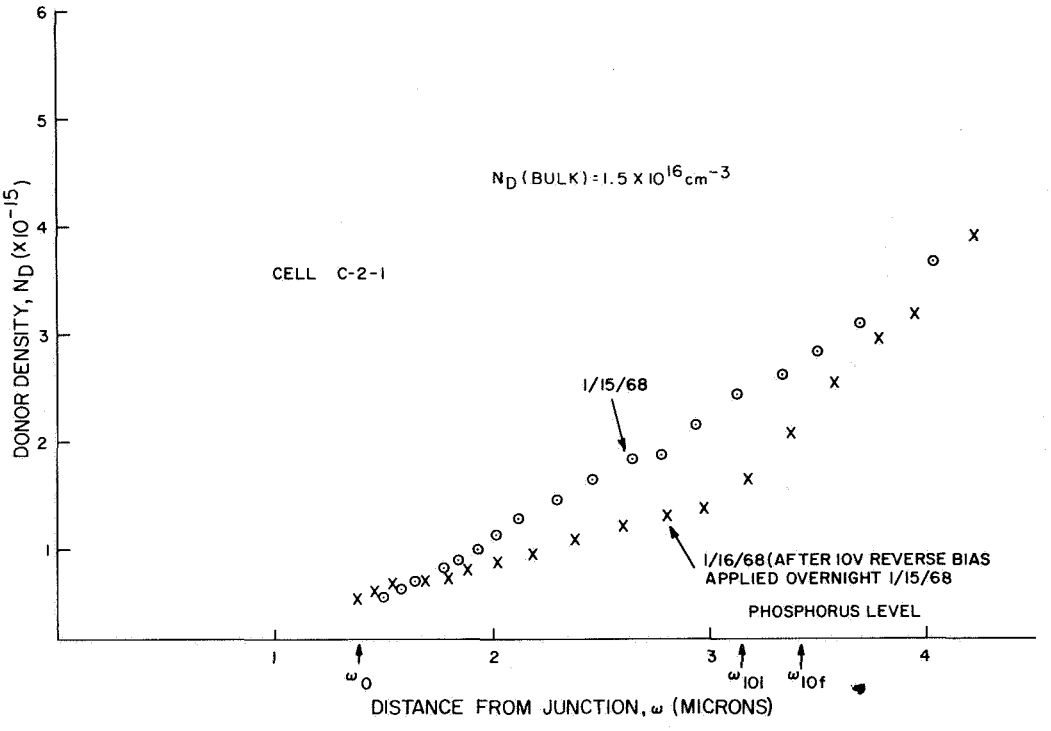

Figure 17. Donor Density Plots of Cell C-2-1

D. RESULTS OF RECOVERY EXPERIMENTS

Measurements of diffusion-length recovery characteristics were made after irradiations of test diodes to a fluence of 10^{13} e/cm^2 and of GFE cells to 10^{13} and 10^{14} e/cm^2. All irradiations and recovery experiments were performed at room temperature. The curves are all plotted as f_r^{-1} vs. time. This form of plot provides a test of Eq. (2) and of the measurements of lithium density profiles and diffusion constants discussed in Paragraphs B and C. Figures 18 and 19 are curves taken at fluences of 10^{13} e/cm^2 and 10^{14} e/cm^2 on GFE cells TI 952, 977, 978, and 981.

Figure 20 gives annealing curves obtained for a set of four test diodes early in the present work. These cells were later employed in the stability tests discussed in Section III. Two of the cells were of 10 Ω-cm Lopex (A-cells) and two were of 30 Ω-cm Lopex (C-cells). In the A-cells the recovery was much more rapid than in C-cells. None of the curves are strictly linear after the expected ~2 minute transient. However, the curves for the A-cells divide into two approximately linear regions, the first for $\tau \leq 100$ minutes with $\delta \sim .016$ min^{-1}, the second for $\tau \geq 100$ min. with $\delta \sim .007$ min.$^{-1}$ The C-cells showed only a very rough approximation to linear behavior. Cell C-1-7 which had a higher lithium concentration than

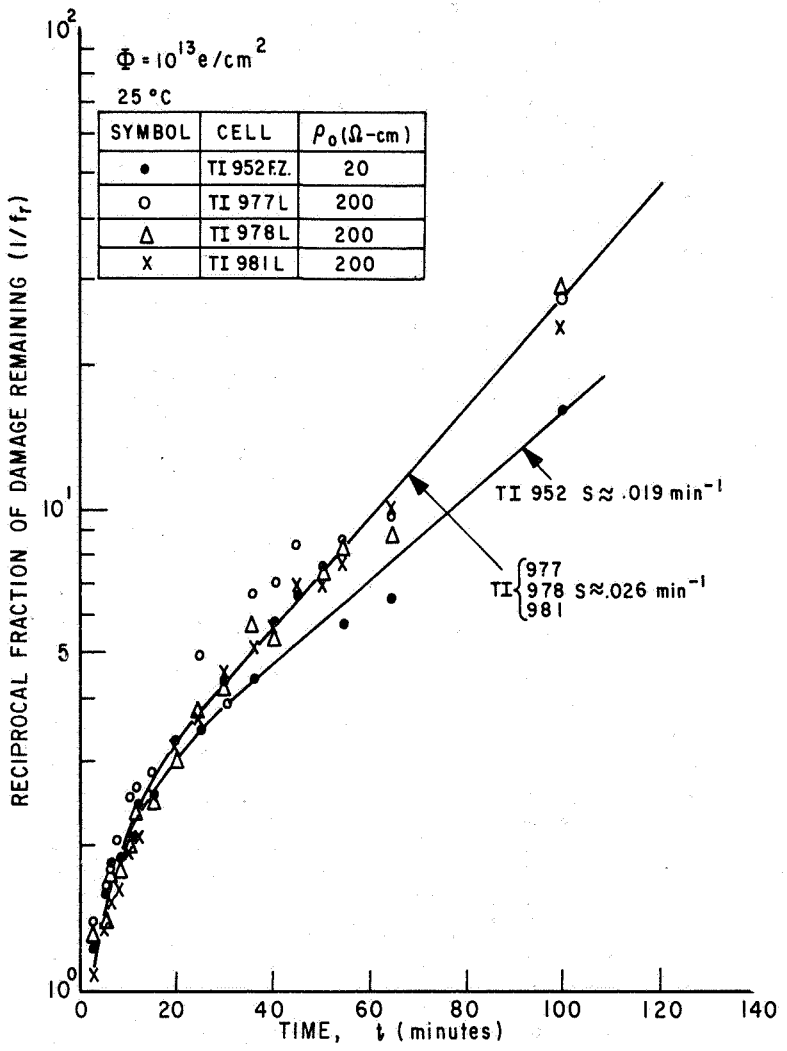

Figure 18. Reciprocal Fraction of Damage Remaining as a Function of Time for Fluence of 10^{13} e/cm^2

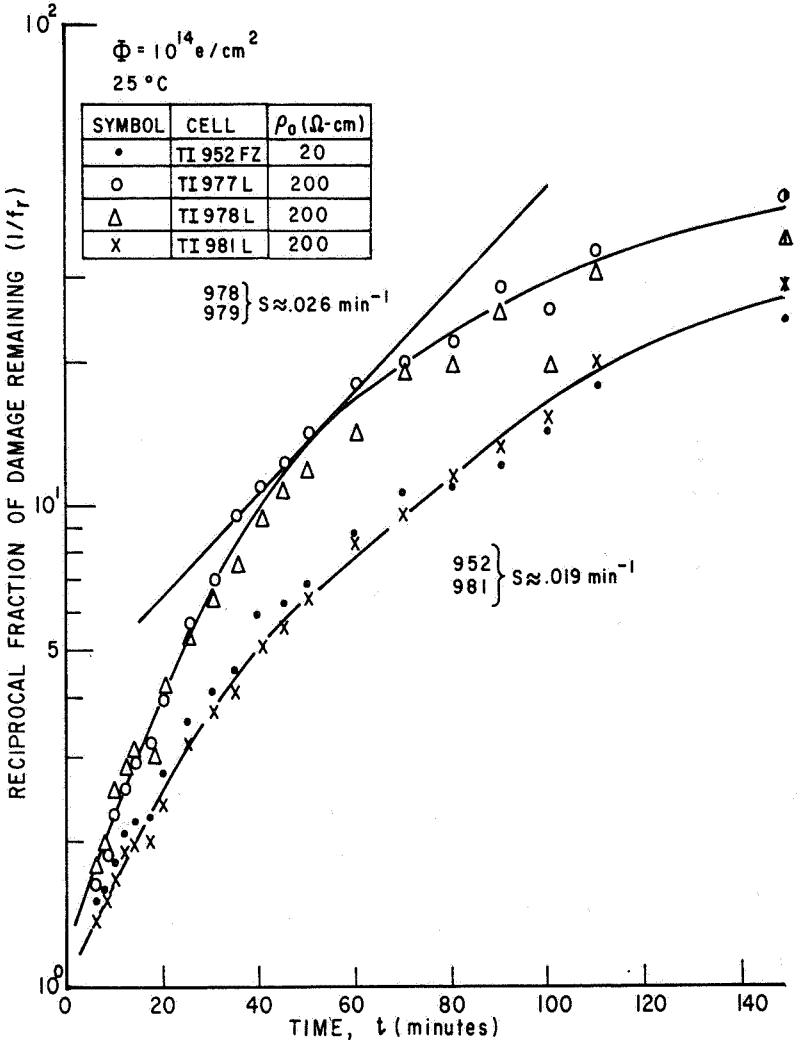

Figure 19. Reciprocal Fraction of Damage Remaining as a Function of Time for Fluence of 10^{14} e/cm^2

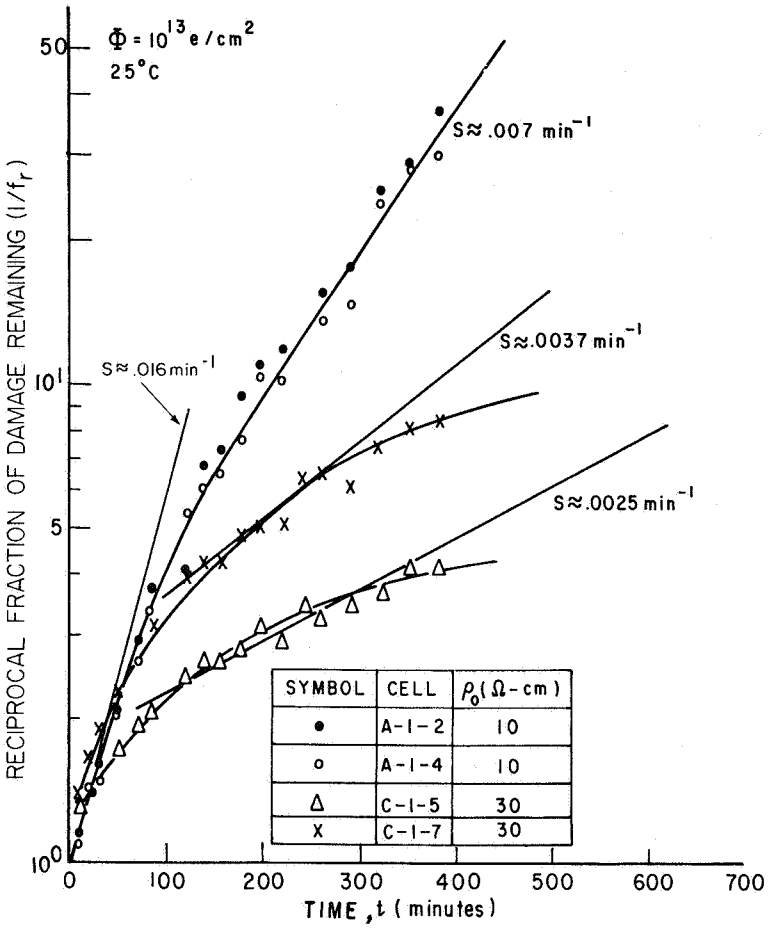

Figure 20. Annealing Curves Obtained for a Set of Four Test Diodes

C-1-5 (and also higher than A-1-2 and A-1-4) also had a faster recovery than C-1-5. If two approximately linear regions are ascribed to cell C-1-5, which had lithium density comparable to the A-cells in Figure 20, the slopes are $\sim .006$ for $\tau \leq 100$ min. and $\sim .003$ for $\tau > 100$ min. Thus the annealing rate for C-1-5, is between 1/2 and 1/3 that for the two A-cells, A-1-2 and A-1-4. Another difference between the A-cells and the C-cells is that the initial region in the A-cells ($\tau \leq$ 100 min.) of high slope encompasses significant annealing, $1/f_r$ reaching ~ 5, ($\sim$ 80% of defects annealed) whereas less annealing occurs in the initial (faster recovery) region of the C-curves ($1/f_r \leq 2$, i.e., 50% defect annealed) for C-1-5 and $1/f_r \leq 3.5$ for C-1-7 in this initial region. In this respect, the C-cells are similar in behavior to the TI cells of Figure 18 (which were also of relatively high resistivity starting material, i.e., 20 and 200 Ω-cm). This behavior, whereby a "transient" of $\geq$ 20 minutes during which $1/f_r$ increased from 1 to ~ 2 was in fact, observed for all test-diodes with starting-material resistivity of 30 Ω-cm, both for Lopex and float-zone silicon. In contrast, the recovery curves were of approximately constant slope in both float-zone and

Lopex cells of 10 Ω-cm starting resistivity from $\tau \lesssim$ 10 min. to $\tau \gtrsim$ 50 min. during which time the same recovery behavior as the other three (2000 Ω-cm Lopex) cells. The recovery curves at a fluence of 10^{13} e/cm^2 are approximately linear after an initial transient of ~ 20 minutes. The observed transient is an order of magnitude longer than that predicted from Eq. (7) of Appendix C and could therefore represent the annealing of some defect which has either a large self-diffusion constant or a large capture radius for lithium. If a straight line is used to approximate the slope of the initial portions of the annealing in Figure 18, the slope is determined to be approximately 0.1 min^{-1}. If this value, along with the highest feasible values of N_L (~3 x 10^{16} cm^{-3}, the estimated bulk doping density) and D_L (i.e., 2 x 10^{-14} cm^2/sec), are inserted in Eq. (2), a value of $r_o \approx 30$ A is obtained. This is not unreasonably high value for a semiconductor defect. After the initial ~ 20 minutes the curves are approximately linear with slopes of ~.025 min^{-1}, a four-fold decrease from the earlier values. This behavior, which was also observed in the test diodes with similarly high (30 Ω-cm) starting resistivity, (but not in 10 Ω-cm diodes), could thus be indicative of two types of defect, one with higher capture cross-section (presumably due to the charge state) than the other. Another possible explanation lies in the influence of internal electric field generated by the donor density gradient. The built-in field of ~ 250 V/cm at the junction edge and ~ 30 V/cm at ~ 7 microns from the junction in cells such as the TI cells should have an appreciable effect on local lithium motion which would be most prevalent during the initial stages of annealing, i.e., when the diffusion length was lowest. This could speed the initial phases of annealing. However, since the local lithium density in the region of the high internal field is ~ 10 times below the bulk density, it is unlikely that the very fast initial annealing would result from the conditions in this region.

The results shown in Figure 19, obtained at a fluence of 10^{14} e/cm^2 indicate only an approximate fit to a straight line. However, the annealing behavior is interesting when compared with that shown in Figure 18. Although the fluence was increased by a factor of 10 (10^{13} to 10^{14} e/cm^2), the curves show practically the same annealing rates. Thus, the first-order nature of the recovery for $N_{LO} >> N_1$, predicted by the theory, is verified experimentally.

It has been proposed (Ref. 4) that the recovery in lithium cells follows second order kinetics. The proposed recovery reaction was

$$R + X = RX$$

where

R is a radiation-produced recombination center,

X is an unknown species with concentration equal to R,

RX is an electrically inactive complex.

The authors of this reference stated that it is extremely unlikely that X is lithium since lithium concentration does not in general equal R concentration. The authors further suggest that, since lithium diffusion is suspected to limit the reaction, it (i.e., lithium) may mobilize one of the components or break down a barrier to their reaction. However, the conditions for a true second-order reaction in lithium-associated recoveries are not feasible for the following reason: Since the presence of lithium is essential for recovery in the annealing process, lithium in some form must diffuse to the defect center even if it is inactive in the actual reaction.

Fourteen cells were put through a complete set of donor density profiles, diffusion constant measurements and recovery measurements after a fluence of $10^{13} e/cm^2$. The cells were made from 10 Ω-cm and 30 Ω-cm starting material. The recovery curves for the 10 Ω-cm cells were linear, to a good approximation, as $1/f_r$ increased from 1 to 5 and 10 (between 80 and 90% of defects annealed). The curves for the 30 Ω-cm cells were more complex. Figures 21 and 22 (10 Ω-cm cells) and Figure 23 (30 Ω-cm cells) illustrate this behavior. These Figures give recovery curves at a fluence of 10^{13} e/cm^2 for six of the total of 14 cells which underwent a complete set of capacitance and recovery tests. Cell A-3-3 (one of seven similar 10 Ω-cm, Lopex A-cells) displayed an approximately linear behavior over the range: 4 min. $\lesssim \tau \lesssim$ 70 min.; $1.3 \lesssim f_r^{-1} \lesssim 10$. Cells E-1-1, E-1-3, and E-2-3 are all 10 Ω-cm float-zone cells, which have quite dissimilar doping profiles and capacitance-time curves as can be seen in Figures 11, 12, 13 and 14.

All of these cells showed approximately linear behavior in Figure 22 for approximately the same intervals as did A-3-3 shown in Figure 19. By contrast, in Figure 23 cell C-2-2, 30 Ω-cm Lopex, and cell F-1-3, 30 Ω-cm float-zone, behaved more like the previous 30 Ω-cm cells, C-1-5 and C-1-7, shown in Figure 20. A total of five other C- and F- cells behaved similarly.

The recovery behavior, therefore, correlated, in a general way, with the phosphorus doping level. The actual phosphorus concentration, measured on control cells by the capacitance method gave: $N_p \approx 4 \times 10^{14}$ cm^{-3} in A cells, $N_p \approx 3 \times 10^{14}$ cm^{-3} in E-cells, $N_p \approx 1.4 \times 10^{14}$ cm^{-3} in C-cells and $N_p \approx 1.0 \times 10^{14}$ cm^{-3} in F-cells. This correlation suggests that a defect center involving phosphorus, perhaps the E-center, is one of the important defects in the lithium-doped cells. This will be discussed in subsequent paragraphs where an attempt will be made to correlate capacitance and recovery measurements with recovery theory.

Table VII lists parameters measured on 12 of the 14 cells on which a complete set of capacitance and recovery data has been taken. The other two cells, made of quartz-crucible silicon, are still in the process of recovery and will not be included in this discussion. The cells are listed in the first column. The second, third, and fourth columns list the donor density N_{DO}, the lithium density, N_{LO}, and the donor density gradient, dN_D/dw, all at the edge of the depletion region, and all taken from capacitance-doping measurements. The fifth column lists the average doping density of the base region as obtained from 4-point probe measurements (Ref. 17). Column 6 lists the diffusion constants, D_{LO}, near the junction from the capacitance-time measurements. The slopes, S, obtained from the recovery data are listed in the seventh column. In the case of the 30 Ω-cm cells,

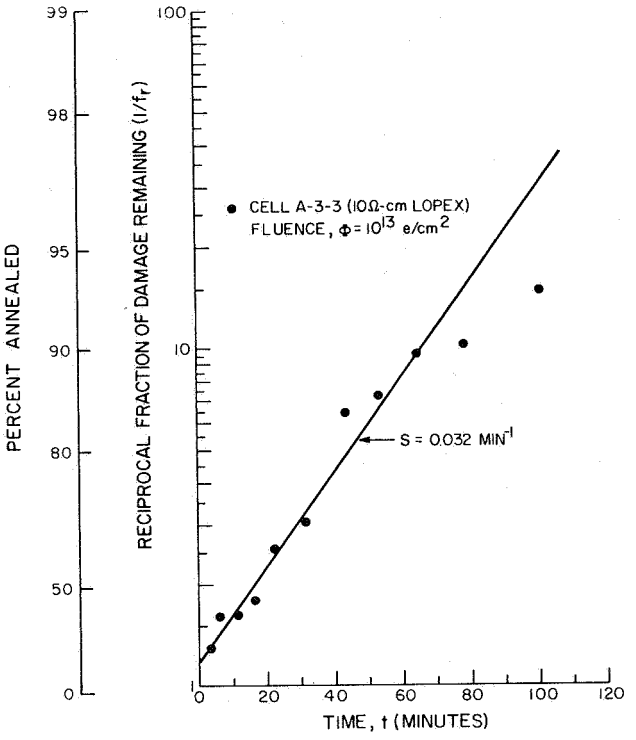

Figure 21. Reciprocal Fraction of Damage Remaining as a Function of Time for Cell A-3-3 (10Ω-cm Lopex)

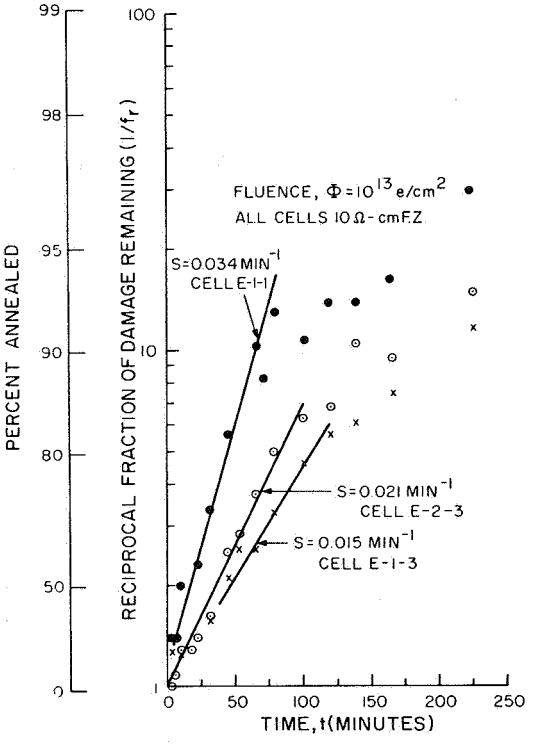

Figure 22. Reciprocal Fraction of Damage Remaining as a Function of Time for Cells E-1-1, E-1-3, and E-23 (all 10Ω-cm F.Z.)

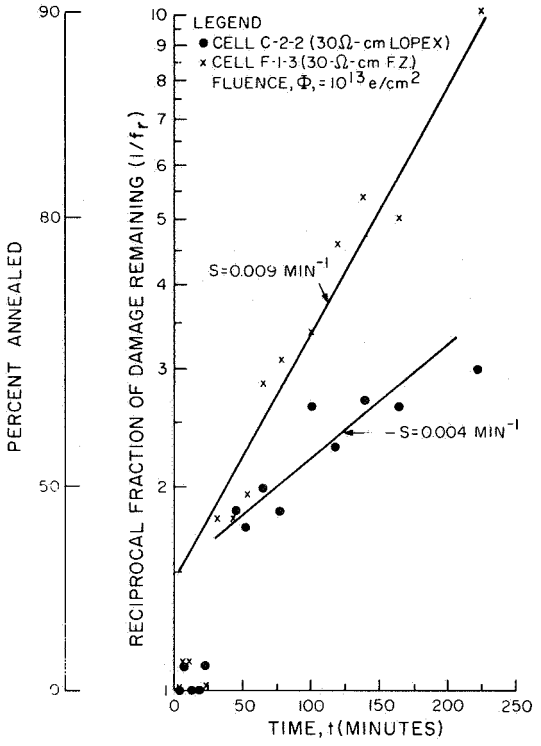

Figure 23. Reciprocal Fraction of Damage Remaining as a Function of Time for Cells C-2-2 (30 Ω-cm Lopex) and F-1-3 (30 Ω-cm F.Z.)

TABLE VII. CORRELATION OF CAPACITANCE AND RECOVERY MEASUREMENTS

Cell	N_{DO} ($cm^{-3} \times 10^{-14}$)	N_{LO} ($cm^{-3} \times 10^{-14}$)	dN_D/dw ($cm^{-4} \times 10^{-19}$)	N_{LB} ($cm^{-3} \times 10^{-16}$)	D_{LO} $cm^2/sec \times 10^{15}$	S ($sec^{-1} \times 10^4$)	r_{01}* (Å)	r_{02}+ (Å)	r_{03}· (Å)
A-3-3	11.8	7.8	2.8	2.0	.55	5.3	270	390	11
A-5-3	12.5	8.5	3.2	2.0	.44	5.3	250	480	11
E-1-1	8.9	5.6	2.0	1.5	1.2	5.7	410	250	15
E-1-3	2.7	.5	.13	1.5	20.0	2.5	800	67	10
E-2-3	5.8	2.5	.60	1.0	3.9	3.5	560	72	14
F-1-3	2.3	1.3	.12	1.0	6.2	1.4	430	18	5.7
F-1-1	4.2	3.2	.78	1.0	2.0	1.4	170	56	5.6
F-1-4	4.5	3.5	.68	1.0	2.0	1.7	190	68	6.8
F-2-4	3.5	2.5	.15	1.0	15.0	1.4	220	7.3	5.6
C-2-2	4.6	3.2	.90	1.1	1.4	.77	96	40	2.9
C-4-4	5.5	4.1	.95	1.5	2.8	3.3	320	63	9.0
C-4-5	6.8	5.4	1.4	1.7	.43	3.3	360	360	7.7

* $r_{01} = \frac{S}{4\pi N_{LO} D_F}$ + $r_{02} = \frac{S}{4\pi N_{LB} D_{LO}}$ · $r_{03} = \frac{S}{4\pi N_{LB} D_F}$

the slopes are taken from the region of the curve where $t \gtrsim 30$ min, $1/f_r \gtrsim 2$, as shown in Figure 23. The remaining three columns give values for r_o, the capture radius for lithium by the defect, calculated by using three different values of the product of the lithium density and the lithium-diffusion constant. The capture radius, r_o, is given, from Equations (1) and (2) by

$$r_o = \frac{S}{4\pi N_L D_L} \tag{13}$$

The appropriate values of lithium density N_L and lithium diffusion constant D_L must be chosen. In previous work (Ref. 7) the value of lithium density at the depletion region edge, N_{LO}, and the free lithium diffusion constant, D_F ($=2 \times 10^{-14}$ cm^2/sec at room temperature) was used. This yielded r_{01}, given in the eighth column of the table. The values of r_{01} range up to 800Å, (i.e., capture cross-sections up to $\sim 2 \times 10^{-10}$ cm^2) which is unreasonably high even for coulomb cross-sections. By extrapolation, the doping profiles in the previous section indicate that the lithium density of most of the cells reaches the bulk value at a distance of about 10 microns from the junction edge. This distance is a small fraction of the diffusion length ($\gtrsim 30$ microns) in the linear regions of the ln $(1/f_r)$ vs t recovery curves. It is therefore most reasonable to choose a density near the bulk value for Eq. (13). In the calculation of r_{02}, the bulk lithium density, N_{LB}, and the diffusion constant, D_{LO}, measured as outlined in Paragraph C of this Section, are used. The values obtained for r_{02}, although lower, in general, than those obtained for r_{01}, are still unreasonably high, ranging up to ≈ 500Å (cross-sections up to $\approx 8 \times 10^{-11}$ cm^2). The capture radius r_{03}, obtained by using the bulk lithium density and the free lithium diffusion constant, gives the most reasonable values ($\approx$10Å), leading to capture cross-sections $\approx 3 \times 10^{-14}$ cm^2 which are reasonable coulomb cross sections. It must therefore be concluded that while the bulk doping density, obtained via the donor density measurements, is the appropriate value for N_L in Eq. (13), the free lithium diffusion constant, D_F, and not the directly measured diffusion constant near the junction, D_{LO}, is the appropriate value for the diffusion constant in this Equation. This somewhat puzzling situation reflects the possibility that, due to the proximity to the cell surface and to the heavily-doped boron region, impurities and crystal defects cause marked local decreases in the effective lithium diffusion constant near the junction. This effect, if it is real, could be a very important factor in long-term lithium cell stability since a local reduction in lithium diffusion constant at the junction would provide a "brake" for the flow of lithium across the junction, thereby reducing this loss of lithium.

Returning to Table VII, it is interesting to compare the values of capture radius, r_{03}, obtained for 10 Ω-cm cells with those obtained for 30 Ω-cm cells. The 10 Ω-cm (A and E-cells) all have values of r_{03} between 10 and 15Å, averaging 12Å; the average value for 30 Ω-cm cells is 6Å. Thus, a factor of two separates the average capture radii. As was previously discussed in reference to Figure 20, the curves can be considered as consisting of two linear regions, one with a high slope followed by one with

lower slope. This would physically approximate two separate defects each having a different capture radius. If the initial ~ 20 to 50 minute period in the 30 Ω-cm cell annealing curves represents one of these linear regions, then the slope of this portion of the curve, although not accurately measureable, would be approximately twice the slope of the portion after ~20 to 50 minutes. This initial slope, which prevails until $1/f_r \simeq 2$ (~50% of defects annealed) would give a lithium capture radius approximating that of the curves obtained for the 10 Ω-cm cells. This is explainable in terms of the phosphorous-vacancy defect on E-center. The 30 Ω-cm cell, having less phosphorus would have a smaller relative fraction of E-centers, in this case about half of all defects, as opposed to ~9/10 of all defects in the 10 Ω-cm cells. It should be noted, however, that the importance of the E-center defect in lithium cells is at this point only a matter of hypothesis. Further work is required with both higher resistivity (>30 Ω cm) and lower resistivity (~ 1 Ω-cm) starting materials.

SECTION V
INJECTION LEVEL EFFECTS

A. INTRODUCTION

The purpose of the investigation of injection level effects was to use the dependence of diffusion length on excess carrier density to obtain information on interactions of lithium with radiation-induced defects in silicon solar cells. A description of injection level measurement, the reasons for using it, and the preliminary results obtained on GFE cells were presented previously (Ref. 7). Briefly, the method provides a rapid and convenient (if, at the moment qualitative) check on the defect-energy-level situation in the base region of the recovering cell. Certain known centers, such as the A- and E-centers, can be tentatively identified. Since the annual Report of last year (Ref. 7) the analysis and presentation of these data has been modified. For this reason and reasons of completeness, the previous data including a brief description of the technique, will be presented in revised form in this report; in addition, new data on newly fabricated test diodes and government-furnished cells will be reported.

B. EXPERIMENTAL TECHNIQUE

The raw data obtained with this measurement technique is the solar-cell diffusion length as a function of Van de Graaff beam current. This electron current generates electron and ion carriers in the solar cell. The excess carrier density is computed from Eq. (14).

$$\Delta n = \frac{L^2 J_B S}{q D_p} \tag{14}$$

where

Δn is the deviation from thermal - equilibrium carrier concentrations (holes) i.e., excess carrier density

L is diffusion length of the cell at any value of J_B (in microns)

J_B is incident electron-beam current density (in amperes/cm^2)

D_p is minority-carrier diffusion constant

S is specific polarization.

Inserting values of the constants,

$$\Delta n = 3.96 \times 10^{15} J_B L^2 \text{ carriers/cm}^3 \quad (15)$$

where $D_p = 10$ cm^2/sec for holes in n-type silicon. The minority-carrier lifetime $\tau = L^2/D_p$ and the relative lifetime $\tau/\tau_o = L^2/L_o^2$, where τ_o and L_o are the lifetime and diffusion length measured at low injection level ($J_B = 1.5 \times 10^{-10}$ A/cm^2). In the present work it was observed that injection level effects appear when the beam current density exceeded 1.3×10^{-9} A/cm^2. The cathode controls of the Van de Graaff generator were modified so that currents as low as 10^{-10} A could be obtained. Measurements of low-injection-level diffusion lengths were made with a standard beam current of 5×10^{-10} A, which is approximately an order of magnitude lower than the value used previously. The experimental techniques involved the sequential measurement of diffusion length at the standard low-injection level, then a high level, and finally the standard low level. This sequence was repeated for all injection levels commencing with the highest beam current obtainable and decreasing to the lowest level. Thus, many diffusion length values at the standard low-injection level were obtained during an experiment. An average value of low-injection level diffusion length, L_o, was determined and this value is tabulated in the figures for each experiment.

C. REVIEW OF PREVIOUS WORK

1. Description of the Work

During the initial contract effort (Ref. 7), commercial n/p, p/n, and lithium-doped p/n cells were bombarded by reactor neutrons and 1-MeV electrons. Doping levels near the junction were measured by the capacitance method before and after bombardment, so that initial and final Fermi-level positions could be specified. Cells were irradiated with a wide range of neutron and electron fluences so that a distribution of cells with post-bombardment diffusion lengths ranging from 2 to 20 microns (a high damage level) were obtained. The diffusion length was measured at room temperature by means of the 1-MeV Van de Graaff electron beam ranging in current from 10^{-8} to 7×10^{-5} A. Beam area scanned could be adjusted and had a minimum size of 1.0 cm^2. With the samples used, these beam currents correspond approximately to excess-carrier densities from $\approx 10^{10}$ to 10^{14} carriers/cm^3. (Note that sun simulators or tungsten light sources, as normally used in optical measurements on cells, produce an excess-carrier density of about 10^{14} carriers/cm^3.) The time spent in making each diffusion-length measurement with the electron beam was minimized by an automatic readout system taking 1 to 2 seconds. As a result, the degradation caused by the electron beam was not allowed to exceed 10% of the initial diffusion-length value. The diffusion lengths of lithium-doped cells were measured several times during a period of 40 days following the electron or neutron bombardments.

2. Results

a. 1-MeV Electrons

The dependence of minority-carrier lifetime τ, relative to the low-injection value τ_o (measured at $I_{beam} = 10^{-8}$ A) vs. injection ratio $\Delta n/n_o$, is shown in Figure 24 for p/n cells bombarded by 1-MeV electrons and then measured by the electron-voltaic method. These cells were made from quartz-crucible grown (Q.C.) and float-zone refined (F.Z.) silicon and thus provide a basis of comparison with lithium-doped cells made from both types of silicon. The average values of six independent measurements of diffusion length which were made each time the lithium cells were measured are shown in Figure 24. Error flags indicate the (rms) deviation of the data. The dominant damage was attributed (Ref. 7) to the A-defect center in the oxygen-containing Q.C. silicon and to the E-center in the oxygen-lean F.Z. silicon. These centers are both located in the upper half of the energy bandgap at a level of 0.18 and 0.4 eV, respectively, below the conduction band. The increase of minority-carrier lifetime with injection level is predicted by Shockley-Read (Ref. 23) statistics for defect levels with a minority-carrier capture cross-section greater than the majority-carrier capture cross section. Thus, $\gamma = \tau_n/\tau_p$ or $c_p/c_n > 1$ (acceptor-like levels) where τ_e and c_e are the electron lifetime and capture cross section, and τ_p and c_p are the hole lifetime and capture cross section, respectively. Note that the τ/τ_o for the F.Z. cell begins to increase at lower values of $\Delta n/n_o$ than the Q.C. cells. This behavior is in qualitative agreement with the description of the E-center as being located deeper in the forbidden gap than the A-center. However, the location of the defect energy levels at E = 0.4 and 0.18 eV (E- and A-center)is not in quantitative agreement with the data. The increase of τ/τ_o with $\Delta n/n_o$ for both Q.C. and F.Z. control cells commences at lower values of $\Delta n/n_o$ than expected for these energy levels. The same behavior was observed in the

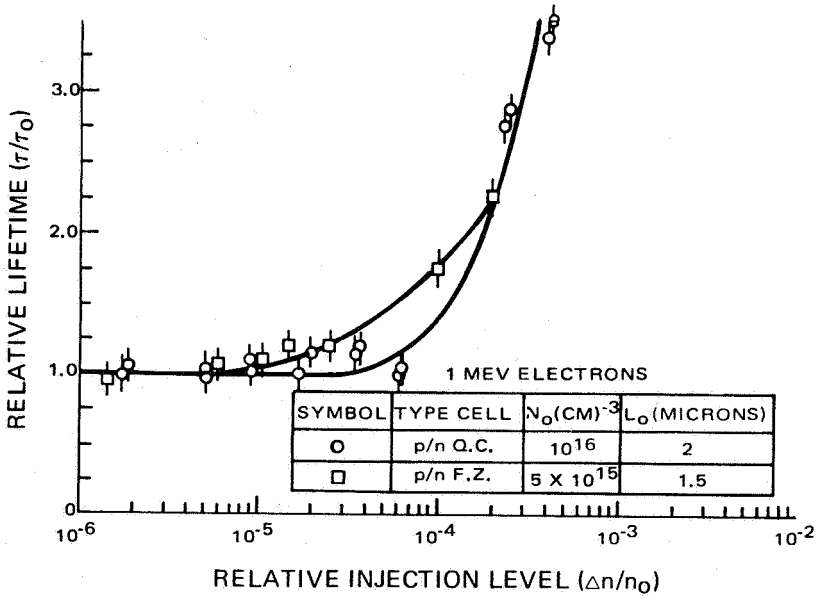

Figure 24. Relative Lifetime vs. Relative Excess Carrier Density for Q.C. and F.Z. Control Cells Bombarded by 1-MeV Electrons

neutron-irradiated control cells. There is no explanation for this behavior except for the unknown effect of the junction in the cell on Shockley-Read theory. The transient lifetime measurements in bulk silicon and/or solar cells as a function of excess-carrier density should provide an explanation. The increase of τ/τ_0 with $\Delta n/n_0$ is linear, which indicates that only one defect level is causing the increase.

Figure 25 shows the dependence of τ/τ_0 both on Δn, the number of carriers/cm^3, and on $\Delta n/n_0$ for lithium-doped F.Z. cells. The cells were measured immediately after irradiation, and then at various times extending to 44 days after the initial measurement. Four of these measurements are shown. Immediately after bombardment, t = 0, there is no significant dependence on injection level. However, as time passes it appears that interaction of lithium with radiation-induced defects takes place. Although heavily damaged, the cells are slowly recovering from the radiation damage as indicated by the tabulated values of the low-injection-level diffusion length, L_0. An interesting feature of this Figure and others on lithium cells is that, although diffusion length values L_0 measured at low injection levels (corresponding to very low light levels) are increasing steadily with time, there are some regions of injection level (say 5×10^{12} cm^{-3}) where L is increasing in an irregular manner or even undergoing reversals, due to the rearrangement of defect energy levels.

Some electron-damaged and also undamaged n/p solar cells were also investigated. It was found that the plots of τ/τ_0 vs. Δn were flat over the range $\Delta n = 10^9$ to 10^{13} cm^{-3}.

The shape of the late-time curves in Figure 25 indicates clearly that more than one defect level is contributing to the dependence on injection level. In Figure 26, the results obtained by the same method, but using lithium-doped cells made from Q.C. silicon are shown. The decrease in τ with Δn, observed in the case of the Li-doped F.Z. cells at later times (say > 500 hours) also occurs for the oxygen-containing cells. However, the behavior of τ at intermediate times (t = 48 to 120 hours) is significantly different. In the case of Figure 26, there is a sharp increase of τ at high injection levels. The A-center exhibits an increase with Δn, shown in Figure 24, and the increase in τ at high injection levels has been sharply reduced. Interaction of the Li-center with the A-center and other defects may have modified the effective lifetime.

b. Reactor Neutrons

Neutron damage differs from electron damage, since neutrons produce large clusters of defects with many recombination levels located in both the lower and upper energy gap. As an exploratory technique, the use of neutrons is of interest as a convenient model experiment which may throw light on the effect of space protons. Protons also produce large clusters of defects. In some cases (Ref. 24), a model defect system consisting of two effective energy levels has been sufficient to explain the experimental data on τ vs. Δn in neutron-damaged silicon. Figure 27 shows the dependence of τ/τ_0 vs. Δn and $\Delta n/n_0$ for commercial n/p and p/n cells both made from Q.C. silicon. The average τ/τ_0 value of ten cells of each type is shown in Figure 27 with the rms deviation of the

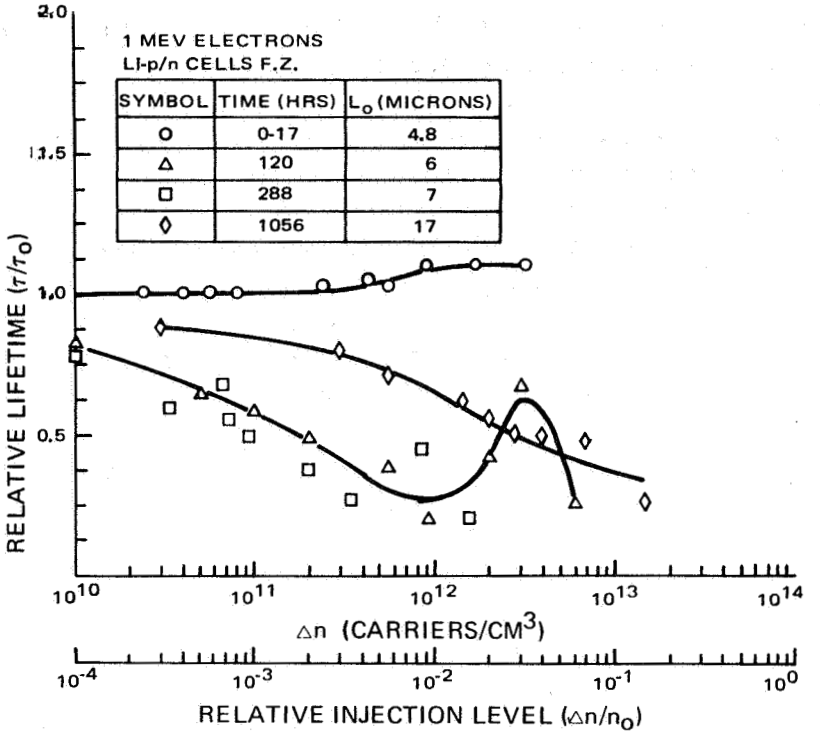

Figure 25. Relative Lifetime vs. Excess Carrier Density for F.Z. Cell Bombarded by 1-MeV Electrons

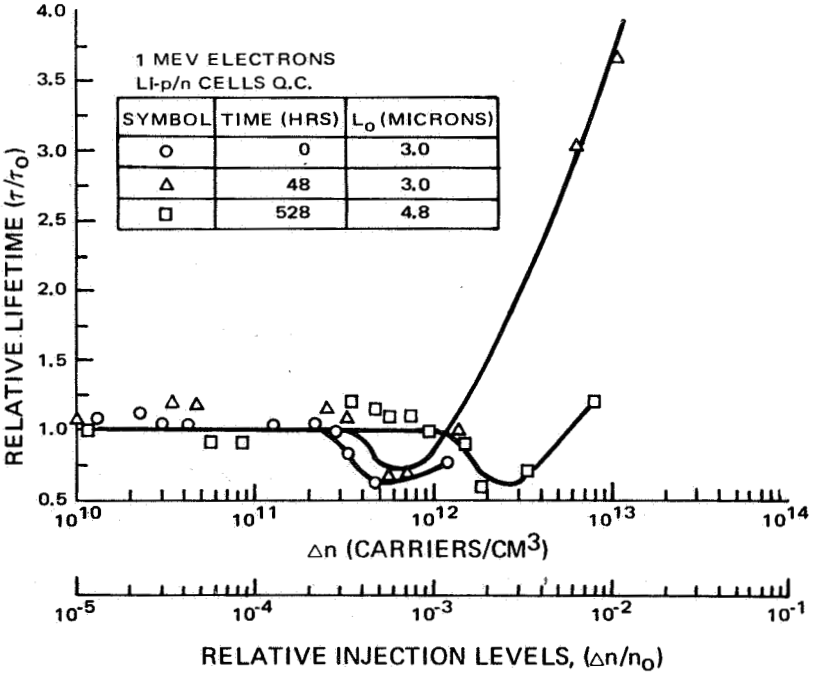

Figure 26. Relative Lifetime vs. Excess Carrier Density for Q.C. Cell Bombarded by 1-MeV Electrons

average value indicated by the error flags. The relative lifetime τ/τ_0 for the p/n cell increases linearly with $\Delta n/n_0$, indicating that within the range of $\Delta n/n_0$ used in the experiment, only a single defect level model is required. This is not the case for the n/p cell results. A model involving at least two energy-defect levels is required. A quantitative comparison of these data on neutron-damaged solar cells with those of Reference 24 for silicon irradiated by neutrons was made. This comparison showed than an increase in τ/τ_0 occurred with lower values of Δn in the solar cells than in the silicon. Thus, in both electron- and neutron-irradiated control cells a consistently more sensitive dependence of τ/τ_0 on excess-carrier density was observed. The average τ/τ_0 values of six lithium cells vs. $\Delta n/n_0$ are shown in Figure 28. The familiar decrease in τ/τ_0, observed before in the electron experiments, is also observed in Figure 28. It seems clear that lithium is responsible for the decrease in lifetime with injection level at $\Delta n \approx 10^{12}$ cm^{-3}. However, the neutron results differ from the electron results since there is a significant increase of lifetime at the higher injection levels. As time passed, interaction of lithium with defects altered the dependence of τ/τ_0 on $\Delta n/n_0$ so that a decrease in τ/τ_0 no longer occurred in the $\Delta n \approx 10^{12}$ cm^{-3} region.

D. RESULTS OF PRESENT WORK

The effects explored in the work described above were examined both in cells made or received in the present contract period and in selected GFE cells which had previously been irradiated or are now under surveillance for stability.

1. Lithium-Doped Test Diodes

Dependence of relative lifetime on excess carrier density in newly fabricated Li-doped test diodes after irradiation by 10^{15} e/cm^2, are shown in Figure 29. Time after irradiation is the parameter. Cell A-2-2 (10 ohm cm) has an effective lithium doping-density of 7 x 10^{13} cm^{-3} in the junction region (after correction for the phosphorus background). This cell exhibited a dependence of τ/τ_0 on Δn similar to a lithium-free control cell, for high Δn, as shown in Figure 24. Capacitance measurements made after completion of the injection-level experiments confirmed the fact that free lithium was depleted in the junction region of the cell. The diode exhibited the decrease of τ/τ_0 with Δn at low levels which appears to be characteristic of cells containing lithium while no recovery of L_0 took place, minor changes in τ/τ_0 did take place. It should be noted that the average value of the low-injection level-diffusion length decreased. This was due to the damage incurred during the injection level measurements. Cell C-1-5 (30 Ω-cm) has an effective lithium density of $\approx 10^{15}$ cm^{-3} in the junction region. It showed a general decrease of τ/τ_0 with increasing Δn. The lifetime of cell A-1-2 decreased sharply with increasing Δn, thus showing a very large effect of the lithium defect on lifetime vs. Δn. From capacitance measurements, it also showed a temporal dependence of lithium-doping density (see Figure 7) which was significantly different from the GFE cells.

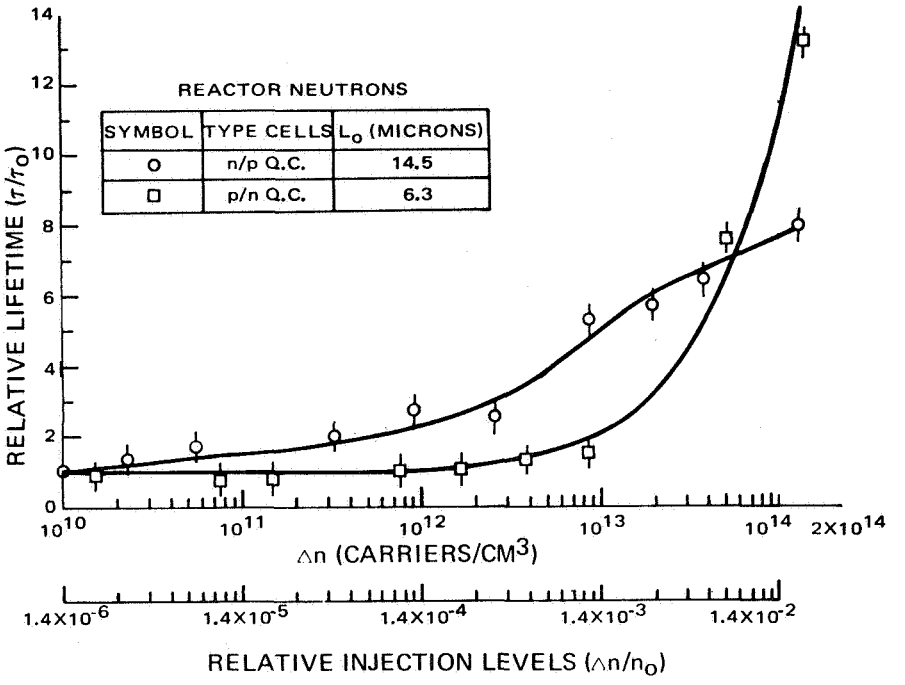

Figure 27. Relative Lifetime vs. Excess Carrier Density for Q.C. n/p and p/n Control Cells Bombarded by Reactor Neutrons

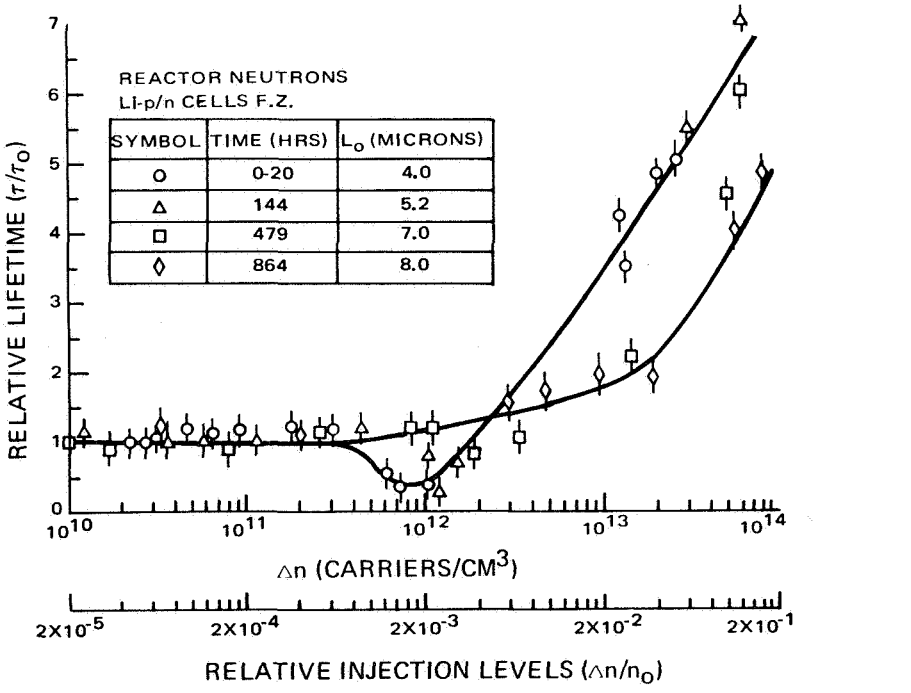

Figure 28. Relative Lifetime vs. Excess Carrier Density for F.Z. Cells Bombarded by Reactor Neutrons

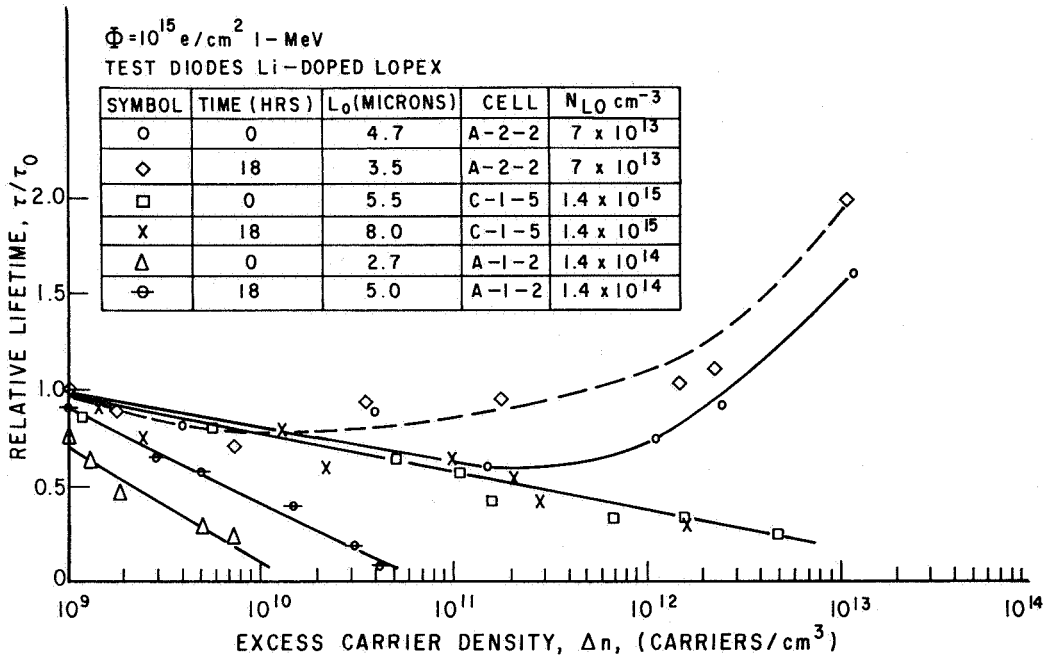

Figure 29. Relative Lifetime vs. Excess Carrier Density for Test Diodes Bombarded by 1-MeV Electrons

2. Long-Term Stability Cells

Three cells from the large group of cells in the long-term stability test were subjected to an injection level experiment — the characteristics of these cells are listed in Table V. Lithium was completely depleted in cell TI 167. Thus, only the phosphorus background was measured in the junction region by capacitance measurements. Cell TI 112 had doping levels only slightly in excess of its phosphorus background, thereby indicating significant lithium depletion. Cell TI 132 was found to have a high junction density of lithium (10^{16} cm^{-3}) which indicated a slight increase of lithium compared with the last measurement made on this cell in June 1967. The results obtained on these cells are shown in Figure 30. It is quite apparent that cells TI 167 and TI 112, with no or little lithium, behaved like standard lithium-free cells. They exhibit an increase of relative lifetime with increasing excess carrier density. Cell TI 132 shows the decrease of τ/τ_0 with increasing Δn, which is characteristic of cells containing lithium.

3. Government Furnished Cells

Three cells of a large group furnished by the government during the final contract period were studied by injection-level measurement after irradiation. Initial characteristics are shown in Table 3-2, Appendix B of this report. These cells were irradiated to 10^{15} e/cm^2. Curves of measurements taken immediately after bombardment and

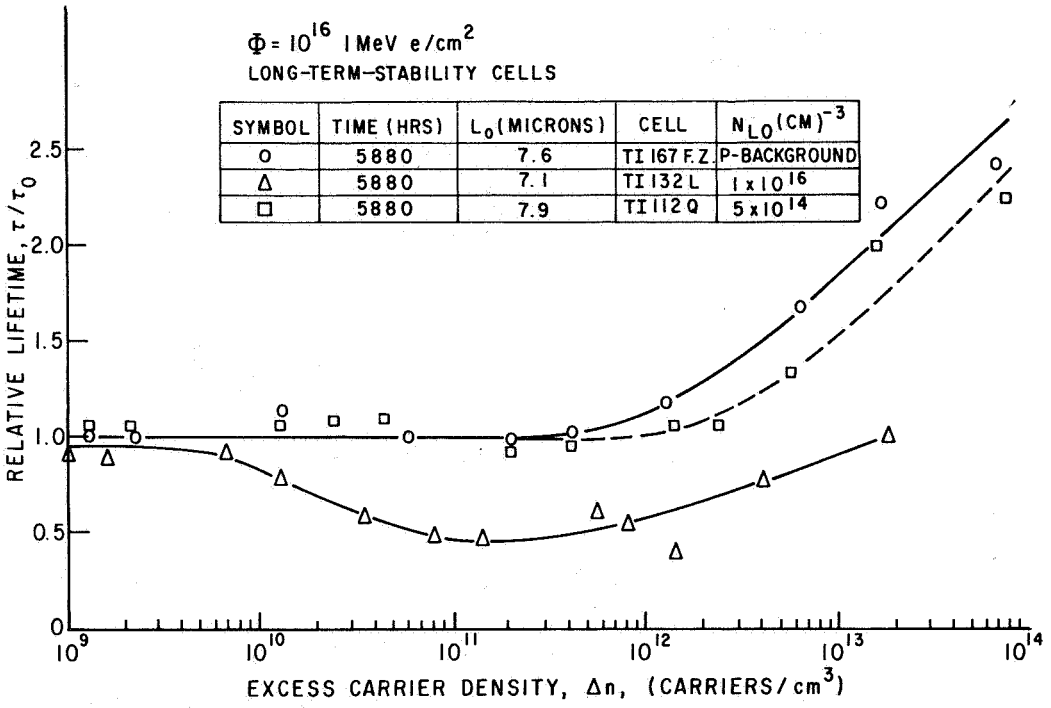

Figure 30. Relative Lifetime vs. Excess Carrier Density for GFE Stability-Study Cells Bombarded by 1 MeV Electron

42 hours later for all three cells are shown in Figure 31. Surprisingly, the cells did not show the characteristic decrease of τ/τ_0 with increasing Δn shown by both types of heavily irradiated lithium cells (F.Z. and Q.C.). Apparently, the concentration of lithium relative to the concentration of damage centers is important in determining the properties of the lifetime dependence on Δn. It appears from the time-dependence of the curves that lithium is interacting with damage centers, and the dependence on Δn is approaching the characteristic behavior of lithium in F.Z. cells as observed in Figures 25 and 29, at latter times namely, τ/τ_0 decreasing steadily with increasing Δn.

The accuracy of the injection-level measurements can be estimated for those measurements which involved a group of similar cells neutron-irradiated n/p, p/n, and Li-p/n cells) or those measurements on cells which were repeated a number of times (electron-irradiated Q.C. and F.Z. control cells). This latter situation occurred only for lithium-free cells since the behavior of Li-doped cells is time-dependent and each measurement represents a different condition of the cell. Average values of a cell group and the rms errors were calculated for the aforementioned cases and the error flags are indicated on the Figures. This calculation allows some degree of confidence in the curves shown in the figures. However, the results on the group of three GFE cells shown in Figure 31 were not averaged, but the data points from all four cells of this group were plotted; then a curve was drawn which fit best all the data points. Both methods of averaging the results

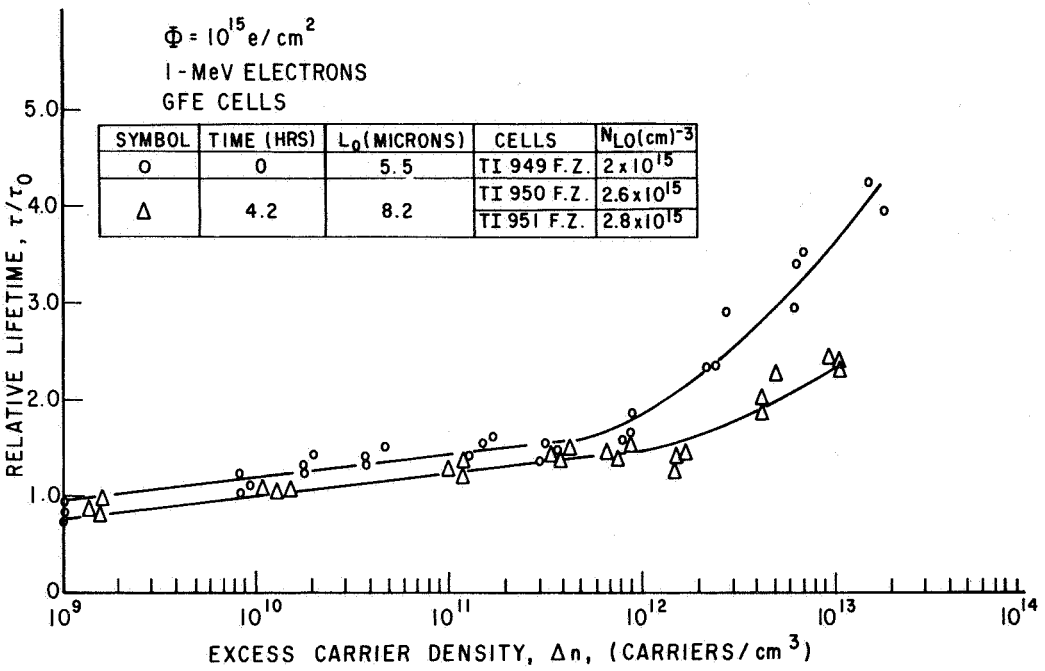

Figure 31. Relative Lifetime vs. Excess Carrier Density for GFE Cells Bombarded by 1-MeV Electrons

yield significant curves. It was more convenient to use an average value at each point for the neutron-irradiated cells because of the larger number of cells in the experiment. The curves for those cells where the estimate of error was not possible are uncertain and are shown only to indicate the general trend of the data.

E. CONCLUSIONS

The experimental evidence suggests that lithium interacting with radiation-induced vacancies and/or acceptor-like damage centers, produces a very efficient recombination center. The recombination statistics of this center exhibit a relative lifetime τ/τ_0 which decreases with excess-carrier density. In addition, this decrease of τ/τ_0 commences at very low Δn (excess-carrier density) indicating that the energy level or levels corresponding to the Li-damage center are deep in the forbidden gap (e.g., a level at E = 0.4 eV would strongly affect τ/τ_0 when $\Delta n \approx 10^{12}$ carriers/cm^2).

For the low fluence levels used in the present work, the interaction of lithium near the junction with the radiation-induced defects is immediately evident. This was especially true in the case of cell A-1-2 where the defect density induced by the irradiation ($\phi = 10^{15}$ e/cm^2) was approximately equal to the lithium concentration near the junction. This is based on the assumption that the density of recombination defects is equal to the introduction rate, η_{CR}, for carrier removal. A value of $\eta_{CR} \approx 1$ cm^{-1} was measured for cell A-1-2. Recovery of cell A-1-2 appears to reduce the slope of τ/τ_0 vs. Δn but τ/τ_0 is still very small at high values of Δn.

The injection-level dependence of cell A-1-2 differed from the other test diodes and GFE cells. This difference in behavior was also found in the capacitance measurements of the lithium-concentration profile as a function of time after irradiation (Section IV.B). The capacitance measurements showed that both the decrease in lithium concentration gradient and the decrease in lithium concentration were large. In the case of the GFE cells, the interaction of lithium with the radiation-induced defects was not immediately evident. The fluence value was below the lithium doping-value and capacitance measurements show that the lithium concentration gradients are not significantly changing. The evidence for the "C"-cells confirmed the "A"-cell behavior. Initial concentration of lithium in the "C"-cells was slightly greater than A-1-2. However, the dependence of τ/τ_0 on Δn was not as sharp as in the "A" cell. This was expected since the level of damage in the "A"-cell was greater than in the "C"-cell. Capacitance measurement of lithium-concentration gradients indicated that large changes of the gradient also took place in the "C"-cells as a function of time after irradiation. Thus, it seems that a large change in lithium distribution takes place in cells where the magnitude of the dependence of τ/τ_0 on Δn is also large. There is still no clear explanation why the density-gradient change for the test diodes differed from the GFE cells. Further experiments are required before a factual explanation can be offered.

The cells in the long-term stability test provided some interesting results. Clearly, cells TI 167 and TI 112 behaved as expected: cell TI 167 was found to be totally depleted of lithium and the dependence of τ/τ_0 on Δn was in agreement with the results obtained on a lithium-free control cell from the same source of silicon, as shown in Figure 24. Annealing has stopped in this cell and a large amount of residual damage remains. These unannealed defect centers cause the dependence of τ/τ_0 on Δn that is observed. In the same way, cell TI 112 was found to have only a small concentration of lithium remaining. Some annealing has occurred in this cell since the last reported measurement in June, 1967 (see Table V). Again, the behavior of the cell is in agreement with the dependence of τ/τ_0 on Δn measured for a control cell made from quartz-crucible silicon (see Figures 24 and 26). The residual damage (probably unannealed A-centers) in this cell causes the injection level response observed for an ordinary lithium-free cell. Cell TI 132 was unusual since the lithium or donor concentration was found to be quite high (10^{16} cm^{-3}) and yet no increase in cell performance is evident since the June 1967 measurement. The dependence of τ/τ_0 on Δn shows the usual evidence of lithium interaction with radiation defects. It is surprising that, after this long period of time (5880 hrs) this characteristic dependence on injection level still exists because one would have expected the annealing of all lithium defects to be completed. At the present time it can only be said that a correlation seems to exist between the temporal variation of the lithium distribution and the dependence of τ/τ_0 on Δn. Thus, the effect of the electric field in the junction region on recombination statistics and on the recovery characteristics of damaged cells is important in understanding the role of lithium in solar cells. It is now apparent that capacitance measurements should be closely correlated with any other type of measurement on solar cells made during the remaining part of the present project.

The existence of injection-level effects in lithium-doped solar cells suggests that measurements of short-circuit current made only at high light levels (e.g., 100 mW/cm^2 of tungsten light, producing $\approx 10^{14}$ carriers/cm^3) can lead to erroneous conclusions. Short-circuit current I_{sc} is related (Ref. 25) to diffusion length by

$$I_{sc} = C \frac{L_o/\lambda}{1 + L_o/\lambda} \tag{16}$$

where C is some constant and λ is the wavelength of the light source. If injection level effects are operating, then I_{sc} is not simply related to the low-injection-level diffusion length, L_o. The constant C is no longer a constant but some function of time. Thus, for this and other reasons high-light level measurements will not always be accurate for measuring changes in minority-carrier lifetimes. This is particularly true for lithium-doped solar cells. The continued use of pulsed or steady-state electron-beam measurement methods with their wide dynamic range and uniform absorption property is advisable although cross-checks of such measurements with light measurements should still be made.

F. RELATION OF PHOTOVOLTAIC OUTPUT AND DIFFUSION LENGTH IN LITHIUM CELLS

Figures 32 and 33 show plots of diffusion length, as measured by electron-voltaic method versus short-circuit current density, as measured for filtered tungsten light set to 100 mW/cm^2. The line drawn on the figure is the empirical dependence found in 1963 by Denney et al (Ref. 26) (quoted in Cooley and Barrett, NASA Special Publication SP 3003 p. S) for non-lithium commercial solar cells under similar measurement conditions. Figure 33 includes some data for the same lithium cells before irradiation, after irradiation, and during recovery, which adds some internal consistency to the data.

It will be noted that the data falls entirely below the line. This would suggest that, in general, it is possible to make lithium cells of higher efficiency than those made out of the same material but without the lithium doping steps. This argument, however, is somewhat weakened by the presence of three points for control cells which do not contain lithium but still lie well below the line.

The conclusion that can be drawn from the data is that within closely related groups of cells the diffusion-length measurement for unirradiated solar cells can be used to give a prediction of tungsten-light photovoltaic performance, using a conversion formula similar to, but not exactly the same as that for non-lithium cells and giving an accuracy no greater than 5%. The dependence is as before, logarithmic (average is $J_{sc} \sim 15.5 \log_{10} L$).

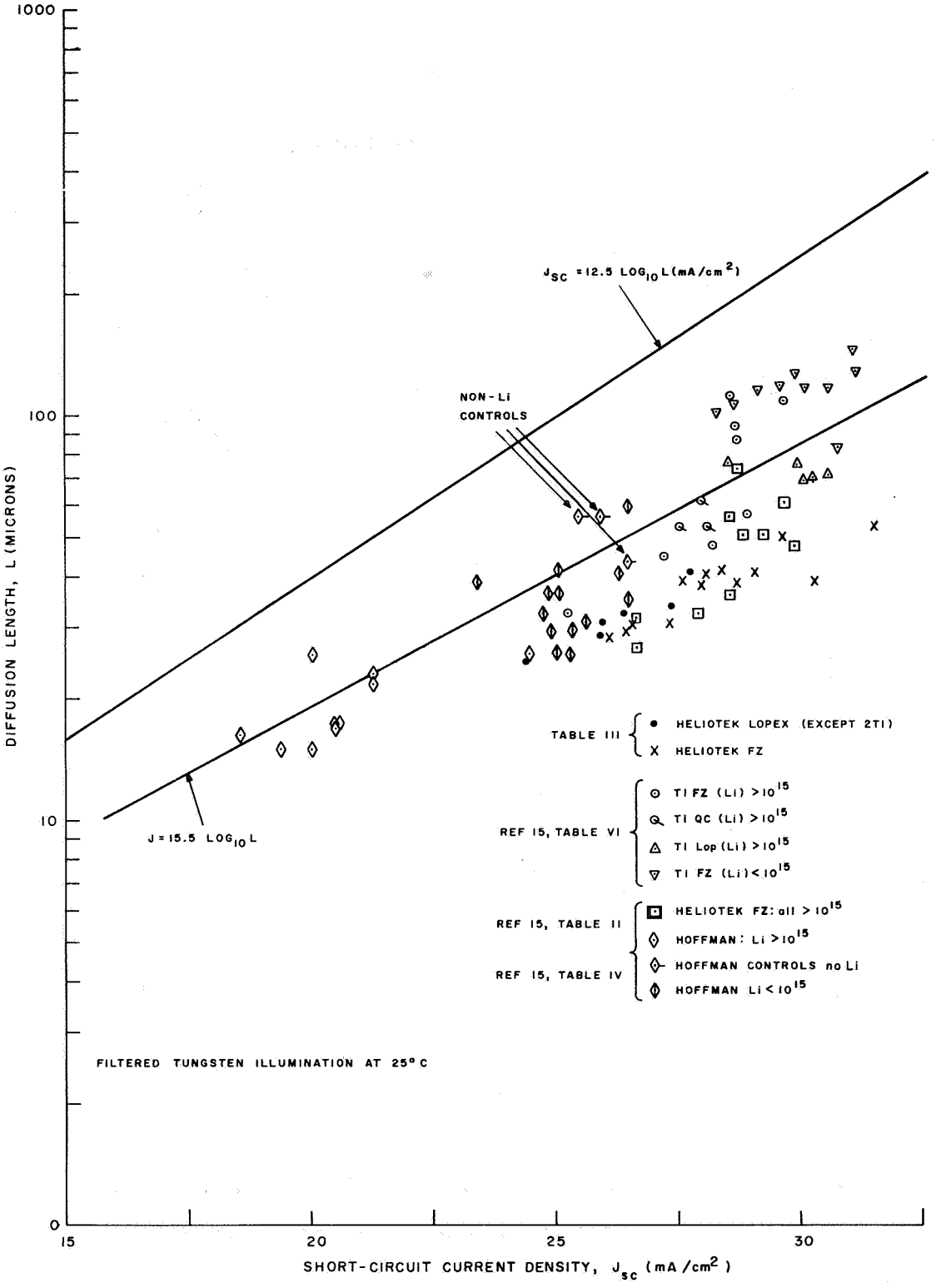

Figure 32. Diffusion Length as a Function of Short-Circuit Current for Unirradiated GFE Cells

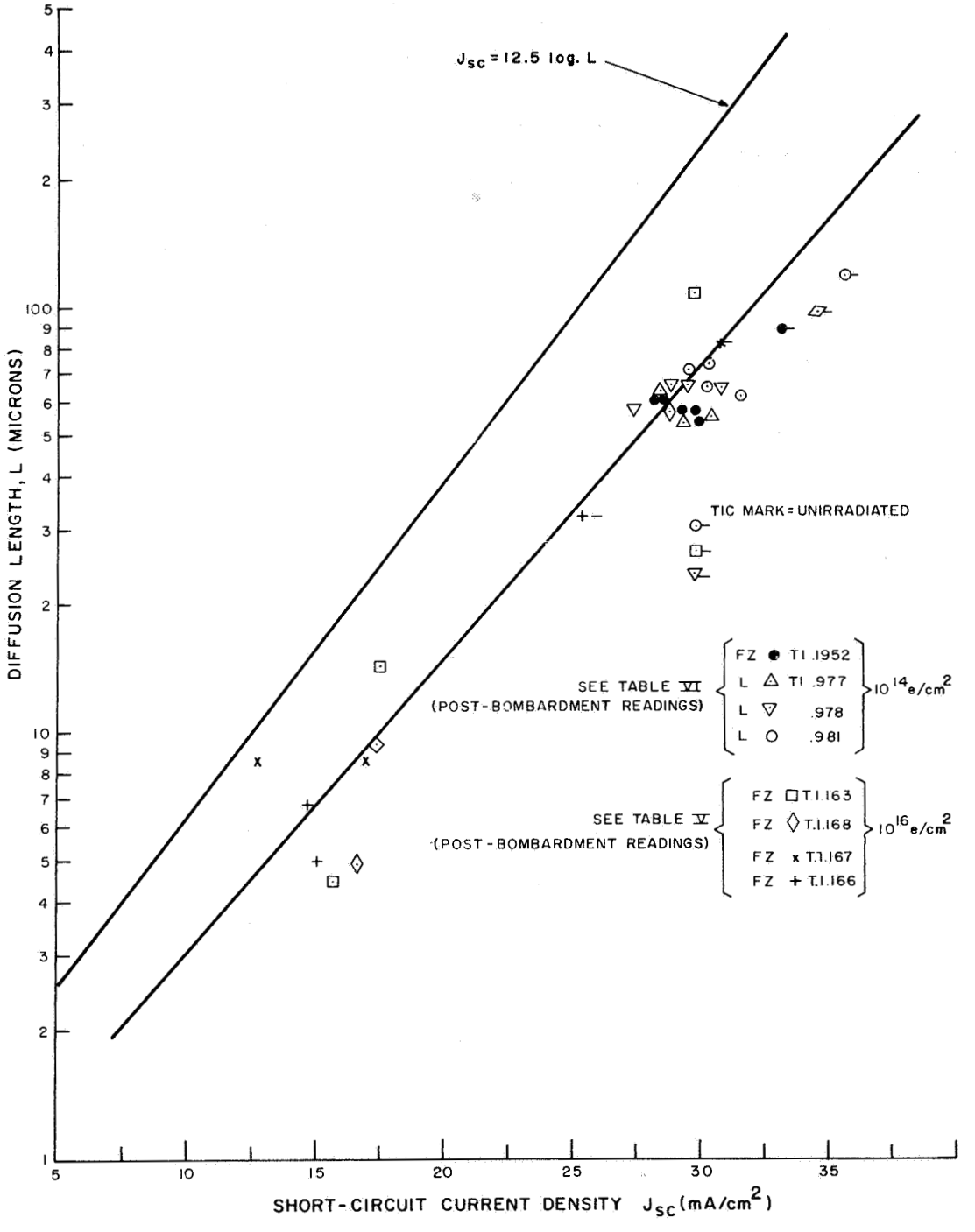

Figure 33. Diffusion Length as a Function of Short-Circuit Current for GFE Cells Before and After Irradiation by 10^{14} e/cm^2 or 10^{16} e/cm^2

Theory predicts that it may be unsafe to extrapolate from diffusion length to short-circuit current in lithium-containing cells; since, as for neutron and proton damage, the diffusion length for lithium solar cells, as measured at low injection levels (the condition under which the routine electron-voltaic measurements quoted here are done) is not necessarily the same as that measured at high injection levels, such as those existing for a 100 mW/cm^2 tungsten-light measurement. However, both in the case of the heavily and the lightly irradiated lithium cells shown, the degradation caused by irradiation caused the data points to move down a curve parallel to the logarithmic dependence curve quoted above. Thus, if due caution is used predictions of short-circuit current or maximum-power degradation can be made from data on diffusion-length degradation in lithium solar cells. This is fortunate, since it paves the way for wide flexibility in test-device design, and makes it possible to relate the behavior of minority-carrier lifetime in bulk samples to that of cell-performance parameters.

SECTION VI
HALL, RESISTIVITY, AND LIFETIME MEASUREMENTS

A. INTRODUCTION

The first set of Hall bars were fabricated but, unfortunately, the lithium-diffusion failed; the bars contained little or no lithium, and the diffusion process had to be repeated. This second diffusion was successful and all of the bars were sufficiently doped with lithium for the measurement program. However since the end of the contract period approached, there was not enough time to commence these measurements. Instead, a control sample, made from 30 Ω-cm Lopex silicon was placed in the Hall apparatus and a probing series of measurements were completed (test diodes labelled with the letter C were made from the same crystal as the "C" test diodes, see Section II). These initial measurements were valuable in troubleshooting the apparatus and defining experimental procedures. The results obtained with this control sample will be presented in the paragraphs that follow.

B. DESCRIPTION OF THE EXPERIMENT

The dimensions of all the Hall bars were approximately the same and are indicated in Figure 34. Ohmic contacts were made to the bars by alloying with an arsenic-tin mixture. Final connection to the alloy dot was made by soldering one end of a fine wire to the dot with indium and the other end to the indium-tinned gold pattern on the ceramic substrate. The gold pattern was fixed to the ceramic substrate by the standard molybdenum silk-screen process. A thermally conductive epoxy was used to attach the Hall bar to the ceramic substrate and the ceramic substrate to the copper plate. Six leads of 0.005 inch diameter formvar wire were soldered to the six points of the bar as shown in Figure 34. A copper-constantan thermocouple was cemented to one of the arms of the bar with thermally-conductive cement. Molybdenum strip heaters mounted on the cold finger were used to vary the temperature of the Hall bar from the temperature of liquid nitrogen to ambient.

Defects responsible for carrier removal were measured by monitoring the Hall coefficient and resistivity. Concurrently with these measurements an attempt was made to measure the lifetime of minority carriers in the Hall bar. This was accomplished by running the Van de Graaff generator in the pulsed mode, and observing the decay of conductivity induced by the pulsed electron beam. It is important to establish whether the defects responsible for carrier removal are also responsible for degradation of lifetime. A concurrent measurement of lifetime on the Hall bar as a function of measuring and bombardment temperature should provide the experimental evidence sought.

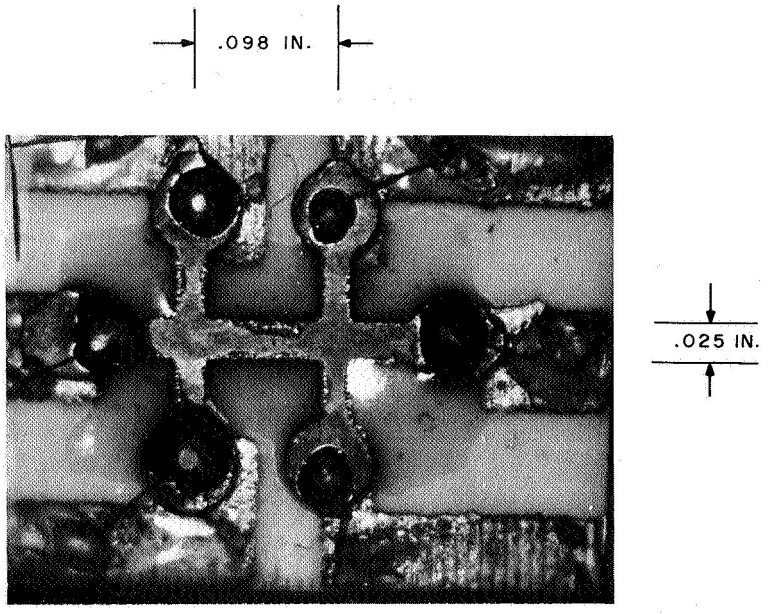

Figure 34. Hall Bar Mounted with Contacts on Alumina Wafer

C. RESULTS OF HALL MEASUREMENTS

The conductivity, σ, of the control sample before and after bombardment by 1.9×10^{16} e/cm^2 is shown in Figure 35 as a function of reciprocal temperature. Sample temperature during bombardment was 100° K. Vook, Stein, and others (Refs. 27, 28, and 29) have shown that there are two types of carrier-removal defects introduced by electron bombardment in n-type silicon at temperatures in the 80° K region. These defects were identified as ITI (irradiation-temperature independent) and ITD defects (irradiation-temperature dependent). As the name implies, the rate of formation of the ITI defects are not dependent on the irradiation temperature; in addition, rates are not influenced by the impurity content of the silicon. For ITD defects, rates of formation are dependent on the temperature and the impurities in the silicon. It should be noted that the above statement does not imply that, as the sample is warmed up after irradiation, both ITD and ITI defects do not alter their form or anneal. In the experiment described here both types of defects were produced. A more detailed explanation of the connection to this program will follow in the discussion of results.

The prebombardment conductivity measured at high temperature exhibits the expected behavior of conductivity dominated by lattice-scattering mobility. At lower temperatures, the loss of carrier density determines the behavior of conductivity. After bombardment, the conductivity decreased sharply with decreasing temperature.

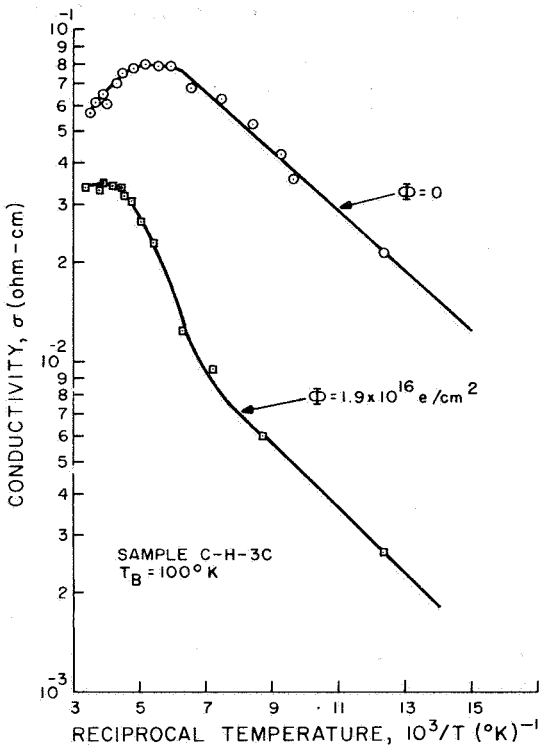

Figure 35. Conductivity of Control Sample C-H-3C Before and After Bombardment by 1.9 x 10^{16} e/cm^2

It was expected that the carrier-removal rate, η, would be an order of magnitude lower than the value measured for a room temperature bombardment. Therefore, in these initial measurements for the purpose of establishing experimental procedures and determining experimental difficulties, a high fluence level of 1.9 x 10^{16} e/cm^2 was chosen. Time did not permit a stepped increase of fluence to be used. A stepped increase of fluence, starting at a low level, will have to be used with the lithium-doped samples, since the authors are not aware of any published data for the temperature dependence of the Li-V defect production rate. It will be shown later that this type of basic information will provide a test of the Vook-Stein model (Refs. 27 and 28) for defect production and will also provide details on the mechanism of Li-V defect formation.

It should be noted that implicit in the method of measurement was the complication of defect annealing as the temperature of the sample was increased. The ITI defects anneal out in the temperature range from 100 to 200° K and the ITD defects anneal at all temperatures. Future measurements will be planned to carefully separate both types of defects by annealing procedures and thus obtain the primary production rates of each type of defect.

The carrier density can be calculated from the Hall coefficient given by

$$n = \frac{1}{qR_H} \frac{\mu_H}{\mu_c} \quad \text{carriers/cm}^3 \tag{17}$$

where

n	is carrier density
R_H	is Hall coefficient
q	is electron charge
μ_H	is Hall mobility
μ_C	is conductivity mobility

The Hall measurements were converted to carrier densities assuming μ_H/μ_C is ≈ 1 and that it does not change with radiation. In these measurements the change in μ_H after bombardment was large and this assumption is poor for the post-bombardment situation. The results are shown in Figure 36. There is nothing unusual about the behavior of n before bombardment. However, the post-bombardment is strange but explainable. The sample was bombarded at an equilibrium temperature of 100° K then then cooled to 81° K at which point the first measurement was made. The ITI defects fects annealed out as the measuring temperature was raised from 81° K to room temperature. It was observed that the sign of the Hall coefficient indicated that the sample was p-type silicon for the temperature range from $10^3/T = 12.3$ to 7 (this region is indicated by dashed curve). Then the silicon type reverted to n-type at the next higher measuring temperature ($10^3/T = 6.3$). Thus, the net carrier concentration changed from acceptor-like to donor-like as the temperature was increased. At some temperature, the net carrier concentration should have reached the intrinsic level as it passed from acceptor to donor. This effect was not detected in these measurements. The original sample was lightly doped with phosphorus and the large fluence could easily convert the sample to p-type at some temperature. The Hall mobility μ_H is calculated from

$$\mu_H = \frac{R_H}{\rho} \tag{18}$$

where ρ is the resistivity in Ω-cm. These results are shown in Figure 37. The dashed curve represents the results of Logan and Peters (Ref. 30) for the lattice mobility dependence on temperature. It appears that the prebombardment Hall mobility follows this dashed curve closely except for the lowest temperatures. At these low temperatures, it appears that the mobility is dominated by another scattering mechanism, for example ionized impurity scattering. It should be recalled that for the lowest three measuring temperatures the post-bombardment sample behaves as p-type silicon rather than n-type. The prebombardment sample behaved as n-type silicon at all temperatures.

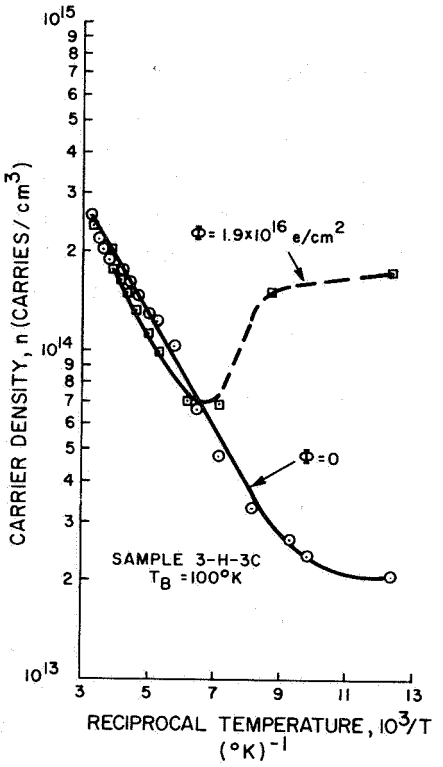

Figure 36. Carrier Density of Control Sample C-H-3C as a Function of Reciprocal Temperature, Before and After Bombardment by 1.9 x 10^{16} e/cm^2

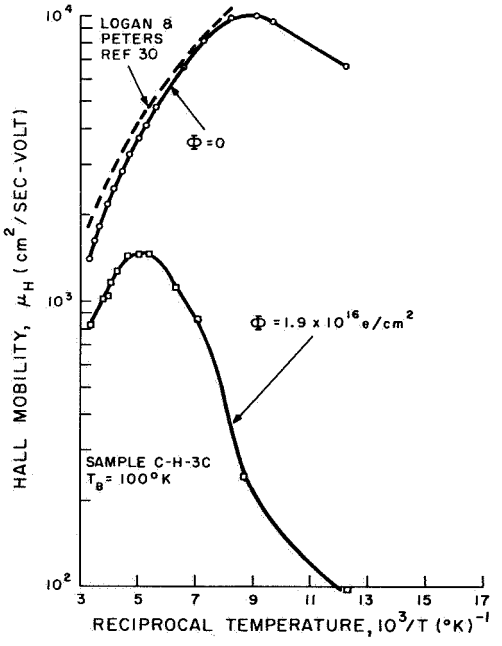

Figure 37. Hall Mobility as a Function of Reciprocal Temperature for Control Sample C-H-3C Before and After Bombardment by 1.9 x 10^{16} e/cm^2

D. RESULTS OF LIFETIME MEASUREMENTS

The electronic system required to present the conductivity decay curve on an oscilloscope is still being developed. The absolute values obtained in these preliminary experiments may be in error, however, general trends are still valid. The results showed that the lifetime of the prebombardment sample, measured at 81° K was greater than the lifetime of the damaged sample. The values were 0.46 microseconds before and 0.2 microseconds after bombardment at a temperature of 81° K. The room temperature values were 0.9 microseconds before bombardment and 0.2 microseconds after bombardment, which is inconsistent with the low-temperature result. The form of dependence of lifetime on temperature indicated the presence of traps since the apparent lifetime increased with decreasing temperature, as is expected for a situation dominated by traps. This trend reversed itself as the temperature decreased to 81°K. Recombination lifetime uncomplicated by trapping effects would decrease with decreasing temperature approaching a limiting value τ_{po}, where τ_{po} is the low-injection level lifetime of holes in n-type silicon. This behavior was observed for the pre- and post-irradiated sample and showed the presence of a high density of short-lived traps in in this particular sample. The lowest beam current used was 4.5 microamperes, which corresponds to an injection level of approximately 5.5×10^{11} carriers/cm^3 or a $\Delta n/n_o$ of 2×10^{-3}; the highest beam current used was one milliampere. The injection-level dependence was measured at several temperatures and, in all cases, the lifetime increased with increasing injection level. This is the behavior reported in the literature for n-type silicon (quartz-crucible) bombarded by 1 MeV electrons, while, in Section V. E of this report, it is shown that injection-level dependence of lithium-free p/n solar cells made from quartz-crucible and float-zone silicon showed an increasing lifetime with injection level under constant beam-current excitation.

E. DISCUSSION

The ITI defect has been identified as a non-reorientable divacancy which anneals when the temperature of the irradiated silicon is increased from 100 to 200°K. The second type of defect is dependent on bombardment temperature and impurity content. Thus, the A, E, and the lithium defect centers fall into this category. Vook and Stein's model for the production of ITD defects is based on the production of a close metastable pair consisting of an interstitual and vacancy. The total probability of defect formation is given by Eq. (19).

$$P_t = \left[1 + \gamma \exp\left(\frac{E_L - E_R^o}{kT}\right)\right]^{-1} \left[1 + g \exp\left\{\frac{E_F(n, T) - E_M}{kT}\right\}\right]^{-1} \qquad (19)$$

where

δ is the ratio of the statistical weights of the jump of the mobile atom or vacancy that annihilates a vacancy interstitial pair to the jump that leads to further separation of the pair

E_L is the energy barrier to the separation or liberation

E_R^o or E_R^+ are energy barriers to recombination of the pair when in charge states designated by the "o" or "+" signs

g is ratio of the number of ways the state can be occupied to the number of ways the state can be unoccupied

$E_F(n, T)$ is the Fermi level for electrons

n is electron concentration

T is absolute temperature of the sample

E_m is the energy level of the metastable interstitial-vacancy pair

It is the second term of Equation (19) which introduces a dependence on the impurity concentration. The energy level of the lithium donor in silicon is located at 0.03 eV below the conduction band, as opposed to 0.05 eV for phosphorus.

Thus, the temperature dependence of damage due to the production of carrier-removal defects should be quite different for the two donors, especially at low temperatures. This fact was pointed out by Watkins (Ref. 31) at the Santa Fe Conference on Radiation Effects in Semiconductors. Basic to our understanding of radiation damage in lithium-doped solar cells is an understanding of the production of the primary lithium-vacancy defect before the annealing process by free lithium takes place.

From the measurements of conductivity and carrier density, it appears that the production rate of carrier-removal defects measured at room temperature is considerably reduced at low bombardment temperatures, as was expected. However, the decrease of mobility was surprisingly high over the entire range of measuring temperatures. The pre-irradiation dependence of μ_H on the reciprocal temperature is in close agreement with the lattice scattering mobility values of Logan and Peters (Ref. 30) over most of the range of measuring temperatures. At the low temperatures, the scattering mechanism changed, and a decrease of mobility with decreasing temperature occurred. Impurity scattering will produce

this type of temperature behavior. The post-irradiation mobility showed a decrease by a factory of 1.7 in the room temperature value, and the change to impurity-like scattering occurred at a higher temperature. It should be noted that the mobility is a parameter which is derived from the measured values of the conductivity and the Hall coefficient.

The complicated behavior of the carrier concentration, n shown in Figure 36 emphasizes the need for careful planning of experimental procedures. As previously discussed, the sample was irradiated at a temperature of 100° K then allowed to cool down to 81° K where the first Hall and resistivity measurements were made. Then the temperature was raised and the next measurement at $10^3/T = 8.7$ was made. The ITI defects anneal out over a temperature range from $10^3/T = 10$ to 5 and approximately 40% of these defects are unannealed at a temperature of 140° K ($10^3/T = 7.1$), based on the length of time required to make the measurements. Thus, the change of n with increasing temperature shows the annealing of ITI defects. In addition, it was observed that the sign of the Hall coefficient indicated that that positively charged carriers were predominant over the temperature range from $10^3/T = 12.35$ to 7.1. At $10^3/T = 6.3$ the sign of the Hall coefficient changed, indicating conduction by negatively charged carriers as in the pre-bombardment measurements. Obviously sufficient defects of an acceptor nature were introduced by the irradiation to alter the compensation that existed at low temperatures. ITI defects are believed to be divacancies and doubly charged. Therefore, the mobility will be strongly affected since it is inversely proportional to the square of the charge on the scattering center. The carrier removal rates for electron irradiation of quartz-crucible silicon at an energy of 1 MeV and a temperature of 81° K are given in Reference (28) as 0.02 for ITI and 0.04 cm^{-1} for ITD defects. Our results indicate a lower rate if the total number of defects produced by 1.9×10^{16} e/cm^2 is assumed equal to the carrier density measured at 81° K. Since the sample was made from Lopex silicon, the production rates of ITD defects should be higher than a sample made from quartz-crucible silicon because every E-center removes two electrons from the conduction band compared to one removal by the A-center. However, it was pointed out in Reference (20), that carrier-removal production rates measured in samples of Lopex silicon varied from sample to sample and were not reproducible. This lack of reproducibility was attributed to the variation of oxygen concentration in the samples. Thus, the production rate of carrier-removal defects in Lopex silicon can vary from a value slightly greater than the one for quartz-crucible silicon to the value obtained for float-zone silicon.

The lifetimes measured in this preliminary experiment show that this technique may prove successful in correlating the production of radiation-induced recombination defects with carrier-removal defects in lithium-doped silicon. It may also be used to monitor the Li-V defect annealing by heat and by lithium diffusion to the defect site at room temperature. These preliminary lifetime results were complicated by the presence of traps. This source of error will be eliminated in further experiments by the addition of a quartz-glass window to the Hall apparatus so that the sample can be illuminated during the measurements.

The following plan is thus proposed for the next experiment. By controlling the bombardment temperature, measurement of the basic defect production rates can be made. Using the present hypothesis (discussed in Section IV. A) of an LiV and Li_2V center, this adjustment of bombardment temperature will allow the observation of LiV center formation by diffusion of a vacancy to a lithium atom but prevent the approach of a second lithium atom since at 80° K, diffusion of lithium is effectively "frozen." Then, the sample temperature can be raised to room temperature and the interaction of free lithium with the LiV centers can be studied as a function of time. This technique eliminates the loss of information caused by the rapidity of recovery during bombardment at room temperature, and also permits a measurement of the basic carrier-removal rate. The parallel measurement of minority-carrier lifetime as a function of bombardment and measuring temperature will show whether the carrier-removal defects also act as recombination centers. This information is vital to the lithium-doped solar cell program since the radiation damage of these solar cells is caused by the degradation of lifetime through increased recombination of minority carriers at defect center.

SECTION VII

CONCLUSIONS AND RECOMMENDATIONS

A. CONCLUSIONS

The most significant findings resulting from this contract effort are as follows:

1. In a solar-cell diode at room-temperature under reverse bias the motion of lithium atoms can be observed by the junction capacitance technique. As a result, it is possible to estimate relative diffusion contents of lithium near the junction in different cells. This could lead to a non-destructive method for measuring the radiation sensitivity of a lithium cell.

2. It has been calculated that low lithium mobility may be desirable in preventing loss of lithium to the p-layer, and perhaps thereby preventing redegradation. Hence, the presence of oxygen or other species which bind lithium may be desirable in silicon for solar cells; damage near the junction due to boron diffusion at high temperature already appears to impede the loss of lithium to the p-layer.

3. Detailed measurements of lithium concentrations near the junction reveal widely differing donor concentration gradients in lithium cells.

4. The observation of changes in the donor concentration profile allows multiple measurements of carrier removal rates near the junction; this rate increases smoothly with lithium concentration.

5. Several observations confirm the theoretical expectation that the observed lithium concentration gradients in lithium cells can lead to significant drift-field effects on minority carriers.

6. Kinetic studies confirm the existing theory of action of lithium as a process controlled by the lithium diffusion rate. In addition, new, though as yet limited, evidence of a role for phosphorus in one of the Li-defect complexes has been found.

7. The use of an n-type starting material with fairly low resistivity can remove the problem of curve power factor degradation of photovoltaic efficiency at high fluences. This effect was postulated by Mandelkorn as being important in cells made from high-resistivity silicon and is due to the loss of lithium as a donor during irradiation and resulting increase in series resistance.

8. The importance to the properties of solar cells of the electric field caused by the distribution of lithium in the junction region of some significance.

9. A continued increase in performance characteristics was observed in cells made from quartz-crucible grown silicon and cells with an added-diffused-layer of phosphorus in the junction region

10. No diffusion-length redegradation was observed in a lightly irradiated set of test diodes made from Lopex silicon and monitored over periods of time ranging up to 154 days after bombardment.

11. Strong redegradation of performance characteristics was observed in a set of heavily irradiated cells, heavily doped with lithium which were monitored for a period of approximately one year.

12. The patterns of injection-level dependence in electron and neutron-irradiated lithium cells indicate that the lithium defect complexes, in each case, lie deep in the forbidden band-gap.

The recovery of test diodes and solar cells from radiation-induced damage was monitored by measuring minority-carrier diffusion length as a function of time after bombardment by 1-mev electrons. The electron fluences were 10^{13} and 10^{14} e/cm^2. Recovery characteristics were correlated to Waite's diffusion-limited theory for annealing with the aid of measurements of lithium density distribution and effective lithium diffusion constant for individual cells.

As predicted by Waite's theory recovery of GFE cells irradiated to fluences of 10^{13} and 10^{14} e/cm^2 has approximated first-order kinetics for these fluences, for which the defect concentration is much less than the lithium concentration. Although the bulk lithium densities of these cells are not known the best estimates (several times 10^{16} cm^{-3}) give reasonable values (tens of angstroms) of capture radius. Recovery characteristics of test diodes (made in-house) after fluences of 10^{13} e/cm^2 also correlate well with theory when the appropriate values of lithium density and lithium diffusion constant are inserted in the recovery equation. Recent capacitance measurements have determined that the lithium concentration at the edge of the depletion region is at least an order of magnitude below the average bulk lithium density. These measurements show a steep density gradient and indicate that, for most cells tested, the bulk lithium density is reached at a distance about 10 microns from the junction. Consequently, after light irradiations, $\phi \approx 10^{13}$ e/cm^2 where the post-bombardment diffusion length is greater than 20 microns, the lithium density pertinent to annealing kinetics is the bulk lithium density, not that at the edge of the depletion region as was assumed in some previous reports on this contract. This was verified by the good correlations between experimental recovery curves and theory when bulk lithium density is used. Comparison of lithium density profiles before and after several irradiations to a fluence of 10^{13} e/cm^2, and in several cases to 10^{14} e/cm^2,

showed that lithium concentration was not severely affected by irradiation to such fluences. However, density profiles taken periodically on cells experiencing no irradiation between measurements showed significant spontaneous changes (usually increases) in lithium density, indicating that mass motion of lithium was taking place in the cells, even under zero bias. The application of reverse bias for tens of hours showed that this mass motion near the junction could be greatly enhanced by applying a voltage across the junction.

Measurements of capacitance change in the latter cases enabled measurement of effective lithium diffusion constants in the region near the junction. Some of the readings, especially in Lopex cells gave diffusion constants well below (up to a factor~50) the diffusion constant expected for free lithium in bulk Lopex silicon. At the same time, the experimental annealing curves correlated with theory only when the free lithium diffusion constant was used, thus indicating the possibility of a strong reduction of the diffusion constant of lithium near the surface, due perhaps to crystal defects or impurities introduced during boron diffusion or other high-temperature proccesses during cell fabrication. If local reduction of lithium diffusion constant does occur near the junction, this effect could be very useful in reducing the flow of lithium across the junction and into the p-region. This could be important in prolonging high-temperature storage life of the cell. Comparison of recovery curves for cells with 10Ω-cm phosphorus-doped starting material with those with higher starting resistivity, i.e., lower phosphorus density, gives, for the first time, direct evidence that the phosphorus-vacancy defect or E-center may be one of the predominant defects in lithium doped p/n solar cells and may be involved in a reaction with lithium. The stability of electrical properties in test diodes and solar cells, both before bombardment and after recovery from bombardment by 1-mev electrons, was evaluated. Test diodes were of 1, 10, and 30 ohm -cm Lopex and float-zone silicon, and of 12 to 16 ohm -cm quartz crucible silicon. Most of the GFE solar cells were made from 20 ohm -cm float-zone silicon, although several cells of other starting resistivities and silicon type were also tested.

Diffusion length measurements on 15 unirradiated test diodes over a four-month period show that only three cells decreased beyond the calculated maximum experimental error of the measurement (10%). Thirty-two GFE cells were tested for preirradiation stability of diffusion length and photo-response over a four month period. All of the readings remained constant over this period with the exception of two decreases (23% and 9 %) and one increase (17%) in output power.

Similar diffusion-length and photo-response measurements were made on GFE cells irradiated to varying fluences from 10^{14} to 10^{16} e/cm^2. These post-irradiation tests have been carried on for times ranging from ~4 to 14 months. Of four float zone cells tested for 14 months after 10^{14} e/cm^2 fluence, one cell has degraded significantly in power output, from 8.0 mW/cm^2 soon after recovery to 4.4 mW/cm^2 eleven months after recovery. The other three cells continued to show good post-recovery stability.

Seventeen cells, twelve float-zone, three Lopex, and two quartz-crucible, have been monitored for approximately one year since bombardment to a fluence of 10^{16} e/cm^2. On all except four of these cells, the photo-response power output is either steady or continues to increase. The four cells with heaviest lithium doping, three of which are Lopex cells, have shown marked re-degradation, the output of one of the cells decreasing to a level equalling that of~1 hour after bombardment.

Four 20Ω-cm float-zone cells irradiated to 10^{15} e/cm^2 have shown good stability over a four-month period since recovery. Four cells, one of 20Ω-cm float-zone silicon and three of 200Ω-cm Lopex silicon were monitored for four months after being irradiated to a fluence of 10^{14} e/cm^2. The float zone cell and one of the Lopex cells have maintained a constant output power since recovery. The other two Lopex cells have shown decreases in output power of 10 and 18%.

Experiments to determine the dependence of diffusion length or lifetime on excess carrier density suggest that lithium interacts with radiation-induced vacancies and/or acceptor-like damage centers to produce a very efficient recombination center. The recombination statistics of this center exhibit a relative lifetime which decreases with excess-carrier density, and this decrease of τ/τ_0 commences at a low value of Δn ($\Delta n \approx 10^9$ carriers/cm^3 excess-carrier density). Assuming that Shockley-Read recombination statistics are applicable in solar cells, this sensitivity of τ/τ_0 to small values of Δn indicates that the energy level or levels corresponding to the lithium-damage center are deep in the forbidden gap (e. g. , a level at E = 0. 4 eV would strongly affect τ/τ_0 when $\Delta n \approx 10^{12}$ carriers/cm^3). The strong dependence of lifetime τ, on excess carrier density, Δn, should engender caution when predicting outer-space sunlight efficiencies in solar cells from low-injection-level diffusion-length data. On the other hand, comparisons of 100 mW/cm^2 tungsten light response with low-injection-level diffusion lengths in many of the GFE cells received indicate that the normal logarithmic relation of these two quantities holds within a few percent, even after irradiation.

The preliminary Hall and lifetime measurements were valuable in anticipating experimental difficulties and in defining the experimental procedures to be used in studies expected to continue in a renewed contract. The objective will be to obtain measurements of carrier removal rates in lithium-doped quartz-crucible and float-zone silicon as a function of extending bombardment temperature from 80°K to 300°K. Parallel measurements of lifetime on the same Hall bars will indicate the relationship of recombination defects to carrier removal defects.

The work described has provided design criteria for radiation-resistant lithium-containing solar cells in the following ways.

(1) Kinetic studies and capacitance measurements have demonstrated the dynamics of lithium motion in the cell. The models indicate that, for a stable cell, lithium mobility should be reduced in cell material where possible. This will ensure that the lithium will not escape too rapidly either into the p-region or into the aggregate state.

(2) Useful guidelines for suitable levels of phosphorus, lithium and other impurity concentrations in the solar cell base region have been obtained. Based on this information it should soon be possible to derive specification for a lithium concentration profile to fit a given radiation environment (i. e. a given flux rate and fluence) and a given shelf and mission life.

(3) The efficacy of the low-injection-level diffusion length method for predicting outer-space sunlight operation, as well as determining absolute defect content, has been established.

(4) Methods of non-destructively characterizing the content and mobility of lithium in a solar cell and hence, ultimately, its precise radiation hardness level, are emerging from recent work.

The general research problem still to be solved is that of the determination of the state of lithium atoms within the silicon lattice defect structure after irradiation lattice. The present work has advanced the ability to detect the position of electrically active lithium donor atoms near the junction and of characterizing active recombination centers containing lithium. However, it is not yet possible to characterize the structure of these centers, nor to assess the form or quantity in which electrically inactive lithium is present. Lithium atoms "disappear" as donors, after irradiation. When this occurs at a certain point in the solar cell, it is not possible to tell whether the lithium atoms have (a) aggregated and precipitated or (b) remained in discrete form, but combined with an impurity to form uncharged (and hence low-recombination) defect centers. Further work at a fairly basic level combined with solar-cell studies will be needed to answer these questions.

B. RECOMMENDATIONS FOR FUTURE WORK

1. Bulk Measurements

The picture gained from the present work suggests that, in the future, investigations of the influence of dopants on lithium interaction with primary and secondary defects can continue to yield information important in selecting the correct material for solar cell construction. Thus, the basic production rates by 1 MeV electrons of carrier-removal and recombination defects must be measured. These measurements can be made by monitoring the Hall-effect and lifetime of minority carriers on bars of silicon uniformly doped with lithium. Wide variation of bombardment and measuring temperatures is required to separate and measure the various interactions of vacancies, phosphorus lithium and oxygen. The production rate dependence of irradiation-temperature dependent (ITD) defects in lithium doped silicon on bombardment temperature should be dramatically different from that in phosphorus-doped silicon.

In addition to the majority-carrier determinations mentioned above (made by Hall-effect measurement), minority-carrier lifetime measurements should be made on bars of the same series of silicon materials which have been used in fabricating cells, with and

without uniform diffusion of the bar with lithium. These measurements should be made as a function of bombardment and measuring temperatures. The lifetime measurements should also be made as a function of injection level, again on samples obtained from the same silicon drystals as are used in the fabrication of test diodes or solar cells.

2. Diode and Solar-Cell Measurements

The above carrier-removal and recombination-center production data can now, with existing techniques be correlated with measurements made on lithium-doped solar cells and help to explain and predict the behavior of the cells at any time after the introduction of the defects. The link is made possible by the recently developed capacitance technique for observing carrier removal rate in cells near the junction, simply by measuring doping density profiles before and after bombardment of lithium-doped cells.

In correlating the minority carrier data (pulsed lifetime vs. diffusion length data) the influence of the electric field in the junction region of solar cells on the damage and annealing rates in irradiated cells will introduce a complicating factor which, however, can be allowed for. In addition, the recombination statistics of minority carriers may be affected by this electric field. Thus, injection-level dependence of minority-carrier lifetime in lithium-doped solar cells bombarded by 1 MeV electrons should be compared to the injection-level dependence of lifetime in the field-free Hall bars. Long-term stability studies on irradiated GFE and test cells must, of course be continued in order to determine the cause of the observed redegradation of recovered solar cells.

Such a program will provide a set of data with the proper balance to determine, with fair assurance, the optimum chemical content and growth method for the basic cell material. In addition, the electrical measurements used are now achieving sufficient repeatability that the data should be useful in developing operational methods for predicting the degradation of a solar cell in many different combinations of high-energy particle and dose rate. However, the practical importance of the particularly correlated pattern of data recommended above lies in the ability to predict changes in degradation or recovery of solar cells with temperature. In an earth-orbit situation, cells are subjected to irregular but cyclic variations of temperature. In certain eclipse situations, array temperature may fall as low as - 120°C (153°K) this lies below the temperature (200°K) at which the familiar room-temperature defects (A, E-center) are formed at the normal rate parallel, but different defect formation processes may take place, especially in the presence of lithium. Array temperatures may also rise to 75°C. Only with a working knowledge of the physical processes taking place is it possible to predict reasonably well the impact of these wide temperature excursions on the radiation-resistance of lithium-containing solar cells.

APPENDIX A

GLOSSARY OF SYMBOLS

A	Cell area
B	Junction capacitance
C_1 and C_2	Junction capacitances measured at voltages V_1 and V_2, effectively
C_n	Capture cross-section for electrons
C_p	Capture cross-section for holes
D_F	Diffusion constant for free lithium in silicon
D_L	Diffusion constant of lithium
D_{Lo}	Effective Li diffusion constant near the junction
D_p	Minority-carrier diffusion constant
E_c	Voltage at edge of conduction band
E_f (n, t)	Fermi level for electrons
E_L	Energy barrier to the liberation
E_m	Energy level of metastable pair
E_r° and E_r+	Energy barriers to recombination
$\mathcal{E}$	Electric field
$\mathcal{E}_A$	Value of electric field at the depletion region edge due to applied bias
F	Fermi level (volts)
f_r	Fraction of damage remaining
g	Uniform generation rate of election-hole pairs by the hombarding radiation
I_{sc}	Short-circuit current
J_B	Incident electron-beam current density
J_{sc}	Short-circuit current density (in mA/cm^2)
k	Boltzmann's constant
L	Diffusion length
L_o	Diffusion length before bombardment
L_i	Diffusion length immediately after bombardment
L_2	Diffusion length, at a time t after bombardment has ceased.
N_c	Effective number of states in conduction band

N_D	Donor density (atoms/cm^3)
N_{Do}	Total donor density
N_{D1}	Density at the junction edge before bias is applied
N_{D2}	Potential at the junction edge after bias is applied
N_L	Lithuim concentration
N_{Lo}	Lithium concentration at edge of the depletion region (hi ions/cm^3)
N_p	Phosphorus density
n	Carrier density
n_o	Thermal-equilibrium minority carrier concentrations (electrons)
n_1	Carrier concentration when the Fermi level is at the energy level of the trap (electrons)
P max	Maximum power
p	Hole concentration
p_o	Thermal equilibrium minority carrier concentrations (holes)
p_1	Carrier concentrations when the Fermi level is at the energy level of the trap (holes)
Q	Total charge in the depletion region
q	Electron charge
R	Radiation-produced recombination center
R_H	Hall coefficient
r_o	Defect capture radius
S	Slope of the annealing curve
s	Specific Ionization
T	Temperature
V_o	P/n junction potential drop
V_{oc}	Open circuit voltage
V_1 and V_2	Voltages employed in capacitance measurements where $V_2 > V_1$
W	Distance from junction
W_o and W_3	Widths of the depletion region for zero and 3 volts reverse bias, respectively
W_{10i}	Initial depletion width at 10V reverse bias
W_{10f}	Final depletion width at 10V reverse bias
X	Unknown species with concentration equal to R
Δn	Excess carrier density (electrons)
Δp	Excess carrier density (holes)
ϵ	Permitivity of silicon
N_{CR}	Carrier removal rate
λ	Wavelength of light source
μ_C	Conductivity mobility

μ_H	Hall mobility
μ_{Lo}	Effective Li mobility near the junction
μ_p	Minority carrier mobility
ρ	Resistivity (in Ω -cm)
σ	Conductivity
τ	Minority carrier lifetime
τ_n	Electron lifetime
τ_{n_o}	Lifetime of electrons in p-type silicon
τ_o	Lifetime at low injection level
τ_p	Hole lifetime
τ_{p_o}	Lifetime of holes in n-type silicon

APPENDIX B

PERFORMANCE PARAMETERS

TABLE B-I. INITIAL PERFORMANCE PARAMETERS FOR CELLS FABRICATED IN-HOUSE

Lopex				Float Zone				Quartz Crucible			
Sample No.	N_{LO} ($cm^{-3} \times 10^{-14}$)	N_{LB} ($cm^{-3} \times 10^{-16}$)	L_O (microns)	Sample No.	N_{LO} ($cm^{-3} \times 10^{-14}$)	N_{LB} ($cm^{-3} \times 10^{-16}$)	L_O (microns)	Sample No.	N_{LO} ($cm^{-3} \times 10^{-14}$)	N_{LB} ($cm^{-3} \times 10^{-16}$)	L_O (microns)
10 Ω-cm				1 Ω-cm				12 to 16 Ω-cm			
A-1-2	7.0	1.0	119	D-1-1		1.8	94	G-1-1	7.5	2.0	40
A-1-4	5.1	1.0	128	D-1-2		1.8	71	G-1-2	7.5	1.9	41
A-2-1	1.0	0.3	83	D-1-3		1.5	72	G-1-5	4.0	1.3	50
A-2-2	1.3	0.3	85	D-1-4		1.5	60	G-2-1	5.5	1.8	33
A-2-3	1.9	0.3	90	D-2-1		1.0	87	G-2-2	5.7	1.8	37
A-3-1	9.0	2.0	118	D-2-2		1.0	86	G-2-3	5.5	1.8	34
A-3-2		2.0	109	D-2-3		1.2	86	G-2-4	5.5	1.8	27
A-3-3	7.8	2.0	109	D-2-4		1.2	99	G-2-5	5.5	1.8	41
A-4-1	13	2.0	132	D-1-6C	0	0	66	G-1-6C	0	0	33
A-4-2	8.5	2.0	109	D-1-7CA	0	0	53	G-1-7C	0	0	33
A-4-3	7.5	2.0	112	D-1-8CA	0	0	65	G-2-6C	0	0	63
A-4-4	7.2	2.0	93	D-2-6C	0	0	50	G-2-7C	0	0	50
A-5-1	9.4	2.0	94	D-2-7CA	0	0	53				
A-5-2	10	2.0	72	D-2-8CA	0	0	46				
A-5-3	8.5	2.0	116	10 Ω-cm							
A-2-4C	0	0	47	E-1-1	5.6	1.5	100				
A-3-7CA	0	0	45	E-1-2	4.4	1.0	94				
A-4-7CA	0	0	55	E-1-3	<.5	1.5	67				
A-5-7CA	0	0	29	E-1-4		0.9	55				
1 Ω-cm				E-2-1	3.0	1.0	129				
B-1-2		1.5	105	E-2-2	1.5	1.0	96				
B-2-1		1.3	141	E-2-3	2.5	1.0	83				
B-2-2		1.3	125	E-2-4		1.0	102				
B-3-1		1.3	100	E-1-6C	0	0	62				
B-3-2		1.5	97	E-1-7CA	0	0	42				
B-1-7CA	0	0	23	E-1-8CA	0	0	58				
B-2-7CA	0	0	30	E-2-6C	0	0	29				
30 Ω-cm				E-2-7CA	0	0	33				
C-1-5	9.0	1.5	131	E-2-8CA	0	0	33				
C-1-7	16	3.5	120	30 Ω-cm							
C-2-1	3.0	1.5	100	F-1-1	3.2	1.0	104				
C-2-2	3.2	1.1	94	F-1-2	3.5	1.0	97				
C-2-3		1.5	95	F-1-3	1.3	1.0	75				
C-2-4	3.0	1.5	97	F-1-4	3.5	1.0	97				
C-2-5		1.7	84	F-2-1	1.4	1.0	79				
C-3-2	2.3	1.5	76	F-2-2	1.0	0.9	69				
C-3-3		1.7	72	F-2-3	1.5	1.0	32				
C-3-4		1.6	83	F-2-4	2.5	1.0	68				
C-4-1	4.4	1.0	57	F-1-6C	0	0	39				
C-4-2		1.1	58	F-1-7CA	0	0	42				
C-4-3	3.0	1.1	64	F-1-8CA	0	0	47				
C-4-4	4.1	1.5	61	F-2-6C	0	0	32				
C-4-5	5.4	1.7	57	F-2-7CA	0	0	32				
C-2-6C	0	0	55	F-2-8CA	0	0	31				
C-2-7C	0	0	52								
C-2-8C	0	0	39								
C-3-6C	0	0	57								
C-3-7C	0	0	53								
C-4-6C	0	0	32								
C-4-7C	0	0	37								

TABLE B-II. INITIAL PERFORMANCE PARAMETERS FOR GFE CELLS PROVIDED DURING PRESENT YEAR

Cell	P_O (Ω-cm)	Gr. Meth	L_o (microns)	J_{sc} (mA/cm^2)	V_{oc} (volts)	P_{max} (mW/cm^2)	N_{Lo} (cm^{-3} x 10^{-14})
TI948	20	FZ	90	33.7	.571	13.3	11
949	20	FZ	89	32.6	.569	12.9	9.5
950	20	FZ	77	32.9	.570	13.0	13
951	20	FZ	76	32.2	.568	12.7	14
952	20	FZ	91	33.0	.564	12.6	9.5
976	200	Lopex	100	32.0	.568	12.1	16
977	200	Lopex	100	34.3	.554	12.0	15
978	200	Lopex	100	34.5	.574	13.4	18
979	200	Lopex	122	32.4	.569	11.8	11
981	200	Lopex	121	35.5	.562	12.4	9.5
He651	20	Lopex	33	26.3	.535	9.8	15
670	20	Lopex	41	27.7	.545	10.8	17
673	20	Lopex	25	24.3	.522	8.8	17
676	20	Lopex	31	25.9	.519	9.1	20
694	20	Lopex	29	25.8	.525	9.4	13
796	20	FZ	29	26.0	.525	9.5	8.9
798	20	FZ	40	27.6	.518	10.4	7.7
808	20	FZ	30	26.4	.532	9.6	7.1
810	20	FZ	39	27.9	.532	9.6	7.1
815	20	FZ	42	28.3	.535	11.0	17
866	20	FZ	42	29.0	.532	10.8	7.7
867	20	FZ	39	28.6	.523	10.7	4.7
868	20	FZ	31	26.5	.527	9.9	8.3
870	20	FZ	41	28.0	.525	10.5	7.1
871	20	FZ	51	29.6	.540	11.2	7.1
872	20	FZ	31	28.0	.535	10.6	5.9
873	20	FZ	44	29.0	.544	11.6	7.1
875	20	FZ	37	28.1	.531	10.7	8.5
876	20	FZ	34	27.6	.523	9.2	8.8
878	20	FZ	36	28.3	.532	11.1	7.3
879	20	FZ	44	30.1	.542	11.9	7.0
881	20	FZ	48	29.6	.539	11.2	9.7
882	20	FZ	51	29.6	.532	11.4	8.3
884	20	FZ	53	30.2	.530	10.8	9.0
885	20	FZ	46	28.9	.530	10.9	7.5
886	20	FZ	45	29.1	.528	10.7	7.6
887	20	FZ	58	30.6	.527	10.8	5.0
890	20	FZ	34	26.4	.527	9.9	8.3
891	20	FZ	51	29.5	.535	11.3	7.5
892	20	FZ	44	28.9	.532	11.0	10

TABLE B-III. INITIAL PERFORMANCE PARAMETERS FOR GFE CELLS PROVIDED IN PREVIOUS YEAR AND MONITORED DURING PREVIOUS YEAR

Cell	P_o (Ω-cm)	Gr. Meth	L_o (microns)	J_{sc} (mA/cm^2)	V_{oc} (volts)	P_{max} (mW/cm^2)	N_{Lo} (cm^{-3} x 10^{-14})
Ho5-1	100	FZ	33	24.7	.500	7.7	
6-1	1000	FZ	39	23.3	.514	6.4	
33-2	10	FZ	26	24.4	.500	6.6	
He55-1	20	FZ	51	29.2	.553	9.2	
248P	1000	FZ	25	24.8	.530	8.4	-
249P	1000	FZ	26	24.2	.543	8.4	-
340	100	FZ	74	28.6	-	-	22
341	100	FZ	57	28.5	-	-	17
342	100	FZ	62	29.6	-	-	12
TI42	20	FZ	89	28.6	.578	9.2	22
63	20	FZ	110	29.6	.582	10.4	15
71	20	FZ	112	28.5	.534	6.3	17
112	20	Q.C.	54	28.0	.586	10.5	20
113	20	Q.C.	54	27.5	.578	9.9	20
127	20	LOPEX	72	30.2	.580	10.2	82
128	20	LOPEX	78	28.5	.594	10.8	70
132	20	LOPEX	78	29.8	-	-	92
161	20	FZ	45	27.2	.584	10.8	50
166	20	FZ	33	25.2	.570	8.7	-
167	20	FZ	84	30.8	.568	10.8	7.5
168	20	FZ	58	28.8	.580	11.1	20

APPENDIX C
DOPANT PROFILES

The capacitance method of obtaining lithium donor concentration as a function of distance from the junction has been extensively employed in this work. The technique of measurement is as follows: doping densities are obtained by applying a reverse bias to the p-n junction and measuring the capacitance of the junction as a function of voltage. As the reverse bias is increased, the width of the depletion region (i.e., field region) increases, sweeping through a small portion of the base region near the junction. By measuring increments of voltage and capacitance, the overall doping concentration vs. distance from the junction can be obtained. Lithium concentration is then obtained by subtraction of the phosphorus doping from the overall value.

The relation (Ref. 11) for determining dopant concentration is a given region of silicon, of thickness Δw is, for a 0.2-inch square diode

$$N_D = 7.7 \times 10^7 \left(\frac{C_1 + C_2}{2}\right)^3 \left(V_2 - V_1\right) \frac{1}{C_2 - C_1)} \qquad \text{(B-1)}$$

where

N_D is donor density, in atoms per cm^3

C_1 and C_2 are junction capacitances measured at voltages V_1 and V_2, respectively

V_1 and V_2 are voltages such that $V_2 > V_1$

For accuracy, V_1 and V_2 must be chosen so that C_2-C_1 is not more than

$$0.1 \left(\frac{C_1 + C_2}{2}\right).$$

This very simple method for the estimation of dopant concentration near the junction has provided a valuable new tool for studying irradiation damage is specific locations, within a diffusion length of the junction, in diodes, without destruction or even special contacting procedures. The fact of important nonuniformities of lithium concentration near the junction, first realized in a previous program, has been confirmed. Not only can the level of damage to minority-carrier lifetime now be related to changes in state of the dopants,

but also changes in dopant state (which may not even be reflected in changes of short-circuit current or diffusion length) can be observed. For example, changes in dopant concentration have been observed to occur even after recovery of minority-carrier lifetime. Furthermore, redistributions of lithium near the junction have been observed over several weeks of storage after fabrication, even before irradiation.

Another important implication of the nonuniformity of lithium can now be studied quantitatively, namely, the effect of drift-fields. The field strength, $\mathcal{E}$, may be obtained from the equations

$$N_D = N_c \exp \frac{-q\,(E_c - F)}{kT} \tag{B-2}$$

$$\mathcal{E} = \frac{-dF}{dw} = \frac{-kT}{q} \frac{1}{N_D} \frac{dN_D}{dw} \tag{B-2a}$$

where

N_c is effective number of states in the conduction band

q is electron charge

E_c is voltage at edge of conduction band

F is Fermi level (in volts)

k is Boltzmann's constant

T is temperature (°K)

w is distance from junction

These drift-fields will assist minority carrier transport toward the junction. This situation in lithium-diffused p-n junctions is made all the more interesting by the fact that both the lithium concentration and the gradient have been observed to decrease after the cell is bombarded by a fluence of sufficient magnitude. Consequently, the electric field due to the ratio of gradient-to-concentration may also decrease. The value of this electric field is sufficiently large that it significantly affects the collection of minority carriers. The changes in lithium distribution and consequently electric field are found to continue after annealing has stopped. Thus, it is possible that the process of neutralization of recombination centers stops while the removal of carriers by defects and other motions of lithium near the junction continues. If the electric field distribution could be specified over a distance equal to a diffusion length, then a

theoretical evaluation of the electric-field effect on short-circuit current could be made. This theoretical evaluation would involve solving the continuity and current equations given by Equations (B-3) and (B-4):

$$\frac{dp}{dt} = g - \frac{1}{q}\frac{dJ_p}{dw} - \frac{p}{\tau_p} \tag{B-3}$$

$$J_{sc} = q\left(p\mu_p \mathcal{E} - D_p \frac{dp}{dw}\right) \tag{B-4}$$

where

p is hole concentration

t is time

g is a uniform generation rate of electron-hole pairs by the bombarding radiation

J_{sc} is hole current density

τ_p is hole lifetime

μ_p is minority-carrier mobility

D_p is minority-carrier (hole) diffusion constant

To date it has not been possible to extend capacitance measurements further than 10 microns from the junction. Efforts will be made in the future to further determine donor concentration and electric-field profiles so that a theoretical analysis can be employed to check the importance of this electric field in the collection of minority carriers.

In addition to the study of the effects of the electric field resulting from the lithium-diffusion process on short-circuit current and annealing properties of solar cells, it is also possible to alter this field by the application of voltage and/or temperature and thus correlate field distribution with the electrical properties of irradiated solar cells.

APPENDIX D

LIFETIME ANNEALING KINETICS

The basic physical parameter measured in this study technique is the diffusion length. This parameter can be measured by means of the photo-voltaic or the electron-voltaic effects. In previous work at RCA and in future work, the electron-voltaic effect will be used to measure diffusion length. Briefly, the technique involves the measurement of short-circuit current produced by the creation of electron ion pairs under electron bombardment. A Van de Graaff generator provides the electron beam of 5×10^{-10} ampere at an energy of 1 MeV. This low value of electron current does not damage the solar cell and, in addition, is less than the value of current at which injection level effects must be considered.

A theoretical treatment of diffusion-length recovery as a function of time after irradiation was given in an earlier analysis (Ref. 15). The analysis is based on a diffusion-limited-kinetic model where unequal concentrations of the annealing species are present. The annealing species were assumed to consist of essentially immobile lithium-vacancy ($Li\text{-}V^-$) damage sites carrying a single negative charge, and mobile lithium ions (Li^+). The $Li\text{-}V^-$, being negatively charged, would have a large capture cross section for minority carriers (i.e., holes) in the n-type region. As Li^+ ions diffuse to and combine with $Li\text{-}V^-$, a complex "Li_2V", with zero charge, and therefore low capture cross section would be formed. The proposed recovery process thus involves the formation of a "Li_2V" complex. The diffusion-limited annealing theory yields the following expression for the defect density, "N" or the fraction of damage remaining $f_r(t)$ at time, t, after bombardment:

$$f_r(t) \quad \frac{N_2}{N_1} = \frac{N_L - N_1}{N_L \exp\left\{ K N_L - N_1 \left[1 + \frac{2r_o}{(\pi D_L t)^{1/2}} \right] t \right\} - N_1} \tag{D-1}$$

$$K = 4\pi r_o D_L \tag{D-2}$$

where

N_2 is defect density at time, t, after bombardment has ceased

N_1 is defect density immediately after bombardment

N_L is free lithium density immediately after bombardment ("free" implies being available for complexing with vacancies and, presumably, in an electrically active, ionizable form)

K is a constant equal to $4\pi r_o D_L$

r_o is defect capture radius for lithium

D_L is diffusion constant of lithium (2×10^{-14} cm^2/sec at room temperature (Ref. 22).

If, as in the case for the experiments discussed in this section; $N_L \gg N_1$. Equation (D-1) reduces to

$$(f_r)^{-1} = \exp \left\{ K N_L \left[1 + \frac{2r_o}{(\pi D_L t)^{1/2}} \right] t \right\} . \qquad \text{(D-3)}$$

The second term in the exponential becomes unimportant when

$$\frac{2r_o}{(\pi D_L t)^{1/2}} \lesssim 0.2.$$

When $r_o \approx 10^{-6}$ cm (100Å), this is satisfied for $t > 20$ minutes. Thus, for $t > 20$ minutes:

$$(f_r)^{-1} = \exp \left(K N_L t \right) , \qquad \text{(D-4)}$$

so that the slope of $\ln (f_r)^{-1}$ vs. time should be a constant equal to $K N_L$

To obtain $(f_r)^{-1}$ as a function of the measured quality, i.e., diffusion length L, the minority carrier (hole) lifetime can be related to the defect density, N, by (Ref. 32):

$$\frac{1}{\tau_p'} = \frac{1}{\tau_p} + k N \qquad \text{(D-5)}$$

where

τ_p is the hole lifetime before irradiation

τ_p' is the hole lifetime after irradiation.

Immediately after bombardment, $N = N_1 = \eta \phi$, where ϕ is the fluence of 1-MeV electrons (e/cm^{-2}), η is the defect introduction rate (cm^{-1}), $k = \sigma f v$, σ is the capture-cross section for holes, f is the Fermi filling factor of the defect level, v is the hole velocity,

and the bombardment is assumed to have occurred in a time negligible by comparison to recovery times.

Inserting the expression for diffusion length, $L = D_p \tau_p$, where D_p is the diffusion constant for (minority carrier) holes, into Equation (D-5) gives

$$(f_r)^{-1} = \left[\frac{1}{(L_1)^2} - \frac{1}{L_o^2}\right] \Bigg/ \left[\frac{1}{(L_2)^2} - \frac{1}{L_o^2}\right] \qquad \text{(D-6)}$$

The quantity $(f_r)^{-1}$ is derived from the raw experimental data by using Equation (D-6)

where

L_1 is diffusion length immediately after bombardment

L_o is diffusion length before bombardment

L_2 is diffusion length at a time, t, after bombardment has ceased.

APPENDIX E
INJECTION-LEVEL DEPENDENCE OF MINORITY-CARRIER LIFETIME

Shockley and Read (Ref. 23) have predicted that the electrical effects of radiation damage in semiconductors would be sensitive to excess minority-carrier injection level. Extensive experimental proof of this prediction has been obtained, including measurements on bulk silicon, silicon transistors, and silicon solar cells. In general, some electrical parameter characterizing damage in these devices was observed to change as the injection level was increased. For example, minority-carrier diffusion length as a function of illumination level has been studied in solar cells damaged by protons, and its value shown to have a fairly strong illumination-level dependence (Ref. 26). The purpose of this investigation technique is to use the dependence of diffusion length on excess carrier density to obtain information on interactions of lithium with radiation-induced defects in silicon solar cells, and energy levels of the defects.

It was first shown by Shockley and Read (Ref. 23) that the minority-carrier lifetime is a function of the injected-carrier concentration. Equation (E-1) describes this dependence of τ_p on excess carrier density, Δn.

$$\tau_p = \tau_{p_o} \frac{(n_o + n_1 + \Delta n)}{(n_o + p_o + \Delta n)} + \tau_{n_o} \frac{(p_o + p_1 + \Delta p)}{(n_o + p_o + \Delta n)} \qquad \text{(E-1)}$$

where

τ_{p_o} is lifetime of holes in n-type silicon (i.e., minority carriers)

τ_{n_o} is lifetime of electrons in p-type silicon (i.e., minority carriers)

n_o and p_o are thermal equilibrium carrier concentrations (electrons and holes, respectively)

n_1 and p_1 are the carrier concentrations when the Fermi level is at the energy level of the trap (electrons and holes, respectively)

Δn and Δp are the deviations from the thermal equilibrium carrier concentrations, i.e., excess carrier density (electrons and holes, respectively).

By setting

$$\frac{\tau_{p_o} + \tau_{n_o}}{\tau_{p_o}(n_o + n_1) + \tau_{n_o}(p_o + p_1)} = a, \tag{E-2}$$

$$\frac{1}{n_o + p_o} = c, \tag{E-3}$$

and

$$\tau_{p_o}\frac{(n_o + n_1)}{(n_o + p_o)} + \tau_{n_o}\frac{(p_o + p_1)}{(n_o + p_o)} = \tau_o, \tag{E-4}$$

Equation (E-1) can be rewritten in the simplified form of Equation (E-5).

$$\tau_p = \tau_o \frac{(1 + a\,\Delta n)}{(1 + c\,\Delta n)} \tag{E-5}$$

It can be seen from Equation (E-5) that the measured lifetime can increase or decrease with excess carrier density Δn, depending on the value of the ratio a/c. Thus, in order for τ_p to increase with Δn, the inequality expressed by Equation (E-6) must hold.

$$\frac{\tau_{p_o}(n_o + n_1) + \tau_{n_o}(p_o + p_1)}{\tau_{p_o} + \tau_{n_o}} < (n_o + p_o) \tag{E-6}$$

For τ_p to decrease, the opposite inequality must hold. Applying Equation (E-6) to n-type silicon where $n_o > p_o$ and $\gamma = \tau n_o/\tau p_o > 1$ (i.e., the recombination level is "acceptor-like"), the inequality becomes:

1. τ_p increases with Δn, $\gamma > 1$, $p_1 < n_o$ Level located in upper or lower half of forbidden gap.

2. τ_p increases with Δn, $\gamma < 1$, $n_1 < p_o$ Level located in lower gap.

3. τ_p decreases with Δn, $\gamma > 1$, $p_1 > n_o$ Level located in lower gap.

4. τ_p decreases with Δn, $\gamma < 1$, $n_1 > p_o$ Level located in upper or lower gap.

Information on relative capture cross section for electrons and holes, together with locations and values of recombination energy levels can be obtained from measurements of lifetime vs. excess carrier density. All of the above equations apply if the radiation-induced defect density N_T is smaller than or equal to $(n_o + p_o)$. The situation is further complicated when more than one recombination level is present. For $N_T < (n_o + p_o)$, the lifetime τ_p is given by Equation (E-7).

$$\frac{1}{\tau} = \Sigma_i \frac{1}{\tau_i} \qquad \text{(E-7)}$$

where the summation is over all recombination levels. However, if N_T is several times larger than $(n_o + p_o)$, lifetimes do not combine as the sum of the reciprocal lifetimes as given by Equation (E-7). Instead, combinations of the recombination level parameters become possible with many corresponding lifetime values possible in the same sample.

Briefly, the technique provides a very rapid and convenient check on the defect-energy-level situation in the base region of the recovering cell. Certain known centers, such as the A- and E-centers, can be tentatively identified. In future work, it will be extremely interesting to correlate electric field changes in the junction region of irradiated solar cells with the dependence of diffusion length on injection level. The effect of the electric field on recombination statistics in the cells is unknown.

The raw data obtained in this measurement technique is the solar-cell diffusion length as a function of Van de Graaff beam current. This electron current generates electron and ion carriers in the solar cell. The excess carrier density is computed from Equation (E-8).

$$\Delta n = \frac{L^2 J_B S}{q D_p} \qquad \text{(E-8)}$$

where

L is the diffusion length of the cell at J_B

J_B is any electron-beam current density

q is the basic electron charge

D_p is minority carrier diffusion constant (hole)

S is specific ionization

Inserting values for the constants results in Equation (E-9).

$$\Delta n = 3.96 \times 10^{15} J_B L^2 \text{ carriers/cm}^3 \qquad \text{(E-9)}$$

where $D_p = 10$ cm^2/sec has been used for holes in n-type silicon, J_B is in A/cm^2, and L is in μ. The minority-carrier lifetime $\tau_p = L^2/D_p$ and the relative lifetime $\tau_p/\tau_o = L^2/L_o^2$, where τ'_p and L_o are the lifetime and diffusion length measured at low injection level ($J_B = 1.5 \times 10^{-10}$ A/cm^2). In previous work it was observed that injection-level effects appear when the beam current density exceeded 1.3×10^{-9} A/cm^2. The cathode controls of the Van de Graaff generator were modified so that currents as low as 10^{-10}A could be obtained. Measurements of low injection level diffusion lengths are now made with a standard beam current of 5×10^{-10} A, which is approximately an order of magnitude lower than the value used previously. The experimental technique involves the sequential measurement of diffusion length at the standard low-injection level, then a high level, and finally the standard low level. This sequence is repeated for all injection levels commencing with the highest beam current obtainable and decreasing to the lowest level. Thus, many diffusion length values at the standard low-injection level are obtained during an experiment. An average value of low-injection level diffusion length, L_o, is determined from these values for use in the analysis of the data.

REFERENCES

1. J. J. Wysocki, P. Rappaport, E. Davison, R. Hand, and J. J. Loferski, Appl. Phys. Letters 9, 44 (1966)

2. J. J. Wysocki, IEEE Transion Nuclear Science NS-13 (6) 168 (1966).

3. G. Brucker, 6th Photovoltaic Spec Conf Mar 1967

4. J. R. Carter, Jr., IEEE Nuclear and Space Radiation Conf, Columbus, Ohio, Jul 1967

5. J. Baicker, et al, RCA, First Semiannual Prog Rept, Cont No. NAS 5-457 Jan 1962

6. C. K. Wertheim and W. M. Augustyniak, Rev. Sci. Instr. 27, 1062 (1956)

7. J. J. Wysocki, G. J. Brucker, A.G. Holmes-Siedle, RCA Annual Prog. Rept. Contr. No. NAS 5-10239, June 1967, Nuclear and Space Radiation Effects Conf. Columbus, Ohio, July, 1967.

8. W. Rosenzweig, Bell System Tech. J. 41, 1573 (1962)

9. E. L. Ralph, 6th Photovoltaic Spec Conf., Mar, 1967

10. P. A. Iles, 6th Photovoltaic Spec Conf, Mar, 1967

11. J. Hilibrand & R. D. Gold, RCA Rev. XXI 245 (1960)

12. R. L. Statler, NRL Rept 6091, Oct. 7, 1964, U.S. Naval Res. Lab., Washington D.C.

13. J. Mandelkorn, Sixth Photovoltaic Specialists Conf. Cocoa Beach, Fla., Mar 1967

14. E. M. Pell, Solid-State Electronics and Communications p. 261, Eds. Desirant and Michiels (Academic Press, New York, 1960)

15. T. R. Waite, Phys. Rev. 107, 463 (1957).

16. L. Valdes, Proc IRE 42, 420 (1954)

17. G. Brucker, T. Faith, A. G. Holmes-Siedle, and R. Neadle, RCA First Prog. Rept. Contr. No. NAS 5-10234, 20 Jun 67, 20 Nov 67.

18. P. Payne, G. Goodelle, and E. L. Ralph, Heliotek First Periodic Report Contr. NAS 5-10272, 24 Aug 1966 - 24 Feb 1967.

19. M. Wolf, Proc IEEE 51, 674 (1963)

20. E. M. Pell, J. Appl. Phys. 31, 291 (1960)

21. E. M. Pell, Phys. Rev. 119, 1222 (1960)

22. H. J. Stein, F. L. Vook, Phys. Rev. 163, 790 (1967)

23. W. Shockley and W. T. Read, Phys. Rev. 87 835 (1952)

24. O. L. Curtis and C. A. Germano, Nuclear and Space Radiations Effects Conf, Columbus, Ohio, July 1967

25. M. E. Beatty and G. F. Hill, NASA TND-2817 June 1965

26. J. M. Denney, et al, STL Report 8653-6017-KU-000 and 8653-6062-KU-000, Contract No. NAS 5-1851

27. F. L. Vook and H. J. Stein, "Production of Defects In n-Type Silicon", Proceedings of the Santa Fe Conference on Radiation Effects in Semiconductors, Plenn-Press, N. Y., p. 99-114, Oct 1967.

28. H. J. Stein and F. L. Vook, "Characteristics of Electron-Induced Defects In n-Type Silicon", Proceedings of the Santa Fe Conference on Radiation Effects in Semiconductors, Plenn-Press, N. Y., p. 415-123, Oct. 1967.

29. B. L. Gregory and C. E. Barnes, "Defect Reordering At Low Temperatures In Gamma Irradiated n-Type Silicon," Proceedings of the Santa Fe Conference on Radiation Effects in Semiconductors, Glenum-Press, N. Y., p. 124-135, Oct 1967.

30. R. H. Logan and A. J. Peters, "Impurity Effects Upon Mobility in Silicon", J. of Appl. Phys, 31, 1, p. 122-124 Jan 1960

31. G. D. Watkins, Comment in Proceedings of the Santa Fe Conference on Radiation Effects in Semiconductors, Glenn-Press, N. Y., p 113, Oct 1967

32. J. J. Loferski and P. Rappaport, Phys. Rev. 111, 432 (1958)